SEARCHING FOR SUPERSYMMETRY AT THE LHC: STUDIES OF SLEPTONS AND STOPS

by

Jonathan Daniel Eckel

A Dissertation Submitted to the Faculty of the

DEPARTMENT OF PHYSICS

In Partial Fulfillment of the Requirements
For the Degree of

DOCTOR OF PHILOSOPHY

In the Graduate College

THE UNIVERSITY OF ARIZONA

2014

THE UNIVERSITY OF ARIZONA
GRADUATE COLLEGE

As members of the Dissertation Committee, we certify that we have read the dissertation prepared by Jonathan Daniel Eckel
entitled Searching for Supersymmetry at the LHC: Studies of Sleptons and Stops
and recommend that it be accepted as fulfilling the dissertation requirement for the Degree of Doctor of Philosophy.

Date: August 8, 2014
Shufang Su

Date: August 8, 2014
Charles Stafford

Date: August 8, 2014
Doug Toussaint

Date: August 8, 2014
Erich Varnes

Final approval and acceptance of this dissertation is contingent upon the candidate's submission of the final copies of the dissertation to the Graduate College.
I hereby certify that I have read this dissertation prepared under my direction and recommend that it be accepted as fulfilling the dissertation requirement.

Date: August 8, 2014
Dissertation Director: Shufang Su

STATEMENT BY AUTHOR

This dissertation has been submitted in partial fulfillment of requirements for an advanced degree at the University of Arizona and is deposited in the University Library to be made available to borrowers under rules of the Library.

Brief quotations from this dissertation are allowable without special permission, provided that accurate acknowledgment of source is made. Requests for permission for extended quotation from or reproduction of this manuscript in whole or in part may be granted by the head of the major department or the Dean of the Graduate College when in his or her judgment the proposed use of the material is in the interests of scholarship. In all other instances, however, permission must be obtained from the author.

SIGNED: Jonathan Daniel Eckel

ACKNOWLEDGEMENTS

This dissertation would not have been possible if it weren't for the help and support of many of my trusted friends and mentors. Pursuing a Ph.D is definitely a transformative experience. I've grown as a researcher, a teacher, a physicist and person. I have many great mentors and friends to thank for the result.

I'd like to thank Daniel Eisenstein, my first advisor, for giving me a chance to work with the BAO group. The experience was incredibly helpful and got me off on the right track in my graduate student career. The computing skills I learned working with the group are fundamental to all of my current (and future) projects. To the BAO group members: Xiao, Kushal, and Marc, remember..."BAO for life!"

To my current advisor, Shufang Su, I thank you for your time, effort and patience with me as a student. I greatly appreciate that I was given the opportunity to spend a year in Irvine, which certainly sped up the process of transitioning from cosmology to particle physics. Special thanks to Felix, Matt, and the rest of the Irvine particle grad students for their guidance and friendship during my stay.

I thank my collaborators Michael Ramsey-Musolf and Will Shepherd for their guidance while working on projects together. It has been a pleasure working with the both of you.

I am indebted to my friends for their compassion and support. Alex, Ian, and Will, you guys helped me get through some stressful times, for which I am grateful. I also want to thank Brokk, Huanian and the ATLAS experimentalists down the hall for helpful discussions. I especially thank our resident Irish astrophysicist and other THING (Theoretical Interest Group) members for enjoyable discussions of physics.

I thank my family, for their continuous support. Lastly, I'd like to thank my wonderful girlfriend Alex, for her love and support through this long process.

DEDICATION

To Mom, Dad, Grandma & Grandpa

TABLE OF CONTENTS

TABLE OF CONTENTS – *Continued*

LIST OF FIGURES

LIST OF TABLES

ABSTRACT

Searches of supersymmetry at the LHC have put stringent constraints on the strong production of squarks and gluinos. Current results exclude colored particles with masses up to roughly 1 TeV. To fully explore the discovery potential of the LHC, we study the challenging signals that are hidden by Standard Model backgrounds but with masses accessible by the LHC. These particles include the sleptons with a weak production cross section, and stops that are hidden by large top-antitop ($t\bar{t}$) backgrounds. In this dissertation, I explore the collider phenomenology of sleptons and stops at the LHC.

Sleptons can be produced at the LHC either through cascade decay or via Drell-Yan pair production. For the cascade decay, we studied neutralino-chargino associated production, with the subsequent decay through on shell sleptons ($\chi_2^0 \to \ell\ell\chi_1^0$ and $\chi_1^\pm \to \nu_\ell\ell\chi_1^0$) resulting in a trilepton plus missing transverse energy ($\not{E}_T$) signal. The invariant mass $m_{\ell\ell}$, from the neutralino decay has a distinctive triangle shape with a sharp kinematic cutoff. We utilized this feature and obtained the effective cross section that is needed for a 5σ discovery of sleptons. We apply these results to the MSSM and find a discovery reach for left-handed sleptons which extends beyond the reach expected in usual Drell-Yan studies.

Slepton pair production searches on the other hand, have limited reach at the LHC. The slepton decay branching fractions, however, depend on the composition of the lightest supersymmetric particle (LSP). We extend the experimental analysis for data collected thus far to include different scenarios for the composition of the LSP. We find that the LHC slepton reach is enhanced up to a factor of 2 for a non-Bino-LSP. We present the 95% C.L. exclusion limits and 5σ discovery reach for sleptons at the 8 and 14 TeV LHC considering Bino-, Wino-, or Higgsino-like LSPs.

Current stop searches at the LHC focus on signals with $t\bar{t}$ (or $bbWW$) plus $\not{E}_T$. However, in many regions of SUSY parameter space, these decay modes are not dominant, leading to weakened experimental limits on stops. We identify stop decays that can have significant

branching fractions to new final states resulting in new signal channels to observe. We investigate stop pair production by considering the channel of $\tilde{t}_1 \to \chi_2^0\ t \to \chi_1^0 h\ t$ and $\tilde{t}_1 \to \chi_1^\pm\ b \to \chi_1^0 W^\pm\ b$ leading to a signal of 4 b-jets, 2 jets, 1 lepton and $\not{E}_T$. We present the 95% C.L. exclusion limits and 5σ discovery reach for stops at the 14 TeV LHC.

CHAPTER 1

Introduction

The study of phenomenology is concerned with the interplay between theory and experiment. Given a theoretical model, phenomenologists identify its possible experimental signatures. Conversely, they can use theoretical models to try to explain anomolous signatures found in experimental data. Ultimately, phenomenologists seek answers to the fundamental questions of the universe.

1.1 State of the Field

The Standard Model is an incredibly successful theory. The theories of Quantum Chromodynamics (QCD), Quantum Electrodynamics (QED), and Glashow-Weinberg-Salam (GWS) are robust formulations describing the strong, electromagnetic and weak interactions of matter respectively. Rigorous tests have found these theories correct to astounding accuracy. The electroweak sector of the Standard Model has been extensively studied at LEP [1, 2] with precision measurements of the W and Z bosons. The QED prediction of the anomolous magnetic moment of the electron matches experiment to 10 significant digits and is the most precisely known quantity in all of physics [3].

The mathematical structure of the Standard Model has lead to the prediction and the subsequent discovery of many particles. For example, the quark model has laid a framework to characterize baryons and mesons by utilizing isospin [4]. The quasi-symmetry of isospin explains the connection between up- and down-type quarks leading to the prediction of the charm quark [5].

The final particle of the Standard Model, the Higgs boson, was discovered at the Large Hadron Collider (LHC) by the ATLAS and CMS collaborations [6, 7]. While the Higgs fits as the missing puzzle piece in the Standard Model, it brings with it many questions. A light Higgs at the weak scale, gains unstable radiative corrections to its mass, which requires an

unnatural cancellation of terms in order to recover the physical Higgs mass of 125 GeV. This is referred to as the hierarchy problem [8]. Another puzzle occurs on the cosmological front, where observations show that the majority of matter in our universe is composed of an unknown component. We exist in a universe filled with "weakly" interacting matter, by which we infer its existence from its gravitational interaction with visible baryonic matter.

One of the most well motivated extensions to the Standard Model is the theory of Supersymmetry (SUSY). SUSY postulates that for every Standard Model fermion/boson there exists an identical bosonic/fermionic superpartner differing only by its intrinsic spin. These superpartners cancel out the divergent component of the mass corrections to the Higgs, effectively solving the hierarchy problem by introducing a new physical scale of SUSY [9]. In addition to solving the hierarchy problem, SUSY brings with it other attactive features. SUSY includes a mechanism for unifying all the Standard Model forces at high energies; an energy known as the "GUT" scale. Additionally, many models lead to stable SUSY particles that could potentially satisfy the dark matter component of the universe.

1.2 Motivation

The current general-purpose experiments at the Large Hadron Collider (LHC), ATLAS and CMS, are searching for new physics at the TeV scale. Current results show the Standard Model is a remarkably accurate theory [10, 11]. Both experiments have verified top quark and electroweak precision measurements, and most recently discovered the elusive Higgs boson [6, 7]. While the confirmation of the Standard Model is exciting, it is also disappointing that there have been no signs of new physics. Where is Supersymmetry, and how might we find it?

To maintain proton stability, an important charge is introduced in supersymmetry called R-parity, under which SUSY and SM particles have opposite charge. If this charge is conserved, there are interesting phenomenological consequences. R-parity conservation requires SUSY particles to be pair produced at the LHC. It also requires that SUSY particles decay through lighter SM and SUSY particles. As a result, the distinctive collider signatures of SUSY are cascade decays. The subsequent cascade decay occurs until the

lightest supersymmetric particle (LSP) is reached, which is stable when R-parity is conserved. The resulting signatures of SUSY particle pair production are high particle mulitplicities coming from the cascade decays, and large amounts of missing energy resulting from the LSP escaping the detector.

New colored particles, the squarks and gluino, whose production is enhanced by the strong coupling strength, were expected to be observed as early as the initial run at $\sqrt{s} = 7$ TeV [12, 13]. Current results exclude gluino masses up to $m_{\tilde{g}} \lesssim 1200$ GeV [14–21]. First and second squark masses are excluded up to $m_{\tilde{q}} \lesssim 800$ GeV [14, 17, 19]. It is entirely possible that these colored particles are too massive to reach at the LHC.

The null search results for new colored particles lead us to search in the electroweak sector where the reach is limited by the weak coupling suppression to the production cross section. Particles of interest in the electroweak sector include the sleptons, neutralinos and charginos. The neutralinos and charginos are mass eigenstates occurring from mixing in the Higgsino and gaugino sectors. We go into more detail in Sec. 3.3.2 and Sec. 3.3.3.

Third generation squarks are expected to be much lighter than the other generation squarks [22]. On the other hand, the signals from stops and sbottoms are masked by large Standard Model backgrounds resulting in weaker exclusion limits. Additionally, the stop and Higgs sectors are closely associated with one another due to large Yukawa couplings. If we gain knowledge of the stop, we also gain a better understanding of the Higgs and the nature of electroweak symmetry breaking.

1.2.1 Sleptons

We often find the particles in the electroweak sector among the lightest SUSY particles and thus should be accessible at the LHC. In this dissertation, I investigate slepton production at the LHC in two ways. In Appendix A, I explore sleptons produced in cascade decays from neutralino-chargino production at the LHC. In Appendix B, I explore sleptons directly produced through Drell-Yan pair production. The former mechanism has a higher production cross-section but requires accessible neutralino and chargino states in order to cascade decay down to sleptons. Whereas, the direct production mechanism is viable as long as the sleptons are light, but suffers from a smaller production cross-section.

Sleptons in particular, lead to relatively clean collider signatures, with final states including multiple charged leptons. Multi-lepton signals are able to significantly reduce Standard Model background and avoid uncertainties from jet reconstruction algorithms. In certain cascade decay topologies with intermediate mass sleptons, a distinctive triangle feature appears in the dilepton signal, which can be detected despite strong Standard Model backgrounds, see Appendix A for further discussion. Direct production searches often utilize a kinematic variable known as M_{T2} in order to further cut down the Standard Model background [23, 24]. In Appendix B, we employ M_{T2} cuts to effectively reduce $t\bar{t}$ background to improve detection of sleptons in pair production mechanisms.

Due to the fact that sleptons can be light, they play an important role in processes occuring at low energies. If the lightest supersymmetric particle is the neutralino, χ_1^0, the slepton mediates a t-channel process which contributes to the overall annihilation cross section [25]. Sleptons also can contribute loop corrections to low energy precision observables, such as the electron and proton weak charges tested in ee Møller scattering and ep scattering experiments respectively [26, 27].

1.2.2 Third Generation Squarks

While first and second generation squark limits are approaching masses of 1 TeV, third generation squarks have less stringent experimental bounds. For a massless LSP, stops and sbottoms with masses $m_{\tilde{t}/\tilde{b}} \lesssim 600$ GeV are excluded by ATLAS and CMS [28–30]. The bounds are weaker since signals resulting from stop and sbottom pair production overlap with the enormous $t\bar{t}$ signal produced at the LHC. Efforts in "tagging" top quarks have attempted to identify the stop signal, but these are still difficult backgrounds to reduce effectively [31]. Stops and sbottoms are hidden in this sense.

Third generation squarks are tightly connected to the Higgs sector due to strong Yukawa couplings. Stop loops provide the dominant radiative corrections to the Higgs mass. The measurement of the Higgs mass of 125 GeV puts constraints on the stop sector and favors a heavily mixed and light stop [32]. Coupled with the fact that the gluino mass is excluded up to approximately 1 TeV so that cascade decays are unlikely, we study pair production of the third generation squarks. We present the discovery reach of the stop/sbottom when

utilizing uncommon decay channels in Appendix C.

1.3 Dissertation Format

The rest of the dissertation is organized as follows. In Chapter 2, I introduce the Standard Model. In particular, I focus on the gauge structure and symmetries present and the subsequent symmetry breaking by the Higgs. In Chapter 3, I discuss the Minimal Supersymmetric Standard Model highlighting the electroweak sector and the stop/sbottom sector. In Chapter 4, I discuss the underlying physics of colliding protons, focusing on the experimental and computational tools used to make measurements and predictions at the LHC. In Chapter 5, I present the conclusions of my dissertation work. Attached in the appendices are my publications with my advisor and other collaborators. In Appendix A, we discuss searching for sleptons by utilizing a distinctive signal feature occuring in production by cascade decay [33]. Appendix B describes our efforts to extend the LHC reach for slepton pair production by adding complementary results to scenarios with Wino- and Higgsino-like LSPs [34]. My work in Appendix C identifies alternative search channels for stop and sbottom pair production and we present the discovery potential at the LHC [35].

CHAPTER 2

Standard Model

The mathematical structure of the Standard Model is one of symmetry; each fundamental force is represented using a symmetry group. Particle interactions with the forces are described mathematically by how the particles transform with the corresponding symmetry group. We find that the gauge structure of $SU(3)_c \otimes SU(2)_L \otimes U(1)_Y$ accurately describes the fundamental interactions of particles, neglecting gravity.

This chapter gives a brief review of the Standard Model. First, I discuss the gauge structure and symmetries present in the Standard Model Lagrangian. Next, I explain the Higgs mechanism and the Higgs's role in electroweak symmetry breaking. Last, I discuss areas where the Standard Model is unsatisfactory; these issues include the hierarchy problem and the unknown identity of dark matter.

2.1 Gauge Structure and Symmetries

The Standard Model gauge structure is governed by symmetry groups. The strong force is gauged by $SU(3)_c$ which corresponds to the theory of QCD, which describes the behavior of colored particles [36, 37]. The electroweak forces are governed by $SU(2)_L \otimes U(1)_Y$ corresponding to weak and hypercharge couplings. Particles in the Standard Model and their charges under each symmetry group are shown in Table 2.1. Prior to electroweak symmetry breaking, all particles are massless; a requirement by the symmetries imposed. The particles are expressed based upon a group representation formalism. Fermions exist as states in the fundamental representation of the symmetry group under which they are charged. The states in the theory are the massless chiral states, ψ_L and ψ_R. A consequence of massless fermionic states is that there is a well defined direction of the particle's momentum relative to its spin. We call particles whose spin and momentum vectors are aligned, right-handed chiral states. Particles with anti-parallel spin and momentum vectors are

Field	$SU(3)_c, SU(2)_L, U(1)_Y$
Q	$\left(\mathbf{3}, \mathbf{2}, \frac{1}{6}\right)$
u_R	$\left(\mathbf{3}, \mathbf{1}, \frac{2}{3}\right)$
d_R	$\left(\mathbf{3}, \mathbf{1}, -\frac{1}{3}\right)$
L	$\left(\mathbf{1}, \mathbf{2}, -\frac{1}{2}\right)$
e_R	$(\mathbf{1}, \mathbf{1}, -1)$
G_μ	$(\mathbf{8}, \mathbf{1}, 0)$
W_μ	$(\mathbf{1}, \mathbf{3}, 0)$
B_μ	$(\mathbf{1}, \mathbf{1}, 0)$
Φ	$\left(\mathbf{1}, \mathbf{2}, \frac{1}{2}\right)$

Table 2.1: Particle content and gauge group representation in the Standard Model. Particles listed include the fermions, gauge bosons and the Higgs. Left-handed fermions are grouped in $SU(2)$ doublets.

left-handed chiral states.

We group the left-handed fermions together in $SU(2)$ doublets where,

$$Q = \begin{pmatrix} u_L \\ d_L \end{pmatrix}, L = \begin{pmatrix} \nu \\ e_L \end{pmatrix} \tag{2.1}$$

and the right handed fermions u_R, d_R, and e_R are singlets. There exists three generations for each fermion. The quarks consist of three up-type quarks, up, charm, top; three down-type quarks, down, strange, bottom. The leptons consist of charged and neutrino states in electron, muon, and tau flavors.

The gauge bosons exist as states in the adjoint representation of the corresponding symmetry groups. This leads to the 8 gluons, G^a_μ of QCD, the 3 weak bosons, W^a_μ and the B_μ for the hypercharge force. The superscript, a, indexes each of the unique bosons in non-abelian gauge theories.

The scalar field in the Standard Model, the Higgs field, Φ, is represented as an $SU(2)$ doublet:

$$\Phi = \begin{pmatrix} \phi^+ \\ \phi^0 \end{pmatrix} \tag{2.2}$$

composed of two complex scalars. We discuss the Higgs sector in more detail in Sec. 2.2.

Now that we have defined the particle content, let's begin to write down the Standard Model Lagrangian. The Standard Model Lagrangian can be split into the following terms.

$$\mathcal{L} = \mathcal{L}_{\text{gauge}} + \mathcal{L}_{\text{fermion}} + \mathcal{L}_{\text{Higgs}} + \mathcal{L}_{\text{Yukawa}} \tag{2.3}$$

The first term contains the pure gauge interactions. The fermion term contains the kinetic part and the gauge couplings for the fermions. The Higgs term contains the kinetic and potential terms in the Higgs sector. The last term contains the Yukawa interactions between the Higgs and fermions. After electroweak symmetry breaking, the Higgs and Yukawa terms also contain the gauge boson and fermion mass terms respectively.

The pure gauge terms are expressed using the field strength tensor represented by $F^a_{\mu\nu} = \partial_\mu A^a_\nu - \partial_\nu A^a_\mu - g f^{abc} A^b_\nu A^c_\mu$, where the f^{abc} terms are the structure constants, arising from the commutation relations between generators of the underlying gauge group. We can now express the gauge term of the Lagrangian simply as:

$$\mathcal{L}_{\text{gauge}} = -\frac{1}{4} F^{i\,a}_{\mu\nu} F^{i\,a\mu\nu} \tag{2.4}$$

where we sum over the indices i and a, corresponding to the gauge group and unique fields in each gauge group respectively. This term encapsulates the gauge kinetic terms and the gauge boson-gauge boson interactions for non-abelian gauge theories [38].

The fermion gauge interactions are represented in the lagragian as:

$$\mathcal{L}_{\text{fermion}} = \bar{Q}_i \not{\mathcal{D}} Q_i + \bar{u}_i \not{\mathcal{D}} u_i + \bar{d}_i \not{\mathcal{D}} d_i + \bar{L}_i \not{\mathcal{D}} L_i + \bar{e}_i \not{\mathcal{D}} e_i \tag{2.5}$$

where the covariant derivative, $\mathcal{D}_\mu$, is represented as:

$$\mathcal{D}_\mu = \partial_\mu - i g_s T^a G^a_\mu - i g \frac{\tau^a}{2} W^a_\mu - i g' Y B_\mu \tag{2.6}$$

which provides the kinetic term and the gauge coupling terms for the $SU(3)_c$, $SU(2)_L$, and $U(1)_Y$ gauge groups with strengths g_s, g and g' respectively. The generators of $SU(2)$ are τ^a which correspond to the Pauli matrices. The generators of $SU(3)$ are the Gell-Mann matrices represented as T^a. The "slash" notation is shorthand for a contraction with a γ^μ.

The gauge structure formalism works in the high energy limit where all particles are massless. Fermion mass terms enter the Lagrangian of the form:

$$\mathcal{L} = m\bar{\psi}_L\psi_R \tag{2.7}$$

Although these terms are completely allowed in Lagrangian, the mass terms cannot be added arbitrarily; doing so would break the $SU(2)_L$ symmetry. The left-handed particles must be able to transform independently from the right-handed particles. However, these terms can be dynamically generated by the Higgs mechanism.

2.2 Electroweak Symmetry Breaking and the Higgs Mechanism

The Higgs field is responsible for electroweak symmetry breaking [39–41] and giving particles their mass [42–45]. Recently discovered at the LHC by the ATLAS and CMS collaborations [6, 7], the Higgs boson is one of kind; the only fundamental scalar particle in the Standard Model. The Higgs sector of the Lagragian:

$$\mathcal{L}_{\text{Higgs}} = |\mathcal{D}_\mu\Phi|^2 + \mu^2\Phi^\dagger\Phi - \lambda(\Phi^\dagger\Phi)^2 \tag{2.8}$$

consists of a kinetic term and potential terms with mass $-\mu^2$ and self-coupling with strength, λ. The Higgs sector in its current form obeys all symmetries present in the Standard Model. When the Higgs gets a vacuum expectation value (VEV):

$$\langle\Phi\rangle = \frac{1}{\sqrt{2}}\begin{pmatrix}0\\v\end{pmatrix} \tag{2.9}$$

where $v = \sqrt{\frac{\mu^2}{\lambda}}$, the potential is minimized. This results in a spontaneous break of the $SU(2)_L \otimes U(1)_Y$ symmetry groups to $U(1)_{EM}$. Whenever, a global symmetry is spontaneously broken, Goldstone's theorem [46] states that N massless real scalar particles are created, where N is the difference of the number of generators in the theory before and after symmetry breaking. The spontaneous symmetry breaking of $SU(2)_L \otimes U(1)_Y \rightarrow U(1)_{EM}$ results in the generation of three massless Goldstone bosons. These are easily seen, by

rewriting the Higgs field in terms of real fields; we have [47]:

$$\Phi = \frac{1}{\sqrt{2}} \begin{pmatrix} -i\left(\phi^1 - i\phi^2\right) \\ v + \left(h + i\phi^3\right) \end{pmatrix} \tag{2.10}$$

where the ϕ^i are the Goldstone bosons. The remaining field h is the Higgs boson.

By breaking the electroweak symmetry, the Higgs mixes the W^a_μ and B_μ fields to construct the weak bosons $W^\pm_\mu$ and Z_μ and the photon, A_μ. The neutral fields Z_μ and A_μ are mixtures of the W^3_μ and B_μ. The charged states $W^\pm_\mu$, are mixtures of the W^1_μ and W^2_μ. The Goldstone bosons are "eaten" by the W and Z bosons to become the longitudinal modes which give the bosons their mass. The photon remains massless.

In addition to giving the vector bosons mass, the Higgs is also responsible for giving mass to the fermions. These masses arise from the Yukawa couplings to the Higgs:

$$\mathcal{L}_{\text{Yukawa}} = y_u \bar{Q}_i \epsilon_{ij} \Phi^\dagger_j u_R + y_d \bar{Q}_i \Phi_i d_R + y_e \bar{L}_i \Phi_i e_R \tag{2.11}$$

where the $SU(2)$ doublets are contracted with the Higgs directly or with the antisymmetric matrix ϵ_{ij}. When the Higgs field gets a VEV, mass terms appear in form $\frac{1}{\sqrt{2}}\, y\, v\, \bar{\psi}_L \psi_R$, where the Yukawa coupling, y corresponds to the fermion ψ. The third generation fermions have the largest mass, so their corresponding Yukawa couplings are also large; the coupling to the top quark the strongest.

After electroweak symmetry breaking, we have a Standard Model which obeys the gauge structure of $SU(3)_c \otimes U(1)_{EM}$ corresponding to the strong and electromagnetic forces respectively. Mass terms for the fermions of the form $m\, \bar{\psi}_L \psi_R$ and for the weak bosons of the form $m^2\, W^\mu W_\mu$ are spontaneously generated by the Higgs mechanism.

2.3 Shortcomings

The Standard Model is a very successful theory, but the prescription is still incomplete. As it stands, the Standard Model is not a very "natural" theory. In this section I discuss the problem a light Higgs presents, known as the hierarchy problem. Addtionally, I discuss the problem of dark matter, whose particle identity is unknown.

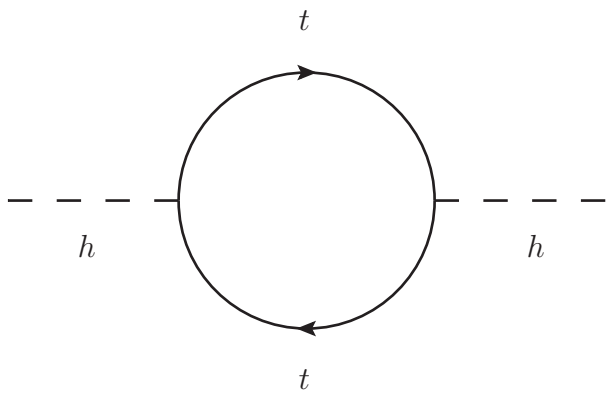

Figure 2.1: Feynman loop diagram of the Yukawa interaction between the top quark and Higgs. The diagram contributes to the Higgs mass of the form shown in Eqn. 2.12, leading to a quadratic divergence.

2.3.1 Hierarchy Problem

The discovery of the Higgs completes the Standard Model as we know it today. However, we are left with an unsatisfactory feature in the model. The Higgs gains radiative corrections to its mass by loop diagrams of the form as shown in Fig. 2.1. The Higgs couples strongly to the top quark, which leads to the dominant contribution of the form [22]:

$$\Delta m_h^2 = -\frac{y_t^2}{8\pi^2}\left(\Lambda^2 - 2m_t^2 \log \Lambda/m_t + ...\right) \tag{2.12}$$

where y_t is the Higgs-top Yukawa coupling and Λ is a cutoff scale at which the theory is no longer valid, creating a quadratic divergence. We know that the Higgs mass is 125 GeV, which means that the loop corrections need to be of order the weak scale ($\sim$ 100 GeV). If we take the cutoff scale $\Lambda^2 \sim m^2_{\text{Planck}}$, then the counter terms need to be precisely tuned to 1 part in 10^{34} in order to recover the physical Higgs mass of 125 GeV. This disparity between the weak and gravitational forces, is in essence, the "Hierarchy Problem" [8]. The level of fine tuning required is highly unnatural and a call for concern. New physics is needed to reconcile the problem.

2.3.2 Cosmological Problems

Analogous to the Standard Model of particle physics, there is a "Standard Model" of cosmology. Under the laws of General Relativity, the model consists of an spatially flat, expanding universe made up of radiation, baryonic matter, a cold dark matter (CDM) component and a dark energy component often referred to as the cosmological constant (Λ). Observations show that the evolution of the universe is dominated by the relatively unknown dark matter and energy components, thus the model is referred to as ΛCDM. Space-based observations of the Cosmic Microwave Background (CMB) [48] combined with ground-based observations of large scale structure using Baryon Acoustic Oscillations (BAO) [49] and a measurement of the expansion rate using Type 1a supernovae (SNe) [50, 51] have verified the model to good accuracy.

The composition of the dark matter component of our universe is relatively unknown. From observations, we have the following constraints on dark matter [52]:

- Massive, due to its inferred gravitational presence
- Stable, or quasi-stable on timescales of order the age of the universe
- "Weakly" coupled to ordinary matter, if at all (excluding gravity)
- Cold, non-relativistic species of matter

These constraints rule out all particles from the Standard Model to comprise the entirety of the dark matter component of the universe. The existence of dark matter implies a need for new physics.

A common type of dark matter falls under the category of weakly interacting massive particle (WIMP). Many extensions of the Standard Model have WIMPs. If WIMPs were produced in the early universe, while in thermal and chemical equilibrium with the hot "soup" of SM particles we can calculate the relic density of WIMPs after freeze out [53]. The relic density is given by [54]:

$$\Omega_\chi h^2 \simeq \frac{0.1\text{pb}}{\langle \sigma_A v \rangle} \simeq 1 \tag{2.13}$$

where σ_A is the annihilation cross section of WIMPs into SM particles, v is the velocity, both quantities thermally averaged. We find a surprising realization that for a weak interaction cross section the distribution of WIMPs would satisfy the dark matter component in the universe. This miraculous coincidence is referred to as the "WIMP Miracle". The theoretical motivations coupled with the presence of WIMPs in many extensions of the Standard Model have led to searches for WIMPs on three fronts: through direct detection [55, 56], indirect detection [57, 58], and collider experiments [59–61]. Supersymmetry can potentially provide a WIMP dark matter candidate in the form of the neutralino. See further discussion in Sec. 3.2.

CHAPTER 3

Minimal Supersymmetric Standard Model

In this section, I introduce Supersymmetry (SUSY) and the Minimal Supersymmetric Standard Model (MSSM). SUSY is a well motivated extension to the Standard Model that provides a solution to the hierarchy problem. Assuming R-parity conservation, SUSY provides interesting collider phenomenology, and most importantly it generates a potential candidate for dark matter. I will focus primarily on the electroweak sector and stop sector, as this will provide useful background for topics discussed in the Appendices. Throughout this chapter, I follow many of the conventions of Martin [22], who provides a complete review on SUSY.

3.1 A New Symmetry

Let us consider a new global symmetry between bosons and fermions, one in which a transformation turns bosons into fermions and vice versa. This transformation can be represented through the use of the operator, Q, which transforms states as follows:

$$Q\left|\text{Boson}\right\rangle = \left|\text{Fermion}\right\rangle, Q\left|\text{Fermion}\right\rangle = \left|\text{Boson}\right\rangle \tag{3.1}$$

When this transformation is applied to SM particles, the result is a set of new particles, which we call *superpartners*. The common nomenclature names the superpartners to the fermions, the *sfermions*, eg. *squarks* and *sleptons*, and the superpartners to the gauge bosons, the *gauginos*, eg. *bino*, *wino*, and *gluino*. The superpartner to the Higgs is the *Higgsino*. The description proposed above, is the simplest extension to the standard model, known as the Minimal Supersymmetric Standard Model (MSSM) [9]. The particle content of the MSSM is shown in Table 3.1. A necessary requirement for a valid Supersymmetric theory is the presence of an additional Higgs doublet [22]. We denote an "up-type" Higgs, H_u and "down-type" Higgs, H_d to generate the up- and down-type masses respectively; we

Fermions	Bosons	$SU(3)_c, SU(2)_L, U(1)_Y$
Q	$\tilde{Q}$	$\left(\mathbf{3}, \mathbf{2}, \frac{1}{6}\right)$
u_R	$\tilde{u}_R$	$\left(\mathbf{3}, \mathbf{1}, \frac{2}{3}\right)$
d_R	$\tilde{d}_R$	$\left(\mathbf{3}, \mathbf{1}, -\frac{1}{3}\right)$
L	$\tilde{L}$	$\left(\mathbf{1}, \mathbf{2}, -\frac{1}{2}\right)$
e_R	$\tilde{e}_R$	$(\mathbf{1}, \mathbf{1}, -1)$
$\tilde{G}_\mu$	G_μ	$(\mathbf{8}, \mathbf{1}, 0)$
$\tilde{W}_\mu$	W_μ	$(\mathbf{1}, \mathbf{3}, 0)$
$\tilde{B}_\mu$	B_μ	$(\mathbf{1}, \mathbf{1}, 0)$
$\tilde{H}_u$	H_u	$\left(\mathbf{1}, \mathbf{2}, \frac{1}{2}\right)$
$\tilde{H}_d$	H_d	$\left(\mathbf{1}, \mathbf{2}, -\frac{1}{2}\right)$

Table 3.1: Particle Content in the MSSM

express the Higgs doublets as:

$$H_u = \begin{pmatrix} H_u^+ \\ H_u^0 \end{pmatrix}, H_d = \begin{pmatrix} H_d^0 \\ H_d^- \end{pmatrix} \tag{3.2}$$

where H_u replaces the use of the charge conjugate $\Phi^\dagger$ in Eqn. 2.11. Additional discussion of the Higgs Sector can be found in Sec. 3.3.1.

3.1.1 Solution to Hierarchy Problem

The primary motivation of Supersymmetry is to provide a solution to the hierarchy problem. We see that the sfermions also couple with the Higgs in a 4-scalar interaction, as shown in Fig. 3.1, leading to additional Higgs mass corrections. Since sfermion couplings are related to the fermion couplings, the resulting mass corrections differ only by a sign difference coming from the scalar loop versus fermion loop. The correction to the mass of the Higgs from a stop is

$$\Delta m_h^2 = \frac{\lambda_s}{16\pi^2}\left(\Lambda^2 - 2m_s^2 \log \Lambda/m_s + ...\right) \tag{3.3}$$

where m_s is the mass of the stop, λ_s is the stop coupling to the Higgs, and Λ is some cutoff scale at which the theory breaks down. But, SUSY requires $\lambda_s = y_t^2$, so when adding the

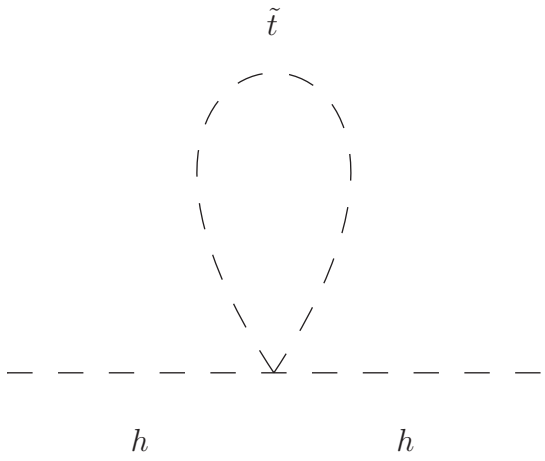

Figure 3.1: Feynman loop diagram of the 4-scalar interaction between the stop and Higgs. The diagram contributes to the Higgs mass of the form shown in Eqn. 3.3. This diagram cancels out the divergent contribution from the top loops shown in Fig. 2.1. and Eqn. 2.12.

Higgs mass divergent contributions from the top, left- and right-handed stops we find a cancellation of the divergent components:

$$\left(\Delta m_h^2\right)^{\text{quad.div.}} = -\frac{y_t^2}{8\pi^2}\Lambda^2 + 2 \times \frac{\lambda_s}{16\pi^2}\Lambda^2 = 0. \tag{3.4}$$

The remaining corrections to the Higgs are terms that only diverge logarithmically. I discuss the corrections from stop loop contributions in Sec. 3.3.5.

3.1.2 SUSY Breaking

For supersymmetry to exist in nature, it must be hidden at low energies. Therefore, SUSY must be broken at some energy scale, M_{SUSY}. If Supersymmetry was not broken, we would observe the existence of light scalar particles with identical quantum numbers and mass to SM particles.

Finding models with spontaneous symmetry breaking is a challenging task. It is very difficult to create a consistent model that is well motivated by physical principles. Currently, there is no consensus model for symmetry breaking. Common models include gravity

mediated (MSUGRA), gauge mediated (GMSB), and anomoly mediated (AMSB) symmetry breaking. See references [62–66] for more detail.

Although each model of spontaneous symmetry breaking leads to different SUSY breaking parameters, we can write down the terms generically. The soft (terms with positive mass dimension) breaking terms in the MSSM are:

$$\begin{aligned}\mathcal{L}_{\text{soft}} = -\frac{1}{2}\Big(M_3\tilde{g}\tilde{g} + M_2\tilde{W}\tilde{W} + M_1\tilde{B}\tilde{B} + \text{c.c.}\Big) \\ - \Big(\tilde{\bar{u}}\ \mathbf{a_u}\tilde{Q}H_u - \tilde{\bar{d}}\ \mathbf{a_d}\tilde{Q}H_d - \tilde{\bar{e}}\ \mathbf{a_e}\tilde{L}H_d + \text{c.c.}\Big) \\ - \tilde{Q}^\dagger\mathbf{m_Q^2}\tilde{Q} - \tilde{u}^\dagger\mathbf{m_u^2}\tilde{u} - \tilde{d}^\dagger\mathbf{m_d^2}\tilde{d} - \tilde{L}^\dagger\mathbf{m_L^2}\tilde{L} - \tilde{e}^\dagger\mathbf{m_e^2}\tilde{e} \\ - m_{H_u}^2 H_u^* H_u - m_{H_d}^2 H_d^* H_d - (bH_uH_d + \text{c.c.}) \quad (3.5)\end{aligned}$$

The first line contains the soft mass terms of the gauginos. The second line contains the (scalar)^3 terms with coupling matrix $\mathbf{a}$, which is a 3 x 3 matrix in flavor space. The third line contains the soft mass terms of the sfermions. Each sfermion mass matrix is also 3 x 3 in flavor space. The last line contains the symmetry breaking terms in the Higgs potential.

3.1.3 Model Framework

The studies explored in this dissertation exist in the framework of the Minimal Supersymmetric Standard Model (MSSM). The MSSM is the minimal extension to the Standard Model that creates a Supersymmetric Lagrangian. We work under the assumption of R-parity conservation, which prohibits couplings that contribute to proton decay, see the discussion in Sec. 3.2. Additionally, the following soft SUSY breaking universality conditions are imposed to avoid large flavor-changing or CP-violating effects.

- Sfermion soft mass matrices are "flavor-blind", that is each generation has the same mass term with no mixing terms, eg. $\mathbf{M_Q^2} = M_Q^2\,\mathbf{1}$. This condition is often relaxed to allow third generation masses to differ.

- The (scalar)^3 couplings are proportional to the corresponding Yukawa matrix in 3 x 3 flavor space, eg. $\mathbf{a_u} = A_u\,\mathbf{y_u}$.

- Soft parameters do not introduce any new complex phases, eg. $\text{Im}\,(\text{M}_1) = 0$.

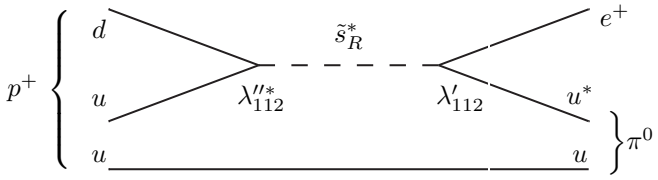

Figure 3.2: Feynman diagram of proton decay via R-parity violating terms of the form shown in Eqn. 3.6.

3.2 R-parity and its Consequences

In general, SUSY allows for terms of the form:

$$\frac{1}{2}\lambda'^{ijk} L_i Q_j \tilde{d}_k, \qquad \frac{1}{2}\lambda''^{ijk} u_i d_j \tilde{d}_k \tag{3.6}$$

which violate lepton and baryon number respectively. Yet in the Standard Model, baryon and lepton number are strictly conserved. Diagrams of the form shown in Fig. 3.2 would lead to proton decay by the process $p^+ \to e^+\pi^0$. However, experiments have placed very strong constraints on the lifetime of the proton [67] requiring that the couplings in Eqn. 3.6, denoted by λ, are extremely small, or forbidden altogether.

Baryon and lepton number conservation arises due to an "accidental" symmetry in the Standard Model so imposing these symmetries by hand in SUSY would be unsatisfactory. Instead, we can resolve the issue by defining a new charge for SM and SUSY particles called R-parity [68]. R-parity can be expressed as:

$$R = (-1)^{3(B-L)+2s} \tag{3.7}$$

where B is baryon number, L is lepton number, and s is the spin of the particle. We see that SM particles have even parity, $R = +1$ and SUSY particles have odd parity, $R = -1$. If we impose R-parity conservation in our theory, then the terms which violate lepton or baryon number are now forbidden.

In addition to eliminating unwanted baryon and lepton number violating terms, R-parity has interesting phenomenological consequences. First, SUSY particles must be pair produced at colliders, and once produced, these particles must decay into other SUSY particles and SM particles. This process continues until it decays into the lightest supersymmetric particle (LSP) which is stable. The LSP must interact weakly, otherwise

experiments would have discovered the stable particle. Therefore, in models of SUSY, the LSP is often considered a dark matter candidate.

Depending on the mechanism of SUSY breaking, there are a number of possible LSPs, eg. the sneutrino, lightest neutralino, or gravitino. If the sneutrino or the lightest neutralino is the LSP, it is a WIMP dark matter candidate. In collider experiments, WIMP LSPs escape the detector, resulting in a missing energy signature. WIMP dark matter is also well motivated by cosmological expectations. Alternatively, the superpartner of the graviton, the gravitino, is also a viable dark matter candidate and would interact only via the gravitational force. Both types of particles are viable through SUSY, but we focus on WIMP-like LSPs, since they lead to more interesting phenomenology. In particular, we consider the lightest neutralino, χ_1^0, as the LSP in our studies, presented in the Appendices.

3.3 Review of SUSY Electroweak and Stop Sectors

In this section, I describe the structure of each of the following sectors of the SUSY electroweak sector: the Higgs (Sec. 3.3.1), neutralino (Sec. 3.3.2), chargino (Sec. 3.3.3), slepton (Sec. 3.3.4), and third generation squark (Sec. 3.3.5). See Martin [22] for more details and references therein.

3.3.1 Higgs Sector

In the MSSM, there exists two Higgs doublets, H_u and H_d. The neutral states, H_u^0 and H_d^0 get separate VEVs,

$$\frac{1}{\sqrt{2}}v_u = \left\langle H_u^0 \right\rangle, \frac{1}{\sqrt{2}}v_d = \left\langle H_d^0 \right\rangle, \tag{3.8}$$

but the electroweak constraints on v remain, such that:

$$v^2 = v_u^2 + v_d^2. \tag{3.9}$$

The ratio is commonly expressed as

$$\tan\beta = v_u/v_d. \tag{3.10}$$

The Higgs doublets participate in the Higgs mechanism, resulting in the usual three Goldstone bosons, $\phi^\pm$ and ϕ^0, which become the longitudinal modes of the $W^\pm$ and Z, and

an additional 5 scalar particles. The particles consist of two CP-even neutral scalars, h^0 and H^0, one CP-odd neutral scalar, A^0, and two charged Higgses $H^{\pm}$.

The fields can be expressed in the terms of the mass eigenstate fields as:

$$\begin{pmatrix} H_u^0 \\ H_d^0 \end{pmatrix} = \frac{1}{\sqrt{2}} \begin{pmatrix} v_u \\ v_d \end{pmatrix} + \frac{1}{\sqrt{2}} R_\alpha \begin{pmatrix} h^0 \\ H^0 \end{pmatrix} + \frac{i}{\sqrt{2}} R_\beta \begin{pmatrix} \phi^0 \\ A^0 \end{pmatrix} \tag{3.11}$$

$$\begin{pmatrix} H_u^+ \\ H_d^{-*} \end{pmatrix} = R_\beta \begin{pmatrix} \phi^+ \\ H^+ \end{pmatrix} \tag{3.12}$$

where the rotation matrices are defined:

$$R_\alpha = \begin{pmatrix} \cos\alpha & \sin\alpha \\ -\sin\alpha & \cos\alpha \end{pmatrix} \tag{3.13}$$

$$R_\beta = \begin{pmatrix} \sin\beta & \cos\beta \\ -\cos\beta & \sin\beta \end{pmatrix} \tag{3.14}$$

Considering the discovery of a Higgs at 125 GeV, commonly we work under the decoupling limit, where $m_A \gg m_Z$, which gives a SM-like Higgs h^0, and pushes the other "Supersymmetric" Higgses to high mass near the SUSY scale.

A consequence of having two VEVs, the third generation quark masses are now defined as:

$$m_t = \frac{1}{\sqrt{2}} y_t \, v \sin\beta, \qquad m_b = \frac{1}{\sqrt{2}} y_b \, v \cos\beta \tag{3.15}$$

where, in the case of large $\tan\beta$, the bottom Yukawa becomes comparable to the top Yukawa. This can lead to enhanced couplings of the Higgs to bottom quarks.

3.3.2 Neutralino Sector

There can also be significant mixing between the Higgsinos and Gauginos. In the gauge-eigenstate basis of $\psi = \left(\tilde{B}, \tilde{W}^0, \tilde{H}_d^0, \tilde{H}_u^0\right)$, the neutralino mass term in the Lagrangian is:

$$\mathcal{L} = -\frac{1}{2} \left(\psi^0\right)^T \mathbf{M}_\chi \psi^0 + \text{cc.} \tag{3.16}$$

where

$$\mathbf{M}_\chi = \begin{pmatrix} M_1 & 0 & -c_\beta\, s_W\, m_Z & s_\beta\, s_W\, m_Z \\ 0 & M_2 & c_\beta\, c_W\, m_Z & -s_\beta\, c_W\, m_Z \\ -c_\beta\, s_W\, m_Z & c_\beta\, c_W\, m_Z & 0 & -\mu \\ s_\beta\, s_W\, m_Z & -s_\beta\, c_W\, m_Z & -\mu & 0 \end{pmatrix} \tag{3.17}$$

where I have introduced the abbreviations, $s_\beta = \sin\beta$, $c_\beta = \cos\beta$, $s_W = \sin\theta_W$, $c_W = \cos\theta_W$ for compactness. If the m_Z terms are small, we end up with the following mass eigenstates:

- χ_1^0, Bino-like, $m_{\chi_1} = M_1$
- χ_2^0, Wino-like, $m_{\chi_2} = M_2$
- χ_3^0, χ_4^0, Higgsino-like, $m_{\chi_{3,4}} = |\mu|$

The common convention is to label the lightest neutralino, χ_1^0. So, in the above case, we have assumed the mass hierarchy of $M_1 < M_2 < \mu$. In many models of SUSY, the lightest neutralino is the LSP. The neutralino is a good WIMP dark matter candidate [69].

3.3.3 Chargino Sector

Similarly for the charged Higgsino and Wino, we use the gauge- eigenstate basis of $\psi^\pm = \left(\tilde{W}^+, \tilde{H}_u^+, \tilde{W}^-, \tilde{H}_d^-\right)$. The chargino mass term in the Lagrangian is:

$$\mathcal{L} = -\frac{1}{2}\left(\psi^\pm\right)^T \mathbf{M}_{\chi^\pm} \psi^\pm + \text{cc.} \tag{3.18}$$

where in 2 x 2 block form,

$$\mathbf{M}_{\chi^\pm} = \begin{pmatrix} \mathbf{0} & \mathbf{X^T} \\ \mathbf{X} & \mathbf{0} \end{pmatrix} \tag{3.19}$$

and where:

$$\mathbf{X} = \begin{pmatrix} M_2 & \sqrt{2} s_\beta m_W \\ \sqrt{2} c_\beta m_W & \mu \end{pmatrix}. \tag{3.20}$$

If the m_W terms are small and if we assume the mass hierarchy $M_2 < \mu$, we have the following mass eigenstates:

- $\chi_1^\pm$, Wino-like, $m_{\chi_1^\pm} = M_2$
- $\chi_2^\pm$, Higgsino-like, $m_{\chi_2^\pm} = |\mu|$

3.3.4 Sleptons

The slepton masses are governed by the $\mathbf{m_L^2}$ and $\mathbf{m_e^2}$ mass matrices. Following the universality conditions, we assume that flavor mixing is negligible. Moreover, the left-right mixing in the slepton sector is proportional to the lepton Yukawa couplings which are small for the first two generations. The resulting mass eigenstates are $\tilde{\ell}_L$ and $\tilde{\ell}_R$, for the lepton flavors $\ell = e, \mu$ with masses $m_{\tilde{\ell}_L}$ and $m_{\tilde{\ell}_R}$ respectively. The masses, in terms of the soft breaking terms m_{SL} and m_{SR}:

$$m^2_{\tilde{\ell}_L} = m^2_{SL} + \Delta_{\tilde{\ell}_L}; m^2_{\tilde{\ell}_R} = m^2_{SR} + \Delta_{\tilde{\ell}_R}, \tag{3.21}$$

where the D-term contributions are $\Delta_{\tilde{\ell}_L} = (-\frac{1}{2} - \sin^2\theta_W) m_Z^2 \cos 2\beta$ and $\Delta_{\tilde{\ell}_R} = -\sin^2\theta_W m_Z^2 \cos 2\beta$. On the other hand, staus have significant Yukawa couplings to the Higgs resulting in mixing between the left and right states. As a result, the stau mass eigenstates are labeled $\tilde{\tau}_1$ and $\tilde{\tau}_2$. The sneutrino states, $\tilde{\nu}_\ell$ also have masses governed by $\mathbf{m_L^2}$ with an additional mass splitting given by:

$$m^2_{\tilde{e}_L} - m^2_{\tilde{\nu}_e} = -\cos 2\beta m_W^2. \tag{3.22}$$

3.3.5 Third Generation Squarks

In gauge basis, the eigenstates are: $(\tilde{t}_L \ \tilde{b}_L), \tilde{t}_R$ and $\tilde{b}_R$. The third generation is tightly coupled to the Higgs due to large Yukawa couplings. These couplings lead to mass terms when the Higgs get a VEV. In practice, these terms are small compared to the soft mass terms and do not influence the masses. However, these terms can play a role in determining the mixing angle and cannot be ignored. The stop mass eigenstates are found by:

$$\mathcal{L} = \begin{pmatrix} \tilde{t}_L^* & \tilde{t}_R^* \end{pmatrix} \mathbf{m_{\tilde{t}}^2} \begin{pmatrix} \tilde{t}_L \\ \tilde{t}_R \end{pmatrix}, \tag{3.23}$$

where the stop mass matrix is:

$$\mathbf{m}_{\tilde{\mathbf{t}}}^{\mathbf{2}} = \begin{pmatrix} M_{3SQ}^2 + m_t^2 + \Delta_{\tilde{u}_L} & m_t \tilde{A}_t \\ m_t \tilde{A}_t & M_{3SU}^2 + m_t^2 + \Delta_{\tilde{u}_R} \end{pmatrix}. \tag{3.24}$$

Along the diagonal, we have M_{3SQ}^2 and M_{3SU}^2, which come from the soft SUSY breaking mass terms. The m_t^2 term comes from the F-terms in the SUSY Lagrangian of the form $y_t^2\, \tilde{t}_L \tilde{t}_L H_u^0 H_u^0$ where both Higgses get VEVs. Finally we have the Δ terms which come from the D-term coupling, given by:

$$\Delta_{\tilde{u}_L} = \left(\frac{1}{2} - \frac{2}{3} \sin^2 \theta_W \right) \cos 2\beta \; m_Z^2 \tag{3.25}$$

$$\Delta_{\tilde{u}_R} = \frac{2}{3} \sin^2 \theta_W \cos 2\beta \; m_Z^2. \tag{3.26}$$

On the offdiagonal, we have combined the soft SUSY breaking $(\text{scalar})^3$ terms and the F-term left/right couplings of the form $\mu\, y_t\, \tilde{t}_L \tilde{t}_R H_d^0$, to define a term $\tilde{A}_t$ given by:

$$\tilde{A}_t = A_t - \mu \cot \beta. \tag{3.27}$$

We can diagonalize the mass matrix (Eqn. 3.24) and define a stop mixing angle θ_t as follows,

$$\begin{pmatrix} \tilde{t}_1 \\ \tilde{t}_2 \end{pmatrix} = \begin{pmatrix} \cos\theta_t & -\sin\theta_t \\ \sin\theta_t & \cos\theta_t \end{pmatrix} \begin{pmatrix} \tilde{t}_L \\ \tilde{t}_R \end{pmatrix} \tag{3.28}$$

where θ_t can be expressed as:

$$\tan 2\theta_t = \frac{2 m_t \tilde{A}_t}{M_{3SQ}^2 - M_{3SU}^2 + \Delta_{\tilde{u}_L} - \Delta_{\tilde{u}_R}} \tag{3.29}$$

In addition to playing a role in determining the mixing angle, the $\tilde{A}_t$ term can generate large mass splittings between the two stops. In cases where the off-diagonal terms are large, the light stop can be the lightest squark. Since the off-diagonal terms originate from Higgs couplings, the $\tilde{A}_t$ plays an important role in the Higgs mass correction. The Higgs mass gains significant corrections from the quartic interaction with the stop. The one-loop correction [70]:

$$\Delta m_h^2 = \frac{3}{4\pi^2} y_t^2 m_t^2 \sin^2 \beta \left(\log \frac{M_S^2}{m_t^2} + \frac{\tilde{A}_t^2}{M_S^2} \left(1 - \frac{\tilde{A}_t^2}{12 M_S^2} \right) \right) \tag{3.30}$$

is a maximum for the maximal mixing case where $\tilde{A}_t = \sqrt{6}M_S$. Minimum corrections occur when $\tilde{A}_t = 0$, which we refer to as the minimal mixing case.

A general form for the stop masses is shown here.

$$m_{\tilde{t}}^2 = \frac{1}{2}\left(M_{3SQ}^2 + M_{3SU}^2 + 2m_t^2 + \Delta_{\tilde{u}_L} + \Delta_{\tilde{u}_R}\right) \pm \frac{1}{2}\sqrt{\left(M_{3SQ}^2 - M_{3SU}^2 + \Delta_{\tilde{u}_L} - \Delta_{\tilde{u}_R}\right)^2 + 4m_t^2\tilde{A}_t^2} \quad (3.31)$$

$$\Delta m_{\tilde{t}}^2 = \sqrt{\left(M_{3SQ}^2 - M_{3SU}^2 + \Delta_{\tilde{u}_L} - \Delta_{\tilde{u}_R}\right)^2 + 4m_t^2\tilde{A}_t^2} \quad (3.32)$$

In the maximal mixing case where $M_{3SQ} = M_{3SU} = M_S$ and $\tilde{A}_t = \sqrt{6}M_S$ and m_Z small, the mass separation is given by:

$$\Delta m_{\tilde{t}}^2 = 2\sqrt{6}m_t M_S \quad (3.33)$$

In a very similar analysis for the sbottom, the mass matrix is given as:

$$\mathbf{m}_{\tilde{\mathbf{b}}}^{\mathbf{2}} = \begin{pmatrix} M_{3SQ}^2 + m_b^2 + \Delta_{\tilde{d}_L} & m_b\tilde{A}_b \\ m_b\tilde{A}_b & M_{3SD}^2 + m_b^2 + \Delta_{\tilde{d}_R} \end{pmatrix} \quad (3.34)$$

where,

$$\tilde{A}_b = A_b - \mu\tan\beta \quad (3.35)$$

The off-diagonal terms are now suppressed by the bottom mass. As a result, considerable mixing among the sbottom mass states is uncommon.

CHAPTER 4

Collider Physics

What happens in the process of colliding two proton beams at the LHC? In this chapter we will go through the physics of colliding protons. First we discuss the requisite physics of the proton, by introducing the parton model. Then we discuss the consequences of QCD, the phenomena of asympotic freedom and color confinement. The next section will be concerned with detecting these processes at the LHC. We end this chapter with numerical methods used by phenomenologists to make predictions at the LHC.

4.1 QCD Primer

As discussed in Chapter 2, Quantum Chromodynamics (QCD) is the theory of the strong interactions between quarks and gluons. QCD follows the gauge structure of $SU(3)_c$, where quarks exist in the fundamental representation and gluons exist in the adjoint representation. The gauge theory is non-Abelian, allowing for self-interactions amongst the gluons. These interactions lead to the phenomena of asympotic freedom at high energy and confinement at low energy. This section will discuss the consequences of an asympotically free theory and its impact on physics at the LHC.

4.1.1 Parton Model

The internal structure of the proton can be well described by the parton model. The parton model takes a parametric approach to describing the proton with multiple structure functions which quantify the probability of finding a given flavor of parton inside the proton. These structure functions are referred to as parton distribution functions (PDFs). Deep inelastic scattering experiments have shown that these partons fall into three categories:

- *Valence quarks*: These partons can be thought of as the bound quark states which form the hadron.

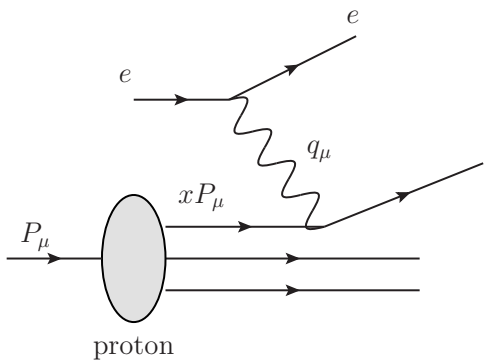

Figure 4.1: Deep inelastic scattering process involving an electron and proton. The electron penetrates the proton and interacts with a single parton with momentum fraction x.

- *Gluons*: The strong force is responsible for keeping quarks bound inside the hadron. Gluons are accessible through scattering off of other colored particles.
- *Sea quarks*: Virtual quark-antiquark pairs created inside the hadron by the aforementioned gluons. In principle, these gluons can produce quarks of any flavor, but the heavier mass quark fractions will be suppressed.

To discern the structure inside the proton, we utilize deep inelastic scattering processes. A schematic of the scattering process is shown in Fig. 4.1. We have a proton with momentum P_μ, scattering via a t-channel process with an electron. The momentum transfer, t can be expressed as $t = -Q^2 = q^\mu q_\mu$. The electron interacts with one of the partons inside the proton, which carries a fraction x, of the proton's momentum. To determine which parton participates in the interaction we use the proton PDFs. The PDFs denoted $f_f(x)$, provide the probability of finding a parton of flavor f, with momentum fraction x. The PDFs must follow certain constraints. The proton is a bound state of 2 u valence quarks and 1 d valence quark. By using the usual definition of quark number, $\mathcal{N}_q = n_q - n_{\bar{q}}$, we can assert the following:

$$\int_0^1 dx\,[f_u(x) - f_{\bar{u}}(x)] = 2 \qquad\qquad \int_0^1 dx\,[f_d(x) - f_{\bar{d}}(x)] = 1 \tag{4.1}$$

to require the expected number of up and down quarks as shown. Calculations of PDFs are non-perturbative and are determined by data-driven methods. Proton PDFs at energies

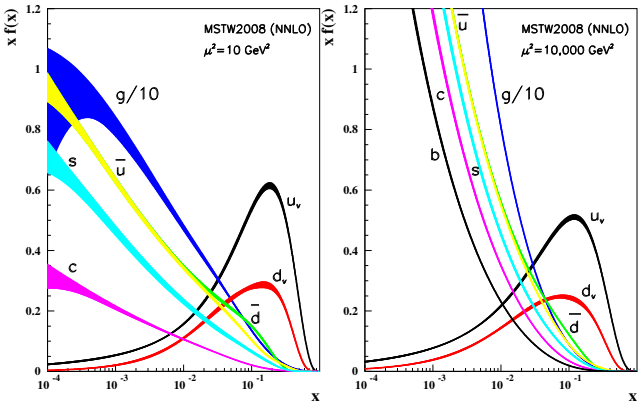

Figure 4.2: Parton distribution functions (PDFs) for the proton compiled by the MSTW collaboration and taken from Beringer et al. [54] published with permission from the Particle Data Group.

$\mu^2 = 10\,(10000)\,\mathrm{GeV}^2$ are shown in the left (right) panels of Fig. 4.2. At high momentum fraction, we find as expected the PDF is dominated by the valence quarks, with a 2:1 ratio of u to d quarks. We also find a large contribution of gluons (scaled by a factor of 10). Since the sea quarks are virtual quark-antiquark pairs from gluon splitting, the sea quarks contribute to the low momentum fraction region, with lighter sea quarks more prevalent. In comparing the left and right panels, at higher interaction energies, μ, we see that the gluons and sea quark curves shift to higher momentum fraction. Subsequently, the valence quark PDFs decrease. This behavior can be explained by additional radiation energy coming from the valence quarks which contributes to the gluon PDF. Having more energetic gluons leads to higher energy sea quarks, thus shifting the curves to higher momentum. At high energies, heavy quarks such as charm and bottom can have non-trivial contributions to the proton PDF.

Utilizing the proton PDFs, we can express the inclusive cross section for deep inelastic scattering in terms of the elastic scattering process of partons as follows:

$$\sigma(e^- p \to e^- + X) = \int_0^1 dx \sum_f f_f(x)\, \sigma(e^- q_f \to e^- q_f) \tag{4.2}$$

where X denotes any hadronic final state. We sum over all flavors of quarks and anti-quarks. The sum is weighted by the PDFs and we integrate over all momentum fractions

x. Generalizing to proton-proton collisions, the inclusive production cross section of final state Y can be expressed as:

$$\sigma(pp \to Y + X) = \int_0^1 dx_1 \int_0^1 dx_2 \sum_{f,f'} f_f(x_1) f_{f'}(x_2)\, \sigma(q_f + q_{f'} \to Y) \tag{4.3}$$

where the sum now includes all flavors of quarks, anti-quarks, and gluons. The possible initial states from proton-proton collisions include: gg, gq, qq', $q\bar{q}$, and $\bar{q}\bar{q}'$. The sums are weighted appropriately by both PDFs.

4.1.2 The Running of α_s

Analogous to the running of the coupling strength, α_{EM} in Electromagnetism, the coupling strength of the strong force also changes with energy. The renormalization group equations describe the evolution of the coupling constant g_s, or similarly $\alpha_s = \frac{g_s^2}{4\pi}$ as [71, 72]:

$$\beta(g_s) = \frac{\partial g_s}{\partial \log \mu}. \tag{4.4}$$

Applying the formula to QCD with three colors and n_f flavors of "massless" quarks ($m_q \ll Q$), we find an equation for β:

$$\beta(g_s) = -\left(11 - \frac{2n_f}{3}\right) \frac{g_s^3}{(4\pi)^2}. \tag{4.5}$$

Most interestingly, the sign of the β function is negative, leading to a weaker coupling strength at higher energy scales, μ. Solving the β function gives an expression for α_s

$$\alpha_s(Q) = \frac{2\pi}{(11 - \frac{2n_f}{3}) \log(Q/\Lambda_{\mathrm{QCD}})} \tag{4.6}$$

where we have introduced a scale, Λ_{QCD}, the scale at which α_s becomes large, requiring use of non-perturbative calculation methods. More formally using Eqn. 4.6, Λ_{QCD} is defined as

$$1 = \frac{g_s^2}{8\pi^2}\left(11 - \frac{2n_f}{3}\right) \log(Q/\Lambda_{\mathrm{QCD}}). \tag{4.7}$$

For three "massless" quarks, measurements find $\Lambda_{\mathrm{QCD}} \approx 200$ MeV [47]. At energies less than Λ_{QCD}, QCD calculations become non-perturbative.

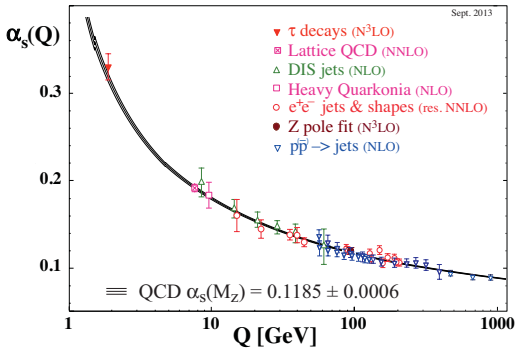

Figure 4.3: Running of α_s, taken from Beringer et al. [54] published with permission from the Particle Data Group.

Experiments have confirmed the running of α_s, the results of which have been compiled in Fig. 4.3. The evolution of α_s is best explained through comparison to the process of Electromagnetic screening. Electromagnetism exhibits charge screening, where the observed charge of a particle decreases with increasing distance. In the vacuum, virtual particle-antiparticle pairs act as electric dipoles and align themselves with the electric field produced by the charge. This phenomenon of vacuum polarization screens the electric charge. As you probe closer to the particle, there is less vacuum between the observer and particle, resulting in a lessened screening effect. A similar process exists for quarks and color charge. However, in QCD the gluon carries color charge. These gluon-gluon interactions contribute to an anti-screening effect. The gluon-gluon interactions dominate over quark-antiquark screening, resulting in an overall anti-screening effect. The color charge of a quark increases with increasing distance. So when probing a quark at high energies (close distances), the quark is effectively free inside a hadron. This phenomenon was discovered by Gross and Wilczek [73] and was coined the term *asympotic freedom*. Asympotic freedom is the foundation for using proton-proton collisions in particle discovery experiments. Scattering processes can be calculated perturbatively, allowing for the utilization of Feynman diagrams to calculate the process effectively.

4.1.3 Hadronization

At low energies, QCD is non-perturbative, meaning we cannot use Feynman diagrams to describe processes. However, we know that quarks bind together to form hadrons and infer their presence from the internal degrees of freedom of hadrons. These quarks can never be observed directly, due to a process known as *color confinement*. Confinement prevents a single quark from being isolated. Quarks must bind together to form mesons or baryons.

Confinement can be best explained by an analogy with Electromagnetism. Let's consider a scenario where we have an electron and positron moving away from each other. We can draw the electric field lines between the two particles which follow a potential $V(r) \sim \frac{1}{r}$. The force between the two particles decreases with increasing distance. Above some escape velocity, the particles will not fall back into each other. Now instead, consider a quark and antiquark. Just as we have electric field lines between the two quarks, we can also consider the strong field lines. The field lines associated with the strong interaction which follow a potential $V(r) \sim r$, can be well approximated by a narrow tube between the two quarks, called color tubes. The force between two colored particles is constant with distance. Classically, we would expect these particles to always fall back into each other. However, quantum mechanics provides another solution. As two quarks move away from each other, the energy in the gluon field gets larger. When there is sufficient energy in the vacuum between the two quarks, it becomes energetically favorable to create quark-anti-quark pairs from the vacuum as opposed to increasing the length of the color tube. These pairs are created with energies near the mass threshold, so these new quarks combine to form hadronic bound states. This process continues until all quarks hadronize. Thus this process is known as hadronization.

4.2 LHC

The Large Hadron Collider (LHC) at CERN in Geneva, Switzerland is the most powerful accelerator in the world. The LHC accelerates two proton beams which collide at designated points along the circular track. These points are the locations of the various LHC detectors. Of particular interest are the general purpose detectors, ATLAS and CMS. As of this work,

the LHC has collected 5 fb^{-1} of integrated luminosity at center-of-mass energy of 7 TeV, and 20 fb^{-1} at 8 TeV. In early 2015, the LHC will begin colliding protons at a center-of-mass energy of 13 TeV. Later upgrades will increase the center-of-mass energy to 14 TeV. During this time, the LHC is expected to collect upwards of 300 fb^{-1} of data. Future high luminosity upgrades are planned to upgrade to the High Luminosity LHC (HL-LHC) [74].

4.2.1 Detectors

The structure of the ATLAS and CMS experiments are very similar [75, 76]. For the discussion in this work, we can simply consider a generic all purpose LHC experiment. The basic structure of the detector can be broken up into four parts: tracker, electromagnetic calorimeter, hadronic calorimeter, and muon spectrometer. Additionally, there exists a strong magnetic field inside the detector to deflect charged particles. The detector readings are combined to attempt to reconstruct events by identifying the following objects: electrons, photons, muons, and jets. Since we know that the momentum in the transverse direction to the beam is initially zero, we can also calculate a missing transverse momentum vector, $\mathbf{p}_T^{\text{miss}}$.

Tracker

At the innermost part of the detector, near the interaction point, lives the tracker. The tracker, composed of primarily of silicon[1], is responsible for tracing out "tracks" of charged particles. These tracks provide useful information in identification of particles.

The tracker is particularly important in the identification of jets originating from bottom quarks, called b-jets. Hadrons containing bottom quarks are relatively long lived. As a result, displaced interaction vertices appear in the tracker between the creation of the b quark and the subsequent B hadron decay. Many processes at the LHC contain b-jets in their final state making proper identification of these jets very important.

[1]The outer ATLAS tracking component, the Transition Radiation Tracker (TRT), is composed of drift tubes filled with Xenon gas.

Calorimeters

The next detector layers are the electromagnetic calorimeter (ECAL) and hadronic calorimeter (HCAL). The goal of the calorimeter layers, is to contain the energy showers produced in pp collisions, typically by using materials with heavy nuclei, such as lead. However, not all heavy nuclei allow for an accurate reading of the energy deposited, so the energy is often sampled using a different material to provide a signal proportional to the energy of the incident particle (for example, ATLAS uses liquid Argon to make ECAL measurements)[2]. The total energy deposited by the showers can then be reconstructed from this signal.

The ECAL is the inner calorimeter designed to contain all electron and photon energy showers. The thickness for the ATLAS ECAL is approximately 22 radiation lengths, which is sufficient for containing the electron and photon energies. The HCAL is the outer calorimeter, responsible for measuring jet energies, as typically jets are not stopped by the electromagnetic calorimeter. The extended size of the HCAL is necessary to contain the hadronic energy showers, which extend out to approximately 9.7 interaction lengths for ATLAS.

Muon Spectrometer

The last detector component is the muon spectrometer. Muons are approximately 200 times more massive than the electron. As a result, it is very difficult to contain muons so that they deposit all of their energy in the detector. Therefore, unlike electrons and photons, muon energies cannot be measured by simply referring to the calorimeters. Muons are reconstructed using combined information from the tracker, calorimeters, and muon spectrometer. The tracks are curved due to the magnetic field inside the experiment. From this information, we can extract the momentum and charge of the muon.

[2]An exception is the CMS ECAL, which uses lead tungstate crystals for both stopping power and detection.

4.2.2 Experimental Complications

Particle Identification

It is a difficult task to reconstruct particles from detector readouts. Common issues include particle fakes and the reconstruction of jets.

Fakes are broadly characterized as signal from the detector components that fakes a signal from a particular object. A common issue which appears in this work, are muon fakes. A jet can fake a muon by having a high momentum muon arise from the decay of a hadron inside of the jet. A common method for reducing fakes, is by instituting constraints on the separation of objects in the detector.

Jets must be reconstructed from calorimeter readouts through various clustering algorithms. In events with high jet multiplicity, jet identification becomes ambigious. If two jets are produced near enough to each other, jet reconstruction algorithms can mistake the two jets as one. These issues become more pronounced at high energies, where jets are more collimated by relativistic beaming effects. Poor jet reconstruction algorithms can also lead to fake missing energy, resulting in an inaccurate calculation of $\mathbf{p}_T^{\text{miss}}$.

Issues at 14 TeV

Efforts are currently underway to upgrade the LHC to center-of-mass energies of 14 TeV. In addition to the collision energy upgrade, the LHC will increase the rate of pp collisions, referred to as instantaneous luminosity. While increased luminosity provides more data over time, we encounter more experimental complications.

The proton beam is composed of bunches of protons. There are two parameters of the proton beam that can be changed to increase luminosity; we can increase the size of the proton bunches, and/or increase the frequency of proton bunches in the beam. But, to maintain beam stability, the frequency of bunches is limited. So ultimately, the bunch size must be increased. However, increasing the bunch size leads to the problem of increased pile-up. Pile-up is the average number of collisions per bunch crossing. Luckily, most proton collisions produce generic QCD background, so experimentalists can identify interesting processes amongst the background. As the number of collisions increases, it

becomes increasingly difficult to disentangle the interesting collisions from the generic ones. Additional issues arise when calculating the total transverse energy of the event, which is necessary to calculate $\mathbf{p}_T^{\text{miss}}$. Pile-up effects need to be corrected for in the momentum sum.

4.3 Monte Carlo

Simulation is essential for both experimentalists and phenomenologists to understand how physical processes present themselves in data. The calculations fall into two categories: numerical calculations and stochastic process generation. Numerical integration is essential for matrix element calculation, the solutions of which feed into decay width and cross section calculations. Monte Carlo simulation is needed to effectively simulate the stochastic processes of event generation, hadronization, and detector simulation.

Given some process at the LHC, we can write down the relevant Feynman diagrams and calculate the matrix elements. These matrix elements are convolved with the proton PDFs to provide a realistic production cross section at the LHC. These calculations involve multi-dimensional integrals which are best suited for Monte Carlo integration. In this dissertation, we make use of CalcHEP [77] for cross section calculations.

Monte Carlo simulation is needed for three aspects of physics at the LHC. Foremost, simulation is needed for the event generation of a given process. We use the software package, Madgraph for event generation in this work [78]. This stage is referred to as parton level or truth level. It can be helpful knowing the truth level for comparison to detector reconstructions to back out the truth. The next step is to incorporate particle showers and hadronization. In our Monte Carlo studies, we utilize the program Pythia [79] to add realistic fragmentation, radiation, and hadronization to our parton level (truth level) data. Lastly, if we want our events to be realistic, we use a detector simulation. In this work we have used the software programs, PGS and Delphes [80] [81]. The goal of the detector simulation is to turn the Pythia level events into detector objects: electron, photon, muon, jets, and missing energy. Once the objects are identified in each event, the events can be combined to form histograms of kinematic variables for further analysis.

CHAPTER 5

Conclusion

In this dissertation, I have presented studies on the prospects of finding supersymmetry at the LHC. Despite the null search results for superpartners, there are still good prospects for discovery in the electroweak and stop sectors.

In Appendix A, I discussed use of a distinctive signal in certain SUSY decay topologies involving onshell sleptons. This triangle signal is present in the dilepton invariant mass, $m_{\ell\ell}$ and when utilized, can extend the mass reach for left-handed sleptons up to 600 GeV for 5σ discovery at the 14 TeV LHC with 100 fb^{-1} of integrated luminosity.

We also considered pair production of sleptons in Appendix B. We extended the experimental analysis reported for 8 TeV to other scenarios with LSPs of different composition than Bino. We found that for a Higgsino-like LSP, the slepton decay fraction to charged leptons is strongly dependent on the Bino-Wino mass ratio, M_1/M_2. The 95% C.L. limit on the left-handed slepton mass can be extended by up to a factor of 2 depending on the LSP composition. We also calculate the expected 95% C.L. limits and 5σ discovery reach for sleptons at the 14 TeV LHC with 100 and 300 fb^{-1} of integrated luminosity. In the best case scenario, sleptons can be discovered with masses up to 850 GeV at 5σ.

In Appendix C, I discuss other significant decay channels of the stop beyond the usual decay to top (or bW) and LSP. In particular, we highlight the decay through intermediate neutralinos, with decay channels $\tilde{t}_1 \to \chi_2^0\, t \to \chi_1^0 h\, t$ and $\tilde{t}_1 \to \chi_1^\pm\, b \to \chi_1^0 W^\pm\, b$ leading to a combined signal of 4 b-jets, 2 jets, 1 lepton and $\not{E}_T$. We find that stops with masses up to 940 GeV can be found with 5σ significance at the 14 TeV LHC with 300 fb^{-1} of integrated luminosity.

We are entering an exciting era in particle physics led by the discovery of the Higgs. As the LHC probes even higher energies, we hope to discover new physics at the TeV scale. Perhaps we will unlock the secrets of supersymmetry.

REFERENCES

[1] The LEP Collaborations: (ALEPH Collaboration, DELPHI Collaboration, L3 Collaboration, OPAL Collaboration, LEP Electroweak Working Group) (2005), hep-ex/0511027.

[2] S. Schael et al. (ALEPH Collaboration, DELPHI Collaboration, L3 Collaboration, OPAL Collaboration, SLD Collaboration, LEP Electroweak Working Group, SLD Electroweak Group, SLD Heavy Flavour Group), Phys.Rept. **427**, 257 (2006), hep-ex/0509008.

[3] D. Hanneke, S. Fogwell Hoogerheide, and G. Gabrielse, Phys.Rev. **A83** (2011), 1009.4831.

[4] M. Gell-Mann, Phys.Lett. **8**, 214 (1964).

[5] S. L. Glashow, J. Iliopoulos, and L. Maiani, Phys. Rev. D **2**, 1285 (1970), URL http://link.aps.org/doi/10.1103/PhysRevD.2.1285.

[6] G. Aad et al. (ATLAS Collaboration), Phys.Lett. **B716**, 1 (2012), 1207.7214.

[7] S. Chatrchyan et al. (CMS Collaboration), Phys.Lett. **B716**, 30 (2012), 1207.7235.

[8] S. Weinberg, Phys.Rev. **D13**, 974 (1976).

[9] S. Dimopoulos and H. Georgi, Phys.Lett. **B117**, 287 (1982).

[10] *Summary plots from the ATLAS standard model physics group*, URL https://atlas.web.cern.ch/Atlas/GROUPS/PHYSICS/CombinedSummaryPlots/SM/.

[11] *Summaries of CMS cross section measurements*, URL https://twiki.cern.ch/twiki/bin/view/CMSPublic/PhysicsResultsCombined.

[12] ATLAS Collaboration, *ATLAS: Detector and physics performance technical design report. Volume 2* (1999).

[13] G. Bayatian et al. (CMS Collaboration), J.Phys. **G34**, 995 (2007).

[14] G. Aad et al. (ATLAS Collaboration) (2014), 1405.7875.

[15] G. Aad et al. (ATLAS Collaboration), JHEP **1406**, 035 (2014), 1404.2500.

[16] G. Aad et al. (ATLAS Collaboration), JHEP **1310**, 130 (2013), 1308.1841.

[17] S. Chatrchyan et al. (CMS Collaboration), JHEP **1406**, 055 (2014), 1402.4770.

[18] S. Chatrchyan et al. (CMS Collaboration), Phys.Lett. **B733**, 328 (2014), 1311.4937.

[19] S. Chatrchyan et al. (CMS Collaboration), Eur.Phys.J. **C73**, 2568 (2013), 1303.2985.

[20] S. Chatrchyan et al. (CMS Collaboration), JHEP **1303**, 037 (2013), 1212.6194.

[21] S. Chatrchyan et al. (CMS Collaboration), Phys.Lett. **B725**, 243 (2013), 1305.2390.

[22] S. P. Martin, Adv.Ser.Direct.High Energy Phys. **21**, 1 (2010), hep-ph/9709356.

[23] C. Lester and D. Summers, Phys.Lett. **B463**, 99 (1999), hep-ph/9906349.

[24] A. Barr, C. Lester, and P. Stephens, J.Phys. **G29**, 2343 (2003), hep-ph/0304226.

[25] M. Drees and M. M. Nojiri, Phys.Rev. **D47**, 376 (1993), hep-ph/9207234.

[26] J. Mammei (MOLLER Collaboration), Nuovo Cim. **C035N04**, 203 (2012), 1208.1260.

[27] D. Androic et al. (Qweak Collaboration), Phys.Rev.Lett. **111**, 141803 (2013), 1307.5275.

[28] G. Aad et al. (ATLAS Collaboration), Phys.Rev.Lett. **109**, 211802 (2012), 1208.1447.

[29] G. Aad et al. (ATLAS), JHEP **1310**, 189 (2013), 1308.2631.

[30] S. Chatrchyan et al. (CMS Collaboration), Eur.Phys.J. **C73**, 2677 (2013), 1308.1586.

[31] Z. Han, A. Katz, D. Krohn, and M. Reece, JHEP **1208**, 083 (2012), 1205.5808.

[32] V. Barger, P. Huang, M. Ishida, and W.-Y. Keung, Phys.Lett. **B718**, 1024 (2013), 1206.1777.

[33] J. Eckel, W. Shepherd, and S. Su, JHEP **1205**, 081 (2012), 1111.2615.

[34] J. Eckel, M. J. Ramsey-Musolf, W. Shepherd, and S. Su, JHEP **1411**, 117 (2014), 1408.2841.

[35] J. Eckel, S. Su, and H. Zhang (2014), 1411.1061.

[36] D. Gross and F. Wilczek, Phys.Rev. **D8**, 3633 (1973).

[37] H. D. Politzer, Phys.Rev.Lett. **30**, 1346 (1973).

[38] C. N. Yang and R. L. Mills, Phys. Rev. **96**, 191 (1954), URL http://link.aps.org/doi/10.1103/PhysRev.96.191.

[39] S. Glashow, Nucl.Phys. **22**, 579 (1961).

[40] S. Weinberg, Phys.Rev.Lett. **19**, 1264 (1967).

[41] A. Salam, Conf.Proc. **C680519**, 367 (1968).

[42] P. W. Higgs, Phys.Lett. **12**, 132 (1964).

[43] P. W. Higgs, Phys.Rev.Lett. **13**, 508 (1964).

[44] F. Englert and R. Brout, Phys.Rev.Lett. **13**, 321 (1964).

[45] T. Kibble, Phys.Rev. **155**, 1554 (1967).

[46] J. Goldstone, Nuovo Cim. **19**, 154 (1961).

[47] M. E. Peskin and D. V. Schroeder, *An Introduction to Quantum Field Theory* (Westview Press, 1995).

[48] E. Komatsu, K. M. Smith, J. Dunkley, C. L. Bennett, B. Gold, G. Hinshaw, N. Jarosik, D. Larson, M. R. Nolta, L. Page, et al., Astrophys.J.Supp. **192**, 18 (2011), `1001.4538`.

[49] D. J. Eisenstein et al. (SDSS Collaboration), Astrophys.J. **633**, 560 (2005), `astro-ph/0501171`.

[50] A. G. Riess et al. (Supernova Search Team), Astron.J. **116**, 1009 (1998), `astro-ph/9805201`.

[51] S. Perlmutter et al. (Supernova Cosmology Project), Astrophys.J. **517**, 565 (1999), `astro-ph/9812133`.

[52] G. Bertone, D. Hooper, and J. Silk, Phys.Rept. **405**, 279 (2005), `hep-ph/0404175`.

[53] T. Padmanabhan, *Theoretical Astrophysics, Volume III: Galaxies and Cosmology* (Cambridge University Press, 2002).

[54] J. Beringer et al. (Particle Data Group), Phys.Rev. **D86**, 010001 (2012).

[55] R. Agnese et al. (SuperCDMS Collaboration), Phys.Rev.Lett. **112**, 241302 (2014), `1402.7137`.

[56] D. S. Akerib, X. Bai, S. Bedikian, E. Bernard, A. Bernstein, A. Bolozdynya, A. Bradley, D. Byram, S. B. Cahn, C. Camp, et al. (Large Underground Xenon (LUX) experiment), Nuclear Instruments and Methods in Physics Research A **704**, 111 (2013), `1211.3788`.

[57] M. Aartsen et al. (IceCube Collaboration) (2013), `1309.7007`.

[58] M. Ackermann, M. Ajello, A. Albert, A. Allafort, L. Baldini, G. Barbiellini, D. Bastieri, K. Bechtol, R. Bellazzini, E. Bissaldi, et al. (Fermi/LAT Collaboration), Phys.Rev. **D88** (2013).

[59] G. Aad et al. (ATLAS Collaboration), Phys.Rev.Lett. **110**, 011802 (2013), 1209.4625.

[60] G. Aad et al. (ATLAS Collaboration), ATLAS-CONF-2012-147 (2012).

[61] S. Chatrchyan et al. (CMS Collaboration), CMS-PAS-EXO-12-047 (2014).

[62] G. Giudice and R. Rattazzi, Phys.Rept. **322**, 419 (1999), hep-ph/9801271.

[63] L. Randall and R. Sundrum, Nucl.Phys. **B557**, 79 (1999), hep-th/9810155.

[64] G. F. Giudice, M. A. Luty, H. Murayama, and R. Rattazzi, JHEP **9812**, 027 (1998), hep-ph/9810442.

[65] T. Gherghetta, G. F. Giudice, and J. D. Wells, Nucl.Phys. **B559**, 27 (1999), hep-ph/9904378.

[66] A. Lahanas and D. V. Nanopoulos, Phys.Rept. **145**, 1 (1987).

[67] H. Nishino et al. (Super-Kamiokande Collaboration), Phys.Rev.Lett. **102**, 141801 (2009), 0903.0676.

[68] G. R. Farrar and P. Fayet, Phys.Lett. **B76**, 575 (1978).

[69] G. Jungman, M. Kamionkowski, and K. Griest, Phys.Rept. **267**, 195 (1996), hep-ph/9506380.

[70] M. S. Carena, J. Espinosa, M. Quiros, and C. Wagner, Phys.Lett. **B355**, 209 (1995), hep-ph/9504316.

[71] J. Callan, Curtis G., Phys.Rev. **D2**, 1541 (1970).

[72] K. Symanzik, Commun.Math.Phys. **18**, 227 (1970).

[73] D. J. Gross and F. Wilczek, Phys.Rev.Lett. **30**, 1343 (1973).

[74] Tech. Rep. CERN-LHCC-2011-012. LHCC-I-020, CERN, Geneva (2011).

[75] G. Aad et al. (ATLAS Collaboration), JINST **3**, S08003 (2008).

[76] S. Chatrchyan et al. (CMS Collaboration), JINST **3**, S08004 (2008).

[77] A. Belyaev, N. D. Christensen, and A. Pukhov, Comput.Phys.Commun. **184**, 1729 (2013), 1207.6082.

[78] J. Alwall, M. Herquet, F. Maltoni, O. Mattelaer, and T. Stelzer, JHEP **1106**, 128 (2011), 1106.0522.

[79] T. Sjostrand, S. Mrenna, and P. Z. Skands, JHEP **0605**, 026 (2006), hep-ph/0603175.

[80] *PGS – Pretty Good Simulator*, http://www.physics.ucdavis.edu /~conway/research/software/pgs/pgs4-general.htm .

[81] J. de Favereau et al. (DELPHES 3), JHEP **1402**, 057 (2014), 1307.6346.

APPENDIX A

Slepton Discovery in Electroweak Cascade Decay

The following manuscript was published as a peer-reviewed article in the Journal of High Energy Physics. The manuscript is reprinted with permission from Springer Science and Business Media. Original reference: J. Eckel, W. Shepherd, and S. Su, "*Slepton Discovery in Electroweak Cascade Decay*", JHEP **1205**, 081 (2012).

Published for SISSA by Springer

Received: November 29, 2011
Revised: March 27, 2012
Accepted: May 1, 2012
Published: May 21, 2012

Slepton discovery in electroweak cascade decay

Jonathan Eckel,[a] **William Shepherd**[b] **and Shufang Su**[a,b]

[a] *Department of Physics, University of Arizona, Tucson, Arizona 85721, U.S.A.*

[b] *Department of Physics and Astronomy, University of California, Irvine, California 92697, U.S.A.*

E-mail: eckel@physics.arizona.edu, shepherd.william@uci.edu, shufang@physics.arizona.edu

Abstract: The LHC studies on the MSSM slepton sector have mostly been focused on direct slepton Drell-Yan pair production. In this paper, we analyze the case when the sleptons are lighter than heavy neutralinos and can appear in the on-shell decay of neutralino states. In particular, we have studied the $\chi_1^\pm\chi_2^0$ associated production, with the consequent decays of $\chi_1^\pm \to \nu_\ell \ell \chi_1^0$ and $\chi_2^0 \to \ell\ell\chi_1^0$ via on-shell sleptons. The invariant mass of the lepton pairs, $m_{\ell\ell}$, from the neutralino decay has a distinctive triangle shape with a sharp kinematic cutoff. We discuss the utilization of this triangle shape in $m_{\ell\ell}$ distribution to identify the slepton signal. We studied the trilepton plus missing E_T signal and obtained the effective cross section, $\sigma \times \mathrm{BR} \times$ acceptance, that is needed for a 5σ discovery as a function of the cutoff mass for the LHC with center of mass energy 14 TeV and 100 fb^{-1} integrated luminosity. Our results are model independent such that they could be applied to other models with similar decay topology. When applied to the MSSM under simple assumptions, it is found that with 100 fb^{-1} integrated luminosity, a discovery reach in the left-handed slepton mass of about 600 GeV could be reached, which extends far beyond the slepton mass reach in the usual Drell-Yan studies.

Keywords: Supersymmetry Phenomenology

ArXiv ePrint: 1111.2615

doi:10.1007/JHEP05(2012)081

JHEP05(2012)081

Contents

1 Introduction

While the Large Hadron Collider (LHC) has great potential in searching for strongly interacting particles, its reach in the electroweak sector of new physics scenarios is limited due to the suppressed electroweak production cross sections. Although those electroweak particles could appear in the cascade decay of heavier colored objects, the discovery reach depends strongly on the mass scale of the colored ones. Current LHC searches in the Minimal Supersymmetric Standard Model (MSSM) are mostly focused on the direct pair production of squarks and gluinos. Null search results from both ATLAS and CMS [1–13] already exclude the mass of those colored particles up to about 1000 GeV for uncompressed spectrum cases. To minimize the dependence on the spectrum of heavy colored objects, we consider the direct production of the electroweak sector of the MSSM in our current study. In particular, we focus on the LHC reach for the discovery of the sleptons. A complementary study on the LHC reach in the neutralino and chargino sector with decoupled sleptons can be found in ref. [14].

If low energy supersymmetry is realized in the nature, sleptons are likely to be light. This happens in the Gauge Mediated Supersymmetry (SUSY) breaking scenarios [15], as well as the Anomaly Mediated SUSY breaking scenarios [16–18], in which the slepton masses are proportional to the electroweak gauge couplings. Even in the minimal Gravity Mediated SUSY breaking scenarios (mSUGRA) [19] where all the scalars have a common mass m_0 at some high energy scale, renormalization group running to low energies typically pushes up the squark mass (due to the contributions of strongly interacting gluinos) while the sleptons remain light. While the masses of the superpartners of the colored objects

JHEP05(2012)081

have already been constrained by current search limits, it is timely to fully explore the discovery potential of the LHC for the superpartners of leptons.

In the R-parity conserving MSSM with the lightest neutralino χ_1^0 being the lightest supersymmetric particle (LSP), χ_1^0 is a good candidate for Weakly Interacting Massive Particle (WIMP) dark matter [20, 21]. When sleptons are light, the t-channel diagram mediated by the exchange of sleptons is important in determining the annihilation cross section of χ_1^0 dark matter [22–24]. Therefore, discovery of the sleptons is not only a verification of low energy supersymmetry in nature; precise measurement of their masses also plays an important role in determining the relic density of the neutralino LSP.

Earlier studies on the slepton discovery potential at the LHC mostly focused on the Drell-Yan pair production of slepton pairs, with sleptons directly decaying down to lepton and χ_1^0 [25–30]. Most of those studies are done either in the mSUGRA framework or for a certain set of benchmark points only. The Drell-Yan production cross sections for slepton pairs are typically small, suppressed both by the electroweak coupling strength, as well as the scalar nature of the sleptons. The LHC reach is very limited: $m_{\tilde{\ell}_L} \gtrsim 300\,\text{GeV}$ and $m_{\tilde{\ell}_R} \gtrsim 200\,\text{GeV}$ for the LHC with center of mass 14 TeV and 30 fb^{-1} integrated luminosity [28–30].

In our study, we focused on an alternative production mechanism for the sleptons via the on-shell decay of heavier neutralino and chargino states [31, 32]. In particular, we considered the scenario where $M_1 < m_{\tilde{\ell}_L} < M_2 \ll \mu$ (M_1, M_2 and μ being the mass parameters for Bino, Winos and Higgsinos, respectively) and studied the pair production of Wino-like[1] $\chi_1^\pm \chi_2^0$ with the subsequent decay of $\chi_2^0 \to \ell\tilde{\ell}_L \to \ell\ell\chi_1^0$ and $\chi_1^\pm \to \ell\tilde{\nu}, \nu\tilde{\ell}_L \to \ell\nu\chi_1^0$. The collider signature is trilepton plus missing E_T.

Compared to the traditional searches of slepton Drell-Yan pair production with dilepton plus missing E_T signature, this channel is advantageous for the following reasons. Firstly, the production cross section for $\chi_1^\pm\chi_2^0$, although also at the electroweak strength, is larger than slepton pair production due to the fermionic nature of the neutralinos and charginos. Secondly, for χ_2^0 and $\chi_1^\pm$ being dominantly Wino, the decay branching fraction into left-handed sleptons is almost 100%. Thirdly, the SM backgrounds for this trilepton signature are also much smaller, with dominant contributions from the leptonic decay of WZ and asymmetric conversion in WZ/γ^*, as well as $t\bar{t}$ with an extra lepton from heavy flavor decay.

In addition, the invariant mass of the dileptons from the χ_2^0 cascade decay chain, $m_{\ell\ell}$, has a distinctive triangle shape, with a sharp kinematic cutoff, m_{cut} completely determined by $m_{\chi_2^0}$, $m_{\chi_1^0}$ and $m_{\tilde{\ell}_L}$ [33]. This triangle feature has been mostly used as a precise determination of the slepton mass [33–35]. It is also used in the recent CMS opposite sign dilepton searches to enhance the signal acceptance [13]. Although this spectral shape can be obvious to the eye, it could easily get washed out when SM backgrounds are considered. In our study, we explore the LHC discovery potential for sleptons by performing a fit to this triangle spectral shape. We also fit the dilepton invariant mass distribution from the

[1] By "Wino-like", we refer to the case that $\chi_1^\pm$ and χ_2^0 are mostly Winos with a small mixture of Higgsino and Bino states that is suppressed by $\mathcal{O}(m_Z/\mu)$ or smaller.

JHEP05(2012)081

dominant SM backgrounds (either containing a Z/γ^* or from $t\bar{t}$). Since we keep the overall normalization of the backgrounds that contain a Z as a fitting parameter, our treatment allows us to include other backgrounds that contain a Z as well, for example, those from other SUSY processes. We obtain the effective cross section, $\sigma\times$ BR $\times$ acceptance, necessary for a 5σ discovery as a function of the cutoff mass. This result is model independent and can be applied to any new physics model that gives rise to the same decay topology and signature. When applied to the MSSM slepton produced in the cascade decay of Wino-like $\chi_1^\pm\chi_2^0$, we obtain the 5σ reach in the parameter space of M_2 vs. $m_{\tilde{\ell}_L}$.

Note that even though we used the cascade decay via left-handed slepton (sneutrino) in our study since our method works more effectively in such scenario, it could be applied to cascade decay via the right-handed slepton as well. The branching fraction of χ_2^0 to the right-handed slepton, however, are typically suppressed, except in the limited parameter space when $\chi_2^0 \to \ell\tilde{\ell}_R$ is the only on-shell two-body decay channel.

A recent analysis by ATLAS on the same sign dilepton plus missing E_T signature [5] studied $\chi_1^\pm\chi_2^0$ associated production with decays of $\chi_1^\pm$ and χ_2^0 via on-shell slepton in a simplified weak gaugino production model. With 1 fb^{-1} at the 7 TeV LHC, masses of $\chi_1^\pm$ (χ_2^0) up to 200 GeV for $m_{\chi_1^0} = 0$ GeV were excluded at 95% C.L., based on event counting. Fitting the dilepton invariant mass distribution was also performed in the opposite sign dilepton plus missing E_T search at CMS [13]. With 0.98 fb^{-1} integrated luminosity at the 7 TeV LHC, 95% C.L. upper limits on the cross section times acceptance of about $4 - 30$ fb is obtained for the cutoff mass scale between 20 to 300 GeV.

The outline of the paper is as follows. In section 2, we discuss the slepton production and decay, focusing on the sleptons produced via neutralino/chargino cascade decay and identify their collider signature. In section 3, we present the triangle spectral shape of the dilepton invariant mass distribution and discuss the parameter dependence of the cutoff mass. In section 4, we review the current collider bounds on sleptons as well as bounds on neutralinos and charginos in the MSSM. In section 5, we discuss in detail our treatment of the signal, as well as the SM backgrounds by fitting to the spectral shape of the $m_{\ell\ell}$ distribution. In section 6, we present the model-independent least effective cross section, $\sigma \times$ BR $\times$ acceptance, that is needed for a 5σ discovery as a function of cutoff mass at the LHC with center of mass energy 14 TeV and 100 fb^{-1} luminosity. In section 7, we apply our study in the MSSM electroweak sector and show the 5σ reach in M_2 vs. $m_{\tilde{\ell}_L}$ parameter space. In section 8, we conclude.

2 MSSM with light gauginos and sleptons

We consider the low lying spectrum of the MSSM electroweak sector, which includes only neutralinos, charginos, and light sleptons. In our discussion below, we assume the canonical case where $M_1 < M_2, \mu$ and the lightest neutralino LSP is dominantly Bino-type. Scenarios with other mass orderings can be studied similarly. The slepton mass spectrum is determined by $(\mathbf{M}^2_{\tilde{\ell}})_{LL}$, $(\mathbf{M}^2_{\tilde{\ell}})_{RR}$ and $(\mathbf{M}^2_{\tilde{\ell}})_{LR}$, where each $\mathbf{M}^2_{\tilde{\ell}}$ is a 3×3 matrix, representing three generations. In our study, we take the simple assumption that the flavor mixing between generations is negligible. The phenomenology and implication of sizable

JHEP05(2012)081

flavor mixing in the slepton sector can be found in ref. [36–39]. Furthermore, the left-right mixing in the slepton sector is typically proportional to the lepton Yukawa, which is small for the first two generations. Therefore, we assume there is no left-right mixing for selectrons and smuons and label the mass eigenstates as $\tilde{\ell}_L$ and $\tilde{\ell}_R$, for $\ell = e,\ \mu$, with masses $m_{\tilde{\ell}_L}$ and $m_{\tilde{\ell}_R}$, respectively. For the stau, left-right mixing could be sizable, especially with large $\tan\beta$. The mass eigenstates are labeled as $\tilde{\tau}_1$ and $\tilde{\tau}_2$. There are three parameters involved for the stau sector: $m_{\tilde{\tau}_1}$, $m_{\tilde{\tau}_2}$ and the left-right mixing angle $\theta_{\tilde{\tau}}$. Our discussion below applies to the simplified case of selectrons and smuons, although it could be adapted to the stau case as well. For sneutrinos, their masses $m_{\tilde{\nu}_\ell}$ are also determined by $(\mathbf{M}_{\tilde{\ell}})^2_{LL}$. Therefore, their masses are related to $m_{\tilde{\ell}_L}$ with a small splitting introduced by electroweak effects: $m^2_{\tilde{\nu}_\ell} = m^2_{\tilde{\ell}_L} + m^2_W \cos 2\beta$; for the allowed range of $\tan\beta > 1$, $m_{\tilde{\nu}_\ell} < m_{\tilde{\ell}_L}$.

The direct production channels of sleptons are Drell-Yan pair productions[2] of $\tilde{\ell}_L\tilde{\ell}_L$, $\tilde{\ell}_L\tilde{\nu}_\ell$, $\tilde{\nu}_\ell\tilde{\nu}_\ell$ and $\tilde{\ell}_R\tilde{\ell}_R$. The production cross sections are typically small due to both the electroweak coupling strength and the scalar nature of the particles. At the LHC with $\sqrt{s} = 14\,\text{TeV}$, the cross sections vary from 0.2 pb to 0.5 fb for $\tilde{\ell}_L\tilde{\ell}_L$ and $\tilde{\nu}_\ell\tilde{\nu}_\ell$, from 0.8 pb to 1.5 fb for $\tilde{\ell}_L\tilde{\nu}_\ell$, and from 0.08 pb to 0.2 fb for $\tilde{\ell}_R\tilde{\ell}_R$, for masses of sleptons in the range of 100 to 500 GeV [26, 27].

The decay of right-handed sleptons is quite straightforward, proceeding dominantly into $\ell\chi^0_1$. In cases when on-shell decay of $\tilde{\ell}_R$ into higher neutralino states is open and when there is a significant Bino component in higher neutralino states (typical for $\mu \sim M_1$), $\tilde{\ell}_R \to \ell\chi^0_{2,3,4}$ could also contribute, although the decay branching fraction is almost always suppressed.

The decay of left-handed sleptons depends on the neutralino and chargino spectrum, in particular, that of Wino-type neutralino and charginos. Since the decay of sleptons into Higgsino-type neutralinos and charginos are typically suppressed, we assume $M_2 \ll \mu$, and thus χ^0_2, $\chi^\pm_1$ are mostly Wino-like. For $m_{\tilde{\ell}_L}$, $m_{\tilde{\nu}_\ell} < M_2$, the branching fractions of $\tilde{\ell}_L \to \ell\chi^0_1$, $\tilde{\nu}_\ell \to \nu_\ell\chi^0_1$ are almost 100%. Once $m_{\tilde{\ell}_L}$, $m_{\tilde{\nu}_\ell} \gtrsim M_2$, the decays of $\tilde{\ell}_L \to \ell\chi^0_2$, $\nu_\ell\chi^\pm_1$, $\tilde{\nu}_\ell \to \nu_\ell\chi^0_2$, $\ell\chi^\pm_1$ become dominant. The branching fraction is about 10% into χ^0_1, 30% into χ^0_2, and 60% into $\chi^\pm_1$. With the subsequent decay of $\chi^0_2 \to Z^{(*)}\chi^0_1$, $h\chi^0_1$ and $\chi^\pm_1 \to W^{(*)}\chi^0_1$, left-handed slepton and sneutrino decay would have multi-lepton, multi-jets, plus missing E_T final states.

For the Drell-Yan pair production of sleptons with dominant direct decay of sleptons into χ^0_1, the collider signatures are dilepton plus missing E_T for $\tilde{\ell}_L\tilde{\ell}_L$ and $\tilde{\ell}_R\tilde{\ell}_R$, single lepton plus missing E_T for $\tilde{\ell}_L\tilde{\nu}_\ell$, and missing E_T only for $\tilde{\nu}_L\tilde{\nu}_L$. The single lepton channel suffers from large SM backgrounds, mainly W. The missing E_T only signature from $\tilde{\nu}_L\tilde{\nu}_L$ needs an extra jet or lepton from initial or final state radiation, which leads to further suppression of signal cross sections. Current collider analyses of slepton Drell-Yan production focus on the final states of two isolated energetic leptons plus missing E_T [26–30]. The SM backgrounds are typically large, dominantly from WW or $t\bar{t}$. The LHC reach is very limited: $m_{\tilde{\ell}_L} \gtrsim 300\,\text{GeV}$ and $m_{\tilde{\ell}_R} \gtrsim 200\,\text{GeV}$ for the LHC with center of mass 14 TeV and 30 fb^{-1} integrated luminosity [28–30].

[2]For the case of stau, additional stau pair productions from b-quark annihilation and gluon fusion could enhance the cross sections by more than one order of magnitude in certain parameter space [41].

JHEP05(2012)081

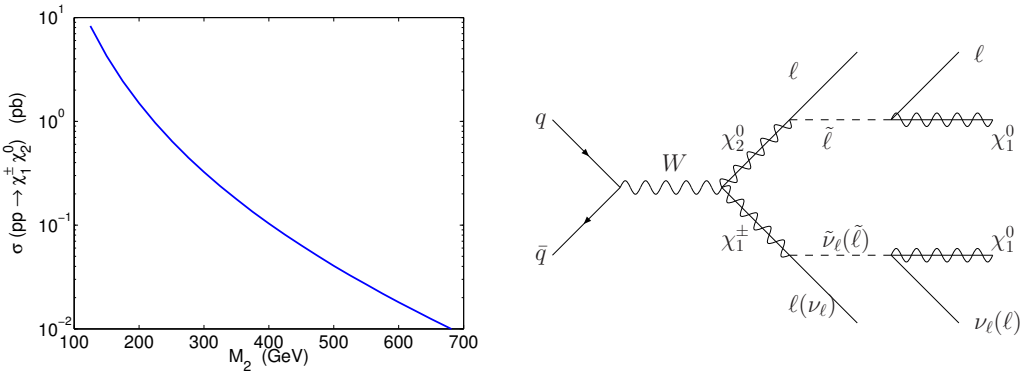

Figure 1. The left plot shows the cross section for $\chi_1^\pm\chi_2^0$ associated production in the pure Wino case at the LHC with center of mass energy 14 TeV. Here we have decoupled both Higgsinos as well as squarks by setting their masses to be 3 TeV. The right plot shows an example of the production of the trilepton plus missing E_T final states via the cascade decay of $\chi_1^\pm\chi_2^0$ through on-shell sleptons.

In this paper, we explore alternative production channels for sleptons, in particular, $\tilde{\ell}_L$ and $\tilde{\nu}_\ell$, via the decay of heavier neutralinos and charginos. The coupling of Higgsinos to sleptons are highly suppressed by the small lepton Yukawa coupling, therefore the production of sleptons from Higgsino decay is negligible. We assume μ is heavy and decouple Higgsinos. Winos, on the other hand, could dominantly decay into $\tilde{\ell}_L$ and $\tilde{\nu}_\ell$ once it is kinematically available, since the competing processes of $\chi_2^0 \to Z\chi_1^0$, $h\chi_1^0$ and $\chi_1^\pm \to W\chi_1^0$ suffer from small neutralino mixing. The pair production cross sections of Wino-like neutralinos/charginos are larger compared to those of sleptons of similar mass. In figure 1, we show the production cross section (calculated in Madgraph 5 version v0.6.2 [40]) for Wino-like $\chi_1^\pm\chi_2^0$ for the LHC with $\sqrt{s} = 14\,\text{TeV}$. The cross section is about 10 pb for M_2 around 100 GeV, which drops to about 10 fb for M_2 around 700 GeV. In principle, $\tilde{\ell}_{L,R}$ could also appear in Bino-like neutralino decay, in cases of $M_1 > m_{\tilde{\ell}}, M_2, \mu$. However, the pair productions of Bino-type neutralino with other neutralinos/charginos are typically suppressed due to the small neutralino mixing effects.

For $M_1 < m_{\tilde{\ell}_L}, m_{\tilde{\nu}_\ell} < M_2$, the lightest chargino $\chi_1^\pm$ dominantly decays into $\ell\tilde{\nu}_\ell$ and $\nu_\ell\tilde{\ell}_L$. With the consequent decay of $\tilde{\nu}_\ell$ and $\tilde{\ell}_L$ directly into χ_1^0, the branching fraction of $\chi_1^\pm \to \ell\nu_\ell\chi_1^0$ is almost 100%. χ_2^0, on the other hand, decays into $\nu_\ell\tilde{\nu}_\ell$ and $\ell\tilde{\ell}_L$ with about the same branching fraction. The former decay leads to $\nu\nu\chi_1^0$ final states, while the latter process has two isolated charged leptons $\ell\ell\chi_1^0$. Considering trilepton plus missing E_T signatures, the overall branching fraction of $\chi_1^\pm\chi_2^0$ into this final state is about 50%. Combining the production cross section of $\chi_1^\pm\chi_2^0$, left-handed sleptons could be produced in the decay products of Wino-like heavier neutralino and charginos states with relatively large cross sections compared to the direct Drell-Yan process. Relatively small SM background for the trilepton final state and the distinctive triangle spectral shape for $m_{\ell\ell}$ render this channel useful in probing the left-handed sleptons at the LHC. Of course it should always be kept in mind that such slepton production is only possible when the slepton masses are less than M_2.

JHEP05(2012)081

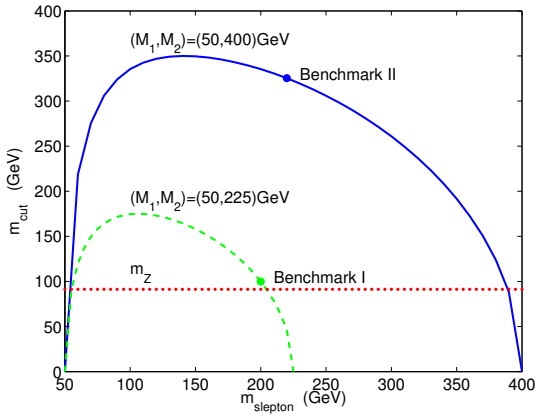

Figure 2. The dependence of the dilepton invariant mass $m_{\ell\ell}$ distribution endpoint $m_{\rm cut}$ on the slepton mass $m_{\tilde{\ell}}$, for (M_1, M_2)=(50,400) GeV (solid curve) and (50,225) GeV (dashed curve). Benchmark point I: $(M_1, M_2, m_{\tilde{\ell}_L}) = (50, 225, 200)$ GeV and benchmark point II: $(M_1, M_2, m_{\tilde{\ell}_L}) = (50, 400, 220)$ GeV are displayed as dots. Also plotted is the Z boson mass in red dotted line.

It should also be noted that such slepton production via cascade decay of heavier neutralinos and charginos works effectively for the left-handed charged sleptons. For the right handed sleptons, even if it is lighter than M_2, the branching fraction is small in general compared to the dominant decays of $\chi_2^0 \to Z\chi_1^0$, $\chi_2^0 \to h\chi_1^0$ since it is suppressed by the small Wino-Bino mixing. It only becomes important in the limited parameter regions with small $M_2 - M_1$ such that the on-shell decay of χ_2^0 into the dominant channels are forbidden. Therefore, in our study below, we focus on the light left-handed sleptons.

In cases when μ is lighter: $M_1 < \mu < M_2$, additional decay modes of heavier Wino states into lighter Higgsino states plus Higgses open, which could lead to the suppression of the branching fractions of Winos decaying into sleptons. The results that we obtained in our study, however, can also be applied to such cases, taking into account the suppressed branching fractions.

3 $m_{\ell\ell}$ distribution and triangle shape

One distinctive feature of the dileptons from the on-shell cascade decay of χ_2^0 (see the right plot of figure 1) is that the invariant dilepton mass $m_{\ell\ell}$ distribution has a triangle shape [33], with a cutoff mass determined by the masses of the $\chi_{1,2}^0$ and $\tilde{\ell}$:

$$m_{\rm cut} = m_{\chi_2^0}\sqrt{1-\frac{m_{\tilde{\ell}}^2}{m_{\chi_2^0}^2}}\sqrt{1-\frac{m_{\chi_1^0}^2}{m_{\tilde{\ell}}^2}}. \tag{3.1}$$

figure 2 shows the dependence of $m_{\rm cut}$ on $m_{\tilde{\ell}}$ for a given set of (M_1, M_2). $m_{\rm cut}$ varies in the range of 0 to $M_2 - M_1$. For $M_2 - M_1 > m_Z$, $m_{\rm cut}$ is larger than m_Z (indicated by the straight red dotted line in figure 2) for a large range of $m_{\tilde{\ell}}$. This is advantageous since we can effectively suppress the dominant SM background from WZ/γ^* by imposing a $m_{\ell\ell}$ cut to be above m_Z.

JHEP05(2012)081

This feature in the $m_{\ell\ell}$ spectral shape is often used as a precise determination of the slepton mass [33]. Even in the case of off-shell sleptons in neutralino decay, there have been studies in the literature exploring the sensitivity of the $m_{\ell\ell}$ spectral shape on the slepton mass [34, 35]. In our study below, we explore how to use this distinctive triangle shape of the $m_{\ell\ell}$ distribution to identify the slepton signal from the SM backgrounds. This triangle shape in $m_{\ell\ell}$ is not unique to the specified χ_2^0 decay in the MSSM; it could appear in many new physics model with a similar cascade decay topology that gives rise to two leptons. Our analysis is therefore model independent and can be applied to a more general set of new physics models.

4 Current collider search limits

The current best limits on the slepton masses come from LEP searches for dilepton plus missing energy signatures [42] with $\sqrt{s}$ up to 208 GeV. For a mass splitting between slepton and neutralino LSP above 15 GeV and considering only the contribution from right-handed sleptons, the mass limits are: $m_{\tilde{e}} > 99.6\,\text{GeV}$, $m_{\tilde{\mu}} > 94.9\,\text{GeV}$ and $m_{\tilde{\tau}} > 85.9\,\text{GeV}$. This is conservative, since the production cross section for the left-handed sleptons is higher. For stau, it is possible to have a large left-right mixing, which could decrease the production cross section for the lightest stau pair. A lower limit of $m_{\tilde{\tau}} > 85.0\,\text{GeV}$ can be obtained when the production cross section for the lightest stau is minimized. It should be noted that the slepton mass limits are obtained with $\mu = -200\,\text{GeV}$ and $\tan\beta = 1.5$, a point at which the neutralino mass limit based on the LEP neutralino and chargino searches is the weakest, and the selectron cross section is relatively small. The gaugino mass unification relation $M_1 = (5/3)\tan^2\theta_W M_2$ is assumed, which is relevant in fixing the masses and field content of the neutralinos. Slepton mass limits would change for a non-unified mass relation between M_1 and M_2, since neutralinos appear in both the slepton decay final states, as well as participating in the t-channel diagram for selectron production. For selectrons, $\tilde{e}_L\tilde{e}_R$ production is also possible via t-channel neutralino exchange. In the case where the $\tilde{e}_R - \chi_1^0$ mass splitting is small and the usual acoplanar dilepton search is insensitive, a single lepton plus missing energy search yields a lower limit on $m_{\tilde{e}_R}$ of 73 GeV, independent of $m_{\chi_1^0}$ [43, 44]. For sneutrinos, a mass limit of 45 GeV can be deduced from the invisible Z decay width [45]. An indirect mass limit on sneutrinos could be derived from the direct search limits on the charged slepton masses.

Since we consider the production of sleptons from heavier neutralino decay, we also summarize the current status of the neutralino and chargino sector. Charginos $\chi_1^\pm$ can be pair produced at LEP via s-channel exchange of Z/γ^* or t-channel exchange of $\tilde{\nu}_e$, with destructive interference. It decays to $f\bar{f}'\chi_1^0$ via a virtual W or sfermion, or dominantly to $f\tilde{f}'$ when two body decay is kinematically accessible. In the case of heavy sfermions and a mass splitting $m_{\chi_1^\pm} - m_{\chi_1^0}$ of at least a few GeV, a robust chargino mass lower limit of 103.5 GeV can be obtained for sneutrino masses larger than 300 GeV [46], assuming the gaugino mass unification relation. For the case of small mass splitting between the lightest chargino and neutralino LSP, limits have been obtained for the degenerate gaugino region ($M_1 \sim M_2$): $m_{\chi_1^\pm} > 91.9\,\text{GeV}$ for large sneutrino mass, as well as the "deep Higgsino"

JHEP05(2012)081

region ($|\mu| \ll M_{1,2}$): $m_{\chi_1^\pm} > 92.4\,\text{GeV}$ [47]. For lower sfermion masses, the limit is worse due to the reduced pair production cross section, as well as the reduction of selection efficiency due to the opening of two body decay channels. In particular, there is a so called "corridor" region where $m_{\chi_1^\pm} - m_{\tilde{\nu}_\ell}$ is small and the lepton from $\chi_1^\pm \to \ell\tilde{\nu}_\ell$ is so soft that it can escape detection. Associated production of $\chi_1^0\chi_2^0$ can be studied in cases where the chargino search becomes ineffective. Limits on chargino and neutralino masses for the light sfermion case, therefore, depend on the sfermion spectrum.

For the lightest neutralino LSP, there is no general mass limit from LEP if the gaugino mass unification relation is not imposed. Production via s-channel exchange of Z/γ^* could be absent for a Bino-like neutralino, and t-channel production could be negligible for heavy selectrons. An indirect mass limit on the neutralino LSP can be derived from chargino, slepton and Higgs boson searches, when gaugino mass (and sfermion mass) unification relation is assumed. A lower mass limit of 47 GeV can be obtained at large $\tan\beta$ [48], while a tighter limit of 50 GeV can be derived in the mSUGRA scenario [49].

Trilepton searches at Tevatron Run II [50–52] study the associated production of $\chi_1^\pm\chi_2^0$ with the subsequent decay of $\chi_1^\pm \to \ell\nu\chi_1^0$ and $\chi_2^0 \to \ell^+\ell^-\chi_1^0$. $\sigma \times \text{BR}(\chi_1^\pm\chi_2^0 \to 3\ell)$ is bounded to be less than about $0.13 - 0.06$ pb ($0.5 - 0.1$ pb) from DØ (CDF) searches for chargino mass in the range of $100 - 180\,\text{GeV}$. For sufficient light sleptons, the leptonic decay branching fractions are large and a mass limit on the lightest chargino can be derived based on the null search results. A chargino mass limit of 138 GeV is obtained based on DØ searches, when the leptonic branching fraction for three body decay is maximized, while no mass limit can be derived in the large m_0 case [52]. A recent CDF analysis with 5.8 fb^{-1} data gives a mass limit on the chargino to be 168 GeV at 95% C.L., for the mSUGRA benchmark point $m_0 = 60\,\text{GeV}$, $\tan\beta = 3$ and $A_0 = 0$ [50, 51].

Limits on $\sigma \times \text{BR}(\geq 3\ell)$ are also obtained based on the recent trilepton search from CMS collaboration using 2.1 fb^{-1} data collected at the LHC with $\sqrt{s} = 7\,\text{TeV}$ [12]. No jet veto is imposed and the dominant contribution to the trilepton signal is from gluino cascade decay. No limit on the chargino mass can be derived based on the direct pair production of $\chi_1^\pm\chi_2^0$.

Recent analyses by ATLAS on the same sign dilepton plus missing E_T [5] studied $\chi_1^\pm\chi_2^0$ associated production with the consequent decay of $\chi_1^\pm$ and χ_2^0 via an on-shell slepton. Assuming $m_{\tilde{\ell}} = \frac{1}{2}(m_{\chi_1^0} + m_{\chi_1^\pm})$, $m_{\chi_1^\pm} = m_{\chi_2^0}$, masses of $\chi_1^\pm$ (χ_2^0) up to 200 GeV for $m_{\chi_1^0} = 0\,\text{GeV}$ are excluded at 95% C.L with 1 fb^{-1} data collected at the 7 TeV LHC. For $m_{\chi_1^0}$ about 50 GeV, the limit on $m_{\chi_1^\pm}$, $m_{\chi_2^0}$ is weakened to be about 150 GeV.

CMS performed an analysis on the opposite sign dilepton plus missing E_T final states by looking for the kinematic edge in the dilepton invariant mass distribution [13]. With 0.98 fb^{-1} integrated luminosity at the 7 TeV LHC, 95% C.L. upper limits on the cross section times acceptance of about $4 - 30\,\text{fb}$ are obtained for the cutoff mass scale between 20 to 300 GeV, assuming the signal efficiency of the LM1 benchmark point: $m_0 = 60\,\text{GeV}$, $m_{1/2} = 250\,\text{GeV}$, $\tan\beta = 10$, $A_0 = 0$ and $\mu > 0$.

JHEP05(2012)081

5 Method

The dominant standard model backgrounds for the trilepton plus missing E_T signal come from the leptonic decay of WZ and asymmetric conversion in WZ/γ^*, as well as $t\bar{t}$ with a fake lepton (dominantly from b decay). Note that trileptons from heavy flavor bottom and charm decay (produced in association with Z/γ^*) could also be a significant background [53]. As explained below, the overall normalization of backgrounds with a Z peak is a fitting parameter in our analysis; backgrounds containing heavy flavor produced in association with Z/γ^* could be included as well. Therefore, we don't simulate such heavy flavor backgrounds in our analyses.

Many SUSY models can generate a trilepton signal, for example, $\chi_1^\pm\chi_2^0$ with $\chi_2^0 \to \chi_1^0 Z^{(*)}$ and $\chi_1^\pm \to \chi_1^0 W^{(*)}$. For large mass splitting of $m_{\chi_2^0} - m_{\chi_1^0} > m_Z$, the dilepton invariant mass distribution from an on-shell Z looks like that of Standard Model WZ. Such SUSY backgrounds, if they exist, are included in our fitting to $m_{\ell\ell}$ from the Z pole, since the overall normalization of the Z contribution is a fitting parameter. For small mass splittings $m_{\chi_2^0} - m_{\chi_1^0} < m_Z$, $m_{\ell\ell}$ is peaked near $m_{\chi_2^0} - m_{\chi_1^0}$. For such a case, a dedicated analysis to distinguish such off-shell Z contributions from the triangle spectral shape is necessary.

The first difficulty in reconstructing the trilepton event is the combinatorial ambiguity arising from the presence of a third lepton in the final state. To resolve this issue we use the standard technique of same-sign subtraction. We construct our invariant mass histograms by including both of the opposite-sign pairs of leptons and then subtract the histogram of same-sign dilepton invariant mass to have a good approximation to the histogram of invariant masses of the correct pair of opposite-sign leptons, which is otherwise not experimentally accessible. While other techniques exist to resolve this ambiguity [54], they all sacrifice statistics for purity, and as our intent is to find the general shape, the statistics will generally be of more value for us than the purity.

We model the dilepton invariant mass distribution by:

$$\frac{d\sigma}{dm_{\ell\ell}} = (f_{\text{triangle}} * g) + f_Z + a_0 f_{t\bar{t}}. \tag{5.1}$$

The first term models the triangle shape of the $m_{\ell\ell}$ from the signal process:

$$f_{\text{triangle}}(m_{\ell\ell}) = \begin{cases} 2N_{\text{sig}}\frac{m_{\ell\ell}}{m_{\text{cut}}^2} & 0 < m_{\ell\ell} < m_{\text{cut}} \\ 0 & \text{otherwise} \end{cases}, \tag{5.2}$$

where N_{sig} and m_{cut} are fit parameters for the number of counts in the triangle and the mass of the cutoff. To take into account the detector effects, we smear the triangle by a convolution of the triangle function with a gaussian with variance σ^2 shown below:

$$(f_{\text{triangle}} * g) \equiv \frac{1}{\sqrt{2\pi}\sigma}\int_{-\infty}^{\infty} dt\, e^{-\frac{t^2}{2\sigma^2}} f_{\text{triangle}}(m_{\ell\ell} - t). \tag{5.3}$$

The second term models the contribution to $m_{\ell\ell}$ from processes that involves a Z peak using the Breit-Wigner function:

$$f_Z(m_{\ell\ell}) = \frac{A}{2\pi}\frac{\Gamma}{(m_{\ell\ell} - m_0)^2 + (\Gamma/2)^2}, \tag{5.4}$$

JHEP05(2012)081

where A, m_0, Γ are fit parameters for the amplitude, centroid, and width of the Z pole. Note that we fit the centroid and the width of the Z pole instead of using the SM values to account for the smearing effects introduced by the detector resolution.

The last term models the contribution to $m_{\ell\ell}$ from $t\bar{t}$ trilepton events, where $f_{t\bar{t}}$ is the $m_{\ell\ell}$ distribution from $t\bar{t}$ dilepton events taken from Monte Carlo, scaled by a factor a_0, a parameter to represent the fake rate of $t\bar{t}$ to give three leptons. This is intended to emulate a data-driven background understanding, where the dilepton mass distribution is measured in a control region and then used to understand the background in the signal region. We choose the dilepton distribution because we expect that the two "wrong" pairs will largely cancel each other out in the subtracted distribution.

Thus, we have in total seven fitting parameters:

- Number of events in triangle: N_{sig}
- Cutoff in triangle distribution: m_{cut}
- Amount of gaussian smearing of the triangle: σ
- Amplitude of Z peak: A
- Apparent width of Z peak: Γ
- Apparent centroid of Z peak: m_0
- Fake rate for $t\bar{t}$ events: a_0

We use Madgraph 5 version v0.6.2 [40] and Madevent v4.4.57 [55] to generate our signal and background events. These events are passed to Pythia v6.4 [56] to simulate initial state radiation, final state radiation, showering and hadronization. Additionally we use PGS4 [57] with the ATLAS detector card to simulate detector effects. The fitted value for Z peak width in the SM WZ/γ^* background sample is 3.121 GeV, which agrees well with the ATLAS public results for the calibrated $Z \to e^+e^-$ invariant mass with 4.6 fb^{-1} data [58] . Note that, in producing and fitting the dilepton invariant mass, we require only that there be three leptons in the event. In particular, there is no requirement of low hadronic activity, which means that strong production of particles which later decay through an on-shell slepton can also be measured using this technique. We also do not require any missing energy, which allows this technique to be applicable in scenarios which do not include an invisible final state particle, such as R-parity violating theories. In general, some minimal requirement will be needed to ensure that events can be triggered on (either through a single lepton trigger or dilepton trigger), but all of the points we consider have spectra which are not compressed enough to have significant loss due to triggering efficiencies.

For signal generation, we considered the simplified case where the lightest neutralino is purely Bino in nature, and the second neutralino is purely Wino, with degenerate charginos which are also purely Wino: $m_{\chi_1^0} = M_1$ and $m_{\chi_1^\pm} = m_{\chi_2^0} = M_2$. This corresponds to taking the Higgsino mass parameter μ to be heavy such that the Higgsinos decouple. We assume

JHEP05(2012)081

there is no left-right mixing, as well as no flavor mixing between slepton generations. We also completely decouple the heavy colored objects. The relevant mass parameters involved are M_1, M_2 and $m_{\tilde{\ell}_L}$.

We simulate the associated production of $\chi_1^\pm\chi_2^0$ with the consequent decay of $\chi_1^\pm$ and χ_2^0 via left-handed sleptons, as shown in figure 1. As discussed earlier in section 2, since χ_2^0 has equal probability to decay into $\tilde{\ell}_L$ or $\tilde{\nu}_\ell$, we obtain trilepton final states $\ell\ell\ell+\not{E}_T$ 50% of the time. For simplicity, we only consider trilepton events with ℓ being either an electron or muon. In cases with lepton universality, $m_{\tilde{e}_L} = m_{\tilde{\mu}_L} = m_{\tilde{\tau}_L}$, we could study the same flavor, opposite sign $m_{\ell\ell}$ distribution. For non-degenerate slepton masses between generations, multiple triangle shapes appear and the analysis is more complicated, though with no flavor mixing they appear in different channels. Note that in the realistic case when the neutralino and chargino mass eigenstates are not the pure gauginos, the corresponding branching fractions for the decay into $\tilde{\ell}_L$ and $\tilde{\nu}_\ell$ need to be considered. For the backgrounds, we generate the SM WZ/γ^* trilepton events, as well as $t\bar{t}$ with both tops decaying leptonically.

We construct our signal and background histograms of the dilepton invariant mass by using our Monte Carlo data as probability distributions from which we select events. For the signal, we draw from the opposite-sign lepton events $2N_{\rm sig}$ times and draw from the same-sign lepton events $N_{\rm sig}$ times and construct the difference between the opposite-sign and same-sign distributions. $N_{\rm sig}$ is the number of events that we are including in the pseudoexperiment we are currently generating. For a given luminosity, $N_{\rm sig} = \mathcal{L} \times \sigma_{\rm sig} \times$ BR $\times$ acceptance. Similarly, we can draw N_{WZ/γ^*} events from the SM WZ/γ^* background and construct the corresponding $m_{\ell\ell}$ distribution.

Purely leptonic $t\bar{t}$ decay could lead to trilepton events with a third faked lepton from b decay. In the pseudoexperiment we are currently generating, we estimate the expected trilepton events $N_{t\bar{t}}$ using the fake rate estimated from PGS simulation: $N_{t\bar{t}} = \mathcal{L} \times \sigma_{t\bar{t}} \times$ BR $\times$ fake rate $\times$ acceptance, where the fake rate is about 4.3×10^{-3}.

In a trilepton $t\bar{t}$ sample, the opposite sign dilepton $m_{\ell\ell}$ distribution originating from W^+W^- decay is the same as the dilepton distribution from dilepton $t\bar{t}$ events. Therefore, we draw from the opposite-sign dilepton distribution of the dilepton $t\bar{t}$ event samples $N_{t\bar{t}}$ times to simulate the expected final distribution of $m_{\ell\ell}$ from W pair decay. The opposite-sign/same-sign dilepton $m_{\ell\ell}$ distributions with one lepton from the W and the other from the b jet originating from the same top/the other top decay can have very different distributions in principle. However, due to poor Monte-Carlo statistics on the three lepton $t\bar{t}$ events, we take the simplified assumption that the same sign and opposite sign $m_{\ell\ell}$ distributions from the Wb combination are very similar. We build two random histograms from the same-sign dilepton distribution of the trilepton $t\bar{t}$ sample with $N_{t\bar{t}}$ entries each to simulate the wrong pair of opposite-sign leptons and the same-sign pair of leptons, respectively. We then combine these histograms appropriately to get our pseudoexperiment result histogram for the $t\bar{t}$ background. While this is not a perfect description of the background in question, it is approximately valid and a more accurate data-driven background method than the one we use will be able to include those differences without great difficulty, so the sensitivities we find using this technique should be valid.

JHEP05(2012)081

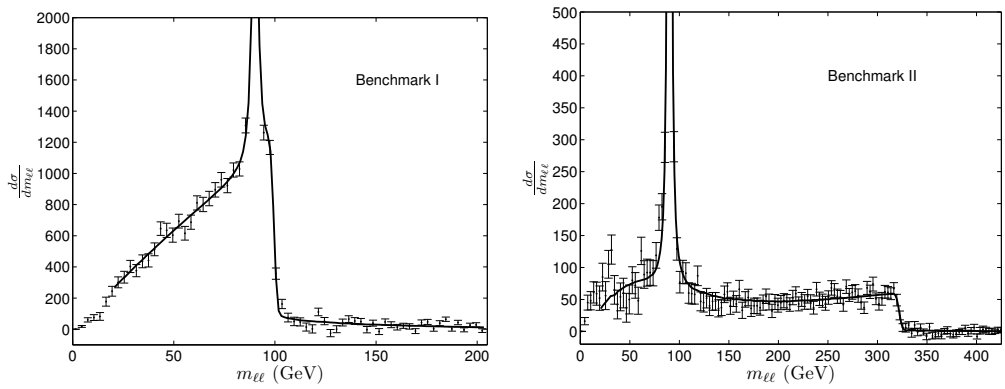

Figure 3. $m_{\ell\ell}$ distribution (after same-sign subtraction) for MSSM trilepton signal and dominant SM backgrounds at the 14 TeV LHC with an integrated luminosity of 100 fb^{-1}. The relevant MSSM parameters are chosen to be benchmark point I: $(M_1, M_2, m_{\tilde{\ell}_L}) = (50, 225, 200)$ GeV with $m_{\rm cut}$ =100 GeV (left plot), and benchmark point II: $(M_1, M_2, m_{\tilde{\ell}_L}) = (50, 400, 220)$ GeV with $m_{\rm cut}$ =325 GeV (right plot). Also shown as black curves are the best fit distribution using eq. (5.1).

In figure 3, we show the $m_{\ell\ell}$ distribution for the MSSM trilepton signal and dominant SM backgrounds at the 14 TeV LHC with integrated luminosity of 100 fb^{-1}, for two benchmark points: I, $(M_1, M_2, m_{\tilde{\ell}_L}) = (50, 225, 200)$ GeV (left plot); II, $(M_1, M_2, m_{\tilde{\ell}_L}) = (50, 400, 220)$ GeV (right plot). The corresponding triangle cutoff masses are 100 GeV and 325 GeV, respectively. For $m_{\rm cut}$ near m_Z (as in Benchmark Point I), the triangle distribution of $m_{\ell\ell}$ from the signal process is buried under the SM Z pole, making the identification of such triangle features much more difficult. For $m_{\rm cut}$ far above m_Z (as in Benchmark Point II), the sharp cutoff feature in $m_{\ell\ell}$ distribution can be easily identified from the SM background, as shown in the right plot of figure 3.

For a given value of integrated luminosity, we fit the $m_{\ell\ell}$ distributions built from the signal and background events generated as described above, using formulae given in eqs. (5.1)–(5.4) with seven fitting parameters. When the cutoff falls near the Z pole, we find that the fitting routine has too much freedom and often fails to identify the cutoff in the proper location. This failure is due to the similarity of the sharp feature of the cutoff and the edge of the Z pole. This results in a large degeneracy in the signal and Z pole fit parameters. Therefore, we fix the Z width, Γ to be 3.121 GeV and centroid position, m_0 to be 90.158 GeV when the cutoff is less than 150 GeV. These values are obtained from the $m_{\ell\ell}$ distribution of the SM WZ/γ^* backgrounds for events passed through the PGS detector simulation.

We perform a χ^2 fit using the MINUIT fitting routine [59]. We fit from 20 GeV to ($m_{\rm cut}$+100 GeV), with a fixed binning scheme of 3 GeV/bin. Note that an initial iteration with a larger fit range is first used to determine the approximate location of $m_{\rm cut}$. We find a good fit to the data with $\chi^2/{\rm dof} \sim 1$ for all cutoff masses. For high cutoff masses, $\chi^2/{\rm dof}$ is slightly lower due to the fact that our fit spans more bins. Conversely, we find a slightly higher $\chi^2/{\rm dof}$ at lower cutoff mass. The data driven approach to fitting the background

JHEP05(2012)081

		A	Γ (GeV)	m_0 (GeV)	a_0 ($\times 10^{-3}$)	$m_{\rm cut}$ (GeV)	$N_{\rm sig}$	σ (GeV)	χ^2/dof
Benchmark	input	3.981×10^3	3.121	90.158	4.280	99.8	1.85×10^4		
Point I	fitted	3.299×10^3	(3.121)	(90.158)	5.420	99.5	1.83×10^4	0.980	1.54
Benchmark	input	3.981×10^3	3.121	90.158	4.280	325.3	3.17×10^3		
Point II	fitted	3.347×10^3	2.914	90.041	4.412	321.9	3.14×10^3	2.319	0.94

Table 1. Input and final fitting parameters to eq. (5.1) for two benchmark points: I, $(M_1, M_2, m_{\tilde{\ell}_L}) = (50, 225, 200)$ GeV; II, $(M_1, M_2, m_{\tilde{\ell}_L}) = (50, 400, 220)$ GeV, for the 14 TeV LHC with $\mathcal{L} = 100$ fb^{-1}. The cutoff for benchmark I is less than 150 GeV so we fix the width and centroid of the Z peak with the values obtained from the $m_{\ell\ell}$ distribution of the SM WZ/γ^* backgrounds based on Monte-Carlo simulation.

works very well providing a best fit χ^2/dof of about 1 when fitting only the background. For high cutoff masses, we also consider fits from 125 GeV to ($m_{\rm cut}$+100 GeV). This to ensure that our fits for the cutoff at high mass are not being influenced too greatly by fitting the Z at low mass. As an illustration, we show in table 1 the input parameters for the simulation, as well as the fitting parameters for the two benchmark points.

6 Results

Using the fitting strategy described above and assuming only the SM backgrounds for trilepton plus missing E_T signals, for a given cutoff mass $m_{\rm cut}$, we fit for the cutoff feature, marginalizing over all the other six fit parameters. This allows us to determine the number of events required for a detection of the cutoff feature with 5σ-level confidence. We consider cutoff masses ranging from 75 to 650 GeV stepping by 25 GeV, with finer stepping around the Z pole. As explained before, for cutoff masses below 150 GeV, we perform a five-parameter fitting with the Z width and centroid fixed. For cutoff masses above 150 GeV, we perform a seven-parameter fitting, allowing the fitting parameters of the Z pole to vary freely.

In the left plot of figure 4 we plot the required effective trilepton cross section, $\sigma \times$ BR $\times$ acceptance, as a function of cutoff mass for 5σ discovery at the 14 TeV LHC with an integrated luminosity of 100 fb^{-1}. The maximum near 100 GeV is due to the difficulty of detecting the cutoff feature near the Z pole. There is a significant parameter degeneracy between the amplitude of the Z and the number of counts in the triangle. The effect also creates a significant scatter amongst the data points. At cutoff masses greater than 150 GeV, the required cross section for detection decreases with increasing cutoff mass. The scatter at high cutoff mass is due to statistical fluctuations in the Monte Carlo during the fitting process. The quality of the fit, however, depends on the range of $m_{\ell\ell}$ that is used in the fitting.

In the right plot of figure 4, we show the 5σ reach in the effective cross section similar to the left plot, but only fitting the $m_{\ell\ell}$ distribution above 125 GeV rather than above 20 GeV, such that the background contributions are significantly less relevant to the fit.

JHEP05(2012)081

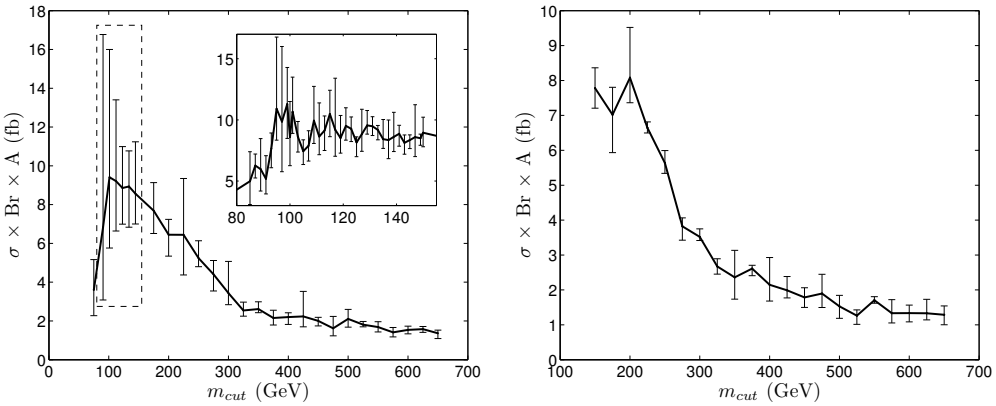

Figure 4. Effective trilepton cross section, $\sigma \times \mathrm{BR} \times$ acceptance, at the 14 TeV LHC required for a 5σ detection of the cutoff feature with an integrated luminosity of 100 fb^{-1}. For the left plot, the cross section reach is obtained with a fitting for $m_{\ell\ell}$ in the range of 20 GeV to ($m_{\rm cut}$+100 GeV). The inserted plot shows the zoom-in region of the dashed box for $m_{\rm cut}$ between 80 to 155 GeV. For the right plot, a fitting range of 125 GeV to ($m_{\rm cut}$+100 GeV) is used. Error bar for each point indicates the minimal and maximum values for $\sigma \times \mathrm{BR} \times$ acceptance that are obtained in our trials.

Comparing to the left plot, in which a blind fitting is performed without prior knowledge of possible range of $m_{\rm cut}$, although the resulting lower limit on the effective cross section is very similar in both cases, the fit with $m_{\ell\ell} > 125$ GeV above the Z pole is more robust since it greatly reduces the dependence on the precise knowledge of the backgrounds, in particular, those containing a Z pole.

Note that the above result is obtained for an integrated luminosity of 100 fb^{-1}. There is no simple scaling behavior of the required effective cross section for a different luminosity because this fitting technique does not have the simple statistical behavior of a counting experiment. In order to understand the sensitivity of this technique at significantly different luminosities it is necessary to generate a new set of pseudoexperiments and analyze them as explained above.

7 Slepton reach in MSSM

The most straightforward application of this search is to a system which gives the maximal branching ratio for the slepton decay of the second neutralino. We therefore consider the simplified MSSM scenario that is described earlier, in which χ_1^0 is purely Bino and $\chi_1^\pm$, χ_2^0 are purely Winos with no left-right mixing in the slepton sector and squarks decoupled. Note that in this simplified scenario, such a trilepton search channel is only sensitive to the intermediate $\tilde{\ell}_L$ since decays to $\tilde{\ell}_R$ are forbidden due to the absence of couplings.

Wino pair production $\chi_1^\pm \chi_2^0$ is completely controlled by gauge couplings in this approximation, which allows us to make robust predictions for the cross section of this process. With our fitting strategy, for a given mass parameter set with known production cross section, we allow the luminosity to shift until the triangle spectral shape in $m_{\ell\ell}$ distribution is

JHEP05(2012)081

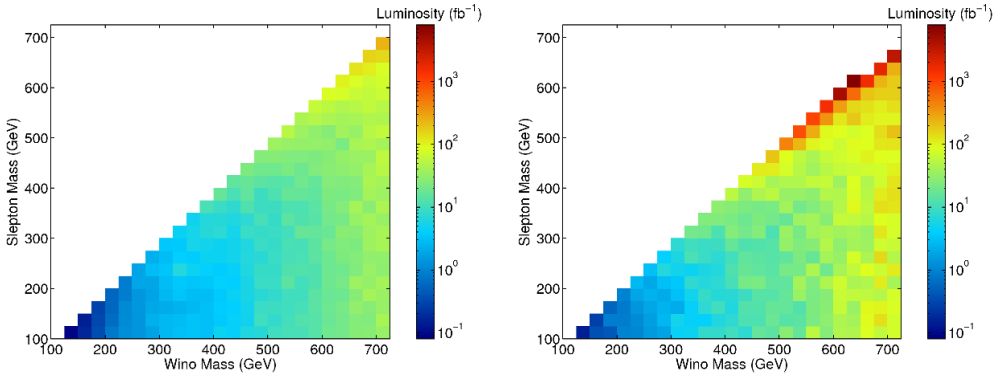

Figure 5. Luminosity required at the 14 TeV LHC for a 5σ detection of the cutoff feature above the SM backgrounds. In the left plot, we assume only the left-handed selectron is accessible in the cascade decay of χ_2^0. In the right plot, we assume that all slepton masses are degenerate. The cross section reaches are obtained considering the final states with electrons and muons only.

detectable at the 5σ level, as defined above. The previous limits from LEP II constrain the left-handed sleptons to be heavier than about 100 GeV, and so we consider only sleptons which are 100 GeV or heavier. While charginos are more weakly constrained in general than the left-handed slepton, they must be heavier than the left-handed slepton in order to be within this framework. We scan $m_{\tilde{\ell}_L}$ and M_2 in the range of $100 - 700$ GeV, with a step size of 25 GeV. The luminosities necessary to discover the slepton in these decays as a function of the masses are shown in figure 5.

In the left plot of figure 5, we assume that only one lepton flavor (selectron in our analysis) is accessible in the cascade decay of χ_2^0. For the 14 TeV LHC with 100 fb^{-1} luminosity, the mass reach for the $\tilde{\ell}_L$ (under pure gaugino assumption) can be reached up to 600 GeV at 5σ level. In the right plot, we assume the lepton universality condition such that $m_{\tilde{e}_L} = m_{\tilde{\mu}_L} = m_{\tilde{\tau}_L}$. Considering only trilepton events with electrons and muons, namely eee, $\mu\mu\mu$, $e^+e^-\mu^\pm$ and $\mu^+\mu^-e^\pm$; additional branching ratio suppression factors need to be applied. The reach for the left-handed slepton mass is reduced in this case, about 500 GeV for $m_{\tilde{\ell}_L}$.

For comparison, Drell-Yan slepton searches were considered in ref. [28–30], with the authors concluding that flavor-diagonal sleptons with masses less than $350-400$ GeV can be discovered by CMS using 100 fb^{-1} of data. Thus, our technique indicates that, in the pure gaugino limit, the reach for left-handed sleptons will be significantly enhanced by looking for the characteristic cutoff shape of $m_{\ell\ell}$ in the decays of the gauginos. Note that right-handed sleptons are not subject to these results because they are a singlet under $\mathrm{SU}(2)_L$.

8 Conclusions and discussion

In this work, we have studied the LHC discovery potential for sleptons, which are produced via the on-shell decay of the heavier neutralino and chargino states. In particular, we have studied the $\chi_1^\pm\chi_2^0$ associated production, with the consequent decays of $\chi_1^\pm \to \nu_\ell\ell\chi_1^0$

JHEP05(2012)081

and $\chi_2^0 \to \ell\ell\chi_1^0$ via on-shell sleptons. Comparing to the conventional slepton searches through Drell-Yan production and dilepton plus missing E_T final states, this trilepton plus missing E_T channel has the advantage of larger production cross sections and less SM backgrounds. In addition, the invariant mass distribution of the dilepton pair from χ_2^0 decay has a distinctive triangle shape, which can be utilized to select out the signals from the dominant SM background of WZ/γ^* and $t\bar{t}$ fakes. We performed a fit to the $m_{\ell\ell}$ distribution of both the signal and the backgrounds. For the LHC with 14 TeV center of mass energy and 100 fb^{-1} integrated luminosity, we obtained the model-independent lower bounds on the effective signal cross section, $\sigma \times \mathrm{BR} \times$ acceptance, as a function of triangle cutoff mass, m_{cut}, at 5σ significance level. Applying this result to the MSSM in the parameter space of $M_1 < m_{\tilde{\ell}_L} < M_2 \ll \mu$, we found that the mass reach for the $\tilde{\ell}_L$ can be up to 600 GeV at 5σ level at the 14 TeV LHC with $\mathcal{L}$ =100 fb^{-1}, when there is only one slepton generation (selectron in our study) lighter than Winos. For a degenerate slepton spectrum with $m_{\tilde{e}_L} = m_{\tilde{\mu}_L} = m_{\tilde{\tau}_L}$, and considering final states with electrons and muons only, the reach is slightly worse due to the suppression of the branching fractions.

Comparing to earlier studies on the LHC reach for sleptons from Drell-Yan production, the reach for left-handed sleptons via Wino decay is greatly enhanced. On the other hand, it should be noted that our study works most effectively for the left-handed slepton, since the decay fraction of heavier neutralino/chargino states to right-handed sleptons is typically suppressed in most of parameter space, either by the small Bino-Wino/Higgsino mixing, or the lepton Yukawa couplings. The right-handed slepton could appear in Bino-like neutralino decay, if it is not the LSP. The associated production cross sections for Bino with other neutralino/chargino states, however, are suppressed in general. Our study does not apply to the parameter region of $m_{\tilde{\ell}_L} > M_2$ since the on-shell decay of Winos into left-handed sleptons is forbidden by kinematics. Therefore, for left-handed sleptons with mass heavier than M_2 or for right-handed sleptons, the usual Drell-Yan production is still the dominant production mode.

It should also be emphasized that the results we obtained for the lower bounds on the effective signal cross section, $\sigma \times \mathrm{BR} \times$ acceptance, as a function of triangle cutoff mass scale m_{cut} is model independent since it can be applied to both MSSM and new physics models other than MSSM, as long as those models give rise to the same cascade decay topology and final states of trilepton plus missing E_T. For new physics models with a given parameter set, we can obtain m_{cut} as well as the production cross sections, branching fractions into the trilepton final states, and signal acceptance via detector simulation. Comparing it with the lower bounds we obtained, we can derive the LHC reach in the parameter space for such new physics models.

More work is needed to fully explore the LHC reach for the slepton sector. Our results on the left-handed slepton reach are obtained under the simple assumption that χ_1^0 is a pure Bino state, $\chi_2^0, \chi_1^\pm$ are pure Wino states, and the heavier Higgsino states are completely decoupled. In addition, we studied only final states including electrons and muons. The analysis strategy in our study can be applied to the general MSSM framework with the mixing of gaugino and Higgsino states, as well as three lepton flavors (and possible left-right mixing in the stau case). The corresponding branching fraction into trilepton final states

JHEP05(2012)081

needs to be taken into account in such general cases. Trilepton final states with all possible flavor combinations could also be studied, although the fitting to the triangle shapes might be more complicated when the slepton masses are not degenerate. For a recent study on the slepton mass determination using kinematic edges with non-degenerate slepton masses and sizable mixing effects, see ref. [60].

In our study, we performed the triangle shape fitting to the trilepton plus missing E_T final states. The triangle shape in $m_{\ell\ell}$ distribution arises from the χ_2^0 cascade decay chain. Therefore, it appears in any process that contains such a heavy neutralino cascade decay. The fitting strategy could be applied to final states containing two opposite sign same flavor dileptons. For example, charginos in $\chi_1^\pm\chi_2^0$ production could decay to jets instead of leptons; or we could consider productions originated from gluinos or squarks, with the cascade decay of gluino or quark containing a χ_2^0. SM backgrounds for dilepton plus jets plus missing E_T signature, of course, are very different from the trilepton plus missing E_T signal that we considered in our study.

We could also consider Wino type $\chi_1^+\chi_1^-$ production with $\chi_1^\pm \to \nu_\ell \ell \chi_1^0$. The final state of dilepton plus missing E_T is similar to the conventional slepton study of Drell-Yan pair production of $\tilde{\ell}_L\tilde{\ell}_L$ with $\tilde{\ell}_L \to \ell\chi_1^0$. Although this channel is not as powerful as the trilepton plus missing E_T study that we explored in this paper, it would still have better reach comparing to the Drell-Yan process given the larger production cross sections.

As we mentioned earlier, our analyses can not be applied to the cases when the sleptons are heavier than M_2, when the Drell-Yan is the dominant production mode. Previous LHC analyses on the Drell-Yan channel focused on the dilepton plus missing E_T final states. When left-handed sleptons are heavier than Wino-like neutralino/charginos, the branching fractions of heavier sleptons into Wino-like states are sizable given its SU(2) coupling strength. Considering the consequent decay of the Wino-like neutralino/charginos, multiple leptons (up to six) + jets + missing E_T final states could appear, which provides additional channels for the left-handed slepton discovery at the LHC. For the right-handed sleptons, however, decays into lepton plus Bino-like χ_1^0 LSP are still dominant.

Light sleptons could also contribute sizably to low energy processes, for example, parity-violating electron scattering, leptonic Pion and Kaon decays, etc. [61–64]. Given the recent progress on both the theoretical and experimental studies in those low energy precision measurements, they have reached a sensitivity which is now able to probe new physics beyond the SM. LHC studies on the slepton sector will be complementary to the indirect probes provided by these precision measurements.

Acknowledgments

We would like to thank M. Ramsey-Musolf, T. Han and S. Padhi for useful discussions. JE and WS would like to thank TASI where some of the work was completed. JE and SS are supported by the Department of Energy under Grant DE-FG02-04ER-41298. SS is also supported by NSF Grants No. PHY-0653656 and PHY-0709742. WS is supported in part by NSF Grant No. PHY-0970171.

JHEP05(2012)081

References

[1] ATLAS collaboration, G. Aad et al., *Search for squarks and gluinos using final states with jets and missing transverse momentum with the ATLAS detector in $\sqrt{s} = 7$ TeV proton-proton collisions*, *Phys. Lett.* **B 710** (2012) 67 [arXiv:1109.6572] [INSPIRE].

[2] ATLAS collaboration, G. Aad et al., *Search for supersymmetry in final states with jets, missing transverse momentum and one isolated lepton in $\sqrt{s} = 7$ TeV pp collisions using 1 fb^{-1} of ATLAS data*, *Phys. Rev.* **D 85** (2012) 012006 [arXiv:1109.6606] [INSPIRE].

[3] ATLAS collaboration, *SUSY searches at ATLAS in multilepton final states with jets and missing transverse energy*, ATLAS-CONF-2011-039 (2011).

[4] ATLAS collaboration, G. Aad et al., *Search for new phenomena in final states with large jet multiplicities and missing transverse momentum using $\sqrt{s} = 7$ TeV pp collisions with the ATLAS detector*, *JHEP* **11** (2011) 099 [arXiv:1110.2299] [INSPIRE].

[5] ATLAS collaboration, G. Aad et al., *Searches for supersymmetry with the ATLAS detector using final states with two leptons and missing transverse momentum in $\sqrt{s} = 7$ TeV proton-proton collisions*, *Phys. Lett.* **B 709** (2012) 137 [arXiv:1110.6189] [INSPIRE].

[6] CMS collaboration, *Search for new physics with same-sign isolated dilepton events with jets and missing energy*, PAS-SUS-11-010 (2011).

[7] CMS collaboration, *Search for new physics in events with a Z boson and missing energy*, PAS-SUS-11-017 (2011).

[8] CMS collaboration, *Search for new physics with single-leptons at the LHC*, PAS-SUS-11-015 (2011).

[9] CMS collaboration, *Search for supersymmetry in all-hadronic events with α_T*, PAS-SUS-11-003 (2011).

[10] CMS collaboration, *Search for supersymmetry in all-hadronic events with missing energy*, PAS-SUS-11-004 (2011).

[11] CMS collaboration, *Search for supersymmetry in all-hadronic events with MT2*, PAS-SUS-11-005 (2011).

[12] CMS collaboration, *Multileptonic SUSY searches*, PAS-SUS-11-013 (2011).

[13] CMS collaboration, *Search for new physics in events with opposite-sign dileptons and missing transverse energy*, PAS-SUS-11-011 (2011).

[14] T. Han, S. Padhi and S. Su, *Searching for charginos and neutralinos at the LHC*, in preparation.

[15] G. Giudice and R. Rattazzi, *Theories with gauge mediated supersymmetry breaking*, *Phys. Rept.* **322** (1999) 419 [hep-ph/9801271] [INSPIRE].

[16] L. Randall and R. Sundrum, *Out of this world supersymmetry breaking*, *Nucl. Phys.* **B 557** (1999) 79 [hep-th/9810155] [INSPIRE].

[17] G.F. Giudice, M.A. Luty, H. Murayama and R. Rattazzi, *Gaugino mass without singlets*, *JHEP* **12** (1998) 027 [hep-ph/9810442] [INSPIRE].

[18] T. Gherghetta, G.F. Giudice and J.D. Wells, *Phenomenological consequences of supersymmetry with anomaly induced masses*, *Nucl. Phys.* **B 559** (1999) 27 [hep-ph/9904378] [INSPIRE].

JHEP05(2012)081

[19] A. Lahanas and D.V. Nanopoulos, *The road to no scale supergravity*, *Phys. Rept.* **145** (1987) 1 [INSPIRE].

[20] H. Goldberg, *Constraint on the photino mass from cosmology*, *Phys. Rev. Lett.* **50** (1983) 1419 [*Erratum ibid.* **103** (2009) 099905] [INSPIRE].

[21] J.R. Ellis, J. Hagelin, D.V. Nanopoulos, K.A. Olive and M. Srednicki, *Supersymmetric relics from the big bang*, *Nucl. Phys.* **B 238** (1984) 453 [INSPIRE].

[22] M. Drees and M.M. Nojiri, *The neutralino relic density in minimal $N = 1$ supergravity*, *Phys. Rev.* **D 47** (1993) 376 [hep-ph/9207234] [INSPIRE].

[23] T. Nihei, L. Roszkowski and R. Ruiz de Austri, *Exact cross-sections for the neutralino WIMP pair annihilation*, *JHEP* **03** (2002) 031 [hep-ph/0202009] [INSPIRE].

[24] A. Birkedal-Hansen and E.-h. Jeong, *Gaugino and higgsino coannihilations. 1. Neutralino neutralino interactions*, *JHEP* **02** (2003) 047 [hep-ph/0210041] [INSPIRE].

[25] F. del Aguila and L. Ametller, *On the detectability of sleptons at large hadron colliders*, *Phys. Lett.* **B 261** (1991) 326 [INSPIRE].

[26] H. Baer, C.-h. Chen, F. Paige and X. Tata, *Detecting sleptons at hadron colliders and supercolliders*, *Phys. Rev.* **D 49** (1994) 3283 [hep-ph/9311248] [INSPIRE].

[27] H. Baer, C.-h. Chen, F. Paige and X. Tata, *Signals for minimal supergravity at the CERN Large Hadron Collider. 2: Multi-lepton channels*, *Phys. Rev.* **D 53** (1996) 6241 [hep-ph/9512383] [INSPIRE].

[28] S. Bityukov and N. Krasnikov, *The search for sleptons and flavor lepton number violation at LHC (CMS)*, *Phys. Atom. Nucl.* **62** (1999) 1213 [hep-ph/9712358] [INSPIRE].

[29] Y. Andreev, S. Bityukov and N. Krasnikov, *Sleptons at post-WMAP benchmark points at LHC(CMS)*, *Phys. Atom. Nucl.* **68** (2005) 340 [hep-ph/0402229] [INSPIRE].

[30] D. Denegri, L. Rurua and N. Stepanov, *Detection of sleptons in CMS, mass reach*, CMS-NOTE-TN-96-059 (1996).

[31] H. Baer, K. Hagiwara and X. Tata, *Gauginos as a signal for supersymmetry at $p\bar{p}$ colliders*, *Phys. Rev.* **D 35** (1987) 1598 [INSPIRE].

[32] H. Baer and X. Tata, *Multi-lepton signals from $W^{\pm}$ and Z_0 decays to gauginos at $\bar{p}p$ colliders*, *Phys. Lett.* **B 155** (1985) 278 [INSPIRE].

[33] I. Hinchliffe, F. Paige, M. Shapiro, J. Soderqvist and W. Yao, *Precision SUSY measurements at CERN LHC*, *Phys. Rev.* **D 55** (1997) 5520 [hep-ph/9610544] [INSPIRE].

[34] A. Birkedal, R. Group and K. Matchev, *Slepton mass measurements at the LHC*, *eConf* **C 050318** (2005) 0210 [hep-ph/0507002] [INSPIRE].

[35] TeV4LHC Working Group collaboration, S. Abdullin et al., *Tevatron-for-LHC report: preparations for discoveries*, hep-ph/0608322 [INSPIRE].

[36] J.L. Feng et al., *Measuring slepton masses and mixings at the LHC*, *JHEP* **01** (2010) 047 [arXiv:0910.1618] [INSPIRE].

[37] J.L. Feng, S.T. French, C.G. Lester, Y. Nir and Y. Shadmi, *The shifted peak: resolving nearly degenerate particles at the LHC*, *Phys. Rev.* **D 80** (2009) 114004 [arXiv:0906.4215] [INSPIRE].

JHEP05(2012)081

[38] N. Krasnikov, *Search for flavor lepton number violation in slepton decays at LHC*, *JETP Lett.* **65** (1997) 148 [hep-ph/9611282] [INSPIRE].

[39] S. Bityukov and N. Krasnikov, *The Search for charged sleptons and flavor lepton number violation at LHC (CMS)*, hep-ph/9806504 [INSPIRE].

[40] J. Alwall, M. Herquet, F. Maltoni, O. Mattelaer and T. Stelzer, *MadGraph 5: going beyond*, *JHEP* **06** (2011) 128 [arXiv:1106.0522] [INSPIRE].

[41] J.M. Lindert, F.D. Steffen and M.K. Trenkel, *Direct stau production at hadron colliders in cosmologically motivated scenarios*, *JHEP* **08** (2011) 151 [arXiv:1106.4005] [INSPIRE].

[42] LEP2 SUSY Working Group, *Combined LEP selectron/smuon/stau results, 183–208 GeV*, LEPSUSYWG/04-01.1 (2004), http://lepsusy.web.cern.ch/lepsusy/.

[43] L3 collaboration, P. Achard et al., *Search for scalar leptons and scalar quarks at LEP*, *Phys. Lett.* **B 580** (2004) 37 [hep-ex/0310007] [INSPIRE].

[44] ALEPH collaboration, A. Heister et al., *Absolute lower limits on the masses of selectrons and sneutrinos in the MSSM*, *Phys. Lett.* **B 544** (2002) 73 [hep-ex/0207056] [INSPIRE].

[45] ALEPH, DELPHI, L3, OPAL, SLD, LEP Electroweak Working Group, SLD Electroweak Group, SLD Heavy Flavour Group collaboration, *Precision electroweak measurements on the Z resonance*, *Phys. Rept.* **427** (2006) 257 [hep-ex/0509008] [INSPIRE].

[46] LEP SUSY working group, *Combined LEP chargino results, up to* 208 *GeV for large* m_0, LEPSUSYWG-01-03.1 (2001).

[47] LEP2 SUSY Working Group, *Combined LEP chargino results, up to* 208 *GeV for low DM*, LEPSUSYWG/02-04.1 (2002), http://lepsusy.web.cern.ch/lepsusy/www/inoslowdmsummer02/charginolowdm_pub.html.

[48] LEP2 SUSY Working Group, *Combined lower bound of the neutralino mass in a constrained MSSM model*, LEPSUSYWG/04-07.1 (2004).

[49] LEP2 SUSY Working Group, *LSP mass limit in minimal SUGRA*, LEPSUSYWG/02-06.2 (2002).

[50] CDF collaboration, T. Aaltonen et al., *Search for supersymmetry in* $p\bar{p}$ *collisions at* $\sqrt{s} = 1.96$ *TeV using the trilepton signature of chargino-neutralino production*, *Phys. Rev. Lett.* **101** (2008) 251801 [arXiv:0808.2446] [INSPIRE].

[51] CDF collaboration, *Search for trilepton new physics and chargino-neutralino production at the collider detector at Fermilab*, CDF note 10636 (2011).

[52] D0 collaboration, V. Abazov et al., *Search for associated production of charginos and neutralinos in the trilepton final state using* $2.3\,fb^{-1}$ *of data*, *Phys. Lett.* **B 680** (2009) 34 [arXiv:0901.0646] [INSPIRE].

[53] Z. Sullivan and E.L. Berger, *Trilepton production at the CERN LHC: standard model sources and beyond*, *Phys. Rev.* **D 78** (2008) 034030 [arXiv:0805.3720] [INSPIRE].

[54] A. Rajaraman and F. Yu, *A new method for resolving combinatorial ambiguities at hadron colliders*, *Phys. Lett.* **B 700** (2011) 126 [arXiv:1009.2751] [INSPIRE].

[55] J. Alwall et al., *MadGraph/MadEvent v4: the new web generation*, *JHEP* **09** (2007) 028 [arXiv:0706.2334] [INSPIRE].

[56] T. Sjöstrand, S. Mrenna and P.Z. Skands, *PYTHIA 6.4 physics and manual*, *JHEP* **05** (2006) 026 [hep-ph/0603175] [INSPIRE].

JHEP05(2012)081

[57] *PGS — Pretty Good Simulator*, http://www.physics.ucdavis.edu/~conway/research/software/pgs/pgs4-general.html.

[58] *Calibrated $Z \to e^+e^-$ mass with* 2011 *data*, https://atlas.web.cern.ch/Atlas/GROUPS/PHYSICS/EGAMMA/PublicPlots/20110512/CalibratedZee/ATL-COM-PHYS-2011-1637/index.html.

[59] F. James and M. Roos, *Minuit: a system for function minimization and analysis of the parameter errors and correlations*, *Comput. Phys. Commun.* **10** (1975) 343 [INSPIRE].

[60] I. Galon and Y. Shadmi, *Kinematic edges with flavor splitting and mixing*, *Phys. Rev.* **D 85** (2012) 015010 [arXiv:1108.2220] [INSPIRE].

[61] A. Kurylov, M. Ramsey-Musolf and S. Su, *Probing supersymmetry with parity violating electron scattering*, *Phys. Rev.* **D 68** (2003) 035008 [hep-ph/0303026] [INSPIRE].

[62] A. Kurylov, M. Ramsey-Musolf and S. Su, *Supersymmetric effects in parity violating deep inelastic electron nucleus scattering*, *Phys. Lett.* **B 582** (2004) 222 [hep-ph/0307270] [INSPIRE].

[63] M.J. Ramsey-Musolf, S. Su and S. Tulin, *Pion leptonic decays and supersymmetry*, *Phys. Rev.* **D 76** (2007) 095017 [arXiv:0705.0028] [INSPIRE].

[64] M. Ramsey-Musolf and S. Su, *Low energy precision test of supersymmetry*, *Phys. Rept.* **456** (2008) 1 [hep-ph/0612057] [INSPIRE].

JHEP05(2012)081

APPENDIX B

Sleptons at the LHC

The following manuscript was published as a peer-reviewed article in the Journal of High Energy Physics. The manuscript is reprinted with permission from Springer Science and Business Media. Original reference: J. Eckel, M. J. Ramsey-Musolf, W. Shepherd, and S. Su, "*Impact of LSP Character on Slepton Reach at the LHC*", JHEP **1411**, 117 (2014).

Published for SISSA by Springer

Received: *August 22, 2014*
Revised: *October 15, 2014*
Accepted: *October 16, 2014*
Published: *November 21, 2014*

Impact of LSP character on Slepton reach at the LHC

Jonathan Eckel,[a] **Michael J. Ramsey-Musolf,**[b,c] **William Shepherd**[d,e] **and Shufang Su**[a]

[a] *Department of Physics, University of Arizona, Tucson, AZ 85721, U.S.A.*
[b] *Amherst Center for Fundamental Interactions, Department of Physics University of Massachusetts-Amherst, Amherst, MA 01003, U.S.A.*
[c] *Kellogg Radiation Laboratory, California Institute of Technology, Pasadena, CA 91125, U.S.A.*
[d] *Department of Physics, University of California - Santa Cruz, Santa Cruz, CA 95064, U.S.A.*
[e] *Santa Cruz Institute for Particle Physics, Santa Cruz, CA 95064, U.S.A.*

E-mail: eckel@physics.arizona.edu, mjrm@physics.umass.edu, wshepher@ucsc.edu, shufang@email.arizona.edu

Abstract: Searches for supersymmetry at the Large Hadron Collider (LHC) have significantly constrained the parameter space associated with colored superpartners, whereas the constraints on color-singlet superpartners are considerably less severe. In this study, we investigate the dependence of slepton decay branching fractions on the nature of the lightest supersymmetric particle (LSP). In particular, in the Higgsino-like LSP scenarios, both decay branching fractions of $\tilde{\ell}_L$ and $\tilde{\nu}_\ell$ depend strongly on the sign and value of M_1/M_2, which has strong implications for the reach of dilepton plus $\not{E}_T$ searches for slepton pair production. We extend the experimental results for same flavor, opposite sign dilepton plus $\not{E}_T$ searches at the 8 TeV LHC to various LSP scenarios. We find that the LHC bounds on sleptons are strongly enhanced for a non-Bino-like LSP: the 95% C.L. limit for $m_{\tilde{\ell}_L}$ extends from 300 GeV for a Bino-like LSP to about 370 GeV for a Wino-like LSP. The bound for $\tilde{\ell}_L$ with a Higgsino-like LSP is the strongest (~ 490 GeV) for $M_1/M_2 \sim -\tan^2\theta_W$ and is the weakest (~ 220 GeV) for $M_1/M_2 \sim \tan^2\theta_W$. We also calculate prospective slepton search reaches at the 14 TeV LHC. With 100 fb^{-1} integrated luminosity, the projected 95% C.L. mass reach for the left-handed slepton varies from 550 (670) GeV for a Bino-like (Wino-like) LSP to 900 (390) GeV for a Higgsino-like LSP under the most optimistic (pessimistic) scenario. The reach for the right-handed slepton is about 440 GeV. The corresponding 5σ discovery sensitivity is about 100 GeV smaller. For 300 fb^{-1} integrated luminosity, the reach is about $50 - 100$ GeV higher.

Keywords: Supersymmetry Phenomenology

ArXiv ePrint: 1408.2841

doi:10.1007/JHEP11(2014)117

Contents

JHEP11(2014)117

1 Introduction

While the discovery of a Standard Model (SM)-like Higgs boson at 125 GeV has been the most significant result obtained at the Large Hadron Collider (LHC) to date [1, 2], no signal for new physics beyond the SM has yet emerged. Any new colored particle would be the best targets for the LHC due to the large QCD production cross sections. Searches for hadronic final states do, however, suffer from the complicated hadronic environment. Hadronically-quiet new physics searches in leptonic final states are typically challenging due to the smaller electroweak production cross sections, yet the associated SM backgrounds are more clearly understood.

Weak scale supersymmetry (SUSY) is one of the most promising new physics scenarios, and the search for supersymmetric particles continues to be one of the main efforts of LHC studies. LHC SUSY searches have largely focused on gluinos and squarks. The null results have set lower limits of about 1200 GeV and 800 GeV, respectively, for the masses of gluinos and degenerate first- and second- generation squarks [3, 4]. The limits on the electroweak sector of the Minimal Supersymmetric Standard Model (MSSM), however, are much less stringent.

If low energy supersymmetry is realized in the nature, sleptons are likely to be light. This feature emerges in the Gauge Mediated SUSY-breaking scenarios [5] and the Anomaly Mediated SUSY-breaking scenarios [6–8], wherein the slepton masses are proportional to the electroweak gauge couplings. Even in the minimal Gravity Mediated SUSY-breaking scenarios (mSUGRA) [9] where all the scalars have a common mass m_0 at a high energy input scale, renormalization group running to low energies typically pushes up the squark

mass (due to the contributions of strongly interacting gluinos) while the sleptons remain relatively light. The observation of sleptons, even in the presence of the strong lower bounds on squark and gluino masses, would be consistent with these expectations. Thus, it is timely to fully explore the discovery potential of the LHC for the lepton superpartners.

In the R-parity conserving MSSM, the lightest neutralino χ_1^0 can be a natural candidate for Weakly Interacting Massive Particle (WIMP) dark matter [10, 11] when it is the LSP. When sleptons are light, the t-channel process $\chi_1^0\chi_1^0 \to \ell^+\ell^-$ mediated by the exchange of sleptons can be important in determining the χ_1^0 annihilation cross section [12–14], and for fairly degenerate spectra of sleptons and χ_1^0, coannihilation processes can also become important [15]. Therefore, discovery of the sleptons would not only provide a verification of low energy supersymmetry in nature; precise measurement of their masses could also play an important role in determining the relic density of the neutralino LSP.

Light sleptons also contribute to low energy precision observables, such as the electron and proton weak charges that can be measured in parity-violation ee Møller scattering and ep scattering [16, 17], respectively, the muon anomalous magnetic moment [18], or tests of first row CKM unitarity [19]. With the precision achieved (attainable) in current (future) measurements [20, 21], these low energy observables provide an indirect probe of the slepton sector that complements the LHC direct search.

Earlier studies of the slepton discovery potential at the LHC focused primarily on the Drell-Yan pair production of slepton pairs, with each slepton decaying directly to a lepton and χ_1^0 [22–24]. Most of those studies have been performed either in the mSUGRA framework or for a certain set of benchmark points only. Dilepton plus missing E_T final states have also been searched for at the LHC. When the results are interpreted in terms of slepton Drell-Yan pair production with direct decays to a Bino-like LSP, the current limit is fairly weak: $m_{\tilde{\ell}_L} \gtrsim 300\,\text{GeV}$ for left-handed sleptons ($\tilde{\ell}_L$) with a relatively light LSP [25, 26].

Sleptons can also be produced in the cascade decay of gauginos when kinematically accessible. The gaugino pair production cross sections are typically larger than that of the direct slepton Drell-Yan process, given the fermionic nature of the gauginos. Once sleptons are lighter than gauginos, the gaugino dominantly decays to a slepton and lepton, with the slepton subsequently decaying to another lepton and the LSP. For heavier neutralinos and charginos, such lepton-rich final states greatly extends the reach of neutralino and charginos at the LHC [27, 28]. In addition, imposing a sharp cut on the invariant mass distribution of two leptons produced in the χ_2^0 decay could provide further discrimination of the signal from the SM backgrounds, potentially allowing for discovery of the slepton in gaugino decays [29].

The implications of null results in the searches of neutralino/chargino decay via sleptons, however, are limited. First, such experimental searches apply only to the case when sleptons are lighter than heavier gauginos; naturally there is no sensitivity to sleptons from gaugino decays once the decay is kinematically forbidden. Second, even when sleptons are lighter than heavier gauginos, the experimental limits apply only to the case of Wino-like pair-produced gauginos with a Bino-like LSP and are, therefore, only sensitive to the stau or the left-handed slepton ($\tilde{\ell}_L$). Finally, when the χ_2^0 and $\chi_1^\pm$ are Higgsino-like states, no

JHEP11(2014)117

reach in the slepton mass can be derived even if the cascade decay is kinematically allowed, since the branching fraction into sleptons is highly suppressed by the small lepton Yukawa couplings and the small gaugino fractions of the the neutralino and chargino states.

Due to these limitations for the production of sleptons via neutralino/chargino decays, we are motivated to investigate the reach for sleptons via direct slepton Drell-Yan pair production, focusing on same flavor, opposite sign dilepton plus $\not{E}_T$ signal. Earlier studies of the slepton searches at the LHC [22–24] assumed a Bino-like LSP. The sensitivity of this channel, however, depends sensitively on the slepton being either left- or right-handed, as well on the composition of the LSP as being either Bino, Wino, or Higgsino dominated. Utilizing the current search channel of dilepton plus $\not{E}_T$ with data collected at the 8 TeV LHC, we re-interpret the results that have been presented by the ATLAS and CMS collaborations assuming a Bino-like LSP for cases with a Wino-like or a Higgsino-like LSP. We also study the exclusion limits and discovery reach for sleptons at the 14 TeV LHC for various choices of the LSP.

The outline of the paper is as follows. In section 2, we give a brief review of the slepton sector in the MSSM and discuss its dominant production and decay channels for various slepton and neutralino/chargino spectra. In section 3, we summarize the current limits on the slepton searches, from both LEP searches and the latest LHC results. In section 4, we interpret the ATLAS results on the opposite sign dilepton plus $\not{E}_T$ search (which assume a Bino-like LSP) in the cases of Wino-like and Higgsino-like LSP, including additional production from sneutrinos in the case of the $\tilde{\ell}_L$ as well. In section 5, we study the reach for sleptons at the 14 TeV LHC. In section 6, we conclude.

2 Sleptons in the MSSM

2.1 Slepton spectrum

The LHC slepton sensitivity considered here depends on both the slepton pair production cross sections and the detailed nature of the branching fractions for the slepton decays. The latter, in turn, is determined by the electroweakino (chargino/neutralino) spectrum. For simplicity, we consider the low-lying spectrum of the MSSM electroweak sector to include only sleptons, neutralinos and charginos. We also assume negligible flavor mixing between the slepton generations and zero left-right mixing of the first two generation sleptons (motivated by their small Yukawa couplings). We can then label the charged slepton mass eigenstates for the first two generations as $\tilde{\ell}_L$ and $\tilde{\ell}_R$, for $\ell = e,\ \mu$, with masses $m_{\tilde{\ell}_L}$ and $m_{\tilde{\ell}_R}$, respectively. These masses are governed by the soft breaking mass terms m_{SL} and m_{SR}: $m^2_{\tilde{\ell}_L} = m^2_{SL} + \Delta_{\tilde{\ell}_L}$ and $m^2_{\tilde{\ell}_R} = m^2_{SR} + \Delta_{\tilde{\ell}_R}$, where the D-term contributions are $\Delta_{\tilde{\ell}_L} = \left(-\frac{1}{2} - \sin^2\theta_W\right) m_Z^2 \cos 2\beta$ and $\Delta_{\tilde{\ell}_R} = -\sin^2\theta_W m_Z^2 \cos 2\beta$. The sneutrino masses are controlled by m_{SL} as well and are, therefore, related to $m_{\tilde{\ell}_L}$ with a small splitting introduced by electroweak effects: $m^2_{\tilde{\nu}_\ell} = m^2_{\tilde{\ell}_L} + m_W^2 \cos 2\beta$; for the range of $\tan\beta > 1$, $m_{\tilde{\nu}_\ell} < m_{\tilde{\ell}_L}$. The phenomenology and implication of sizable flavor mixing in the slepton sector can be found in refs. [30–32]. For the third generation charged leptons (staus), left-right mixing may be sizable, especially if $\tan\beta$ is large. We focus here on the first two

JHEP11(2014)117

generations of sleptons, although our approach could be adapted to the stau case as well by taking the tau tagging efficiency and stau left-right mixing into account.

The decay of sleptons depends on the composition and spectrum of neutralinos and charginos, which is set mainly by the Bino, Wino, and Higgsino mass parameters M_1, M_2 and μ, respectively. We consider three representative cases:

- Bino-like LSP: $|M_1| < |M_2|,\ |\mu|$, yielding a neutralino LSP χ_1^0 that is Bino-like.
- Wino-like LSP: $|M_2| < |M_1|,\ |\mu|$, yielding a Wino-like LSP χ_1^0 degenerate with $\chi_1^\pm$.
- Higgsino-like LSP: $|\mu| < |M_1|,\ |M_2|$, yielding a Higgsino-like LSP χ_1^0 degenerate with χ_2^0 and $\chi_1^\pm$.

In the Wino-like LSP and Higgsino-like LSP cases, $\chi_1^\pm$ (and χ_2^0 in the Higgsino-like LSP case) decay to the neutralino LSP with very soft jets or leptons that cannot be identified at the LHC. For mass splittings $\Delta m = m_{\chi_1^\pm} - m_{\chi_1^0} \lesssim 200\,\text{MeV}$, however, the associated $\chi_1^\pm$ disappearing charged track can be resolved, allowing for a dedicated $\chi^\pm$ search. The current ATLAS analysis of disappearing-track searches [33] gives a 95% C.L. exclusion of nearly degenerate charginos for masses up to about 500 GeV for $\Delta m \sim 140\,\text{MeV}$. The limits get weaker for increasing Δm. For $\Delta m \gtrsim 200\,\text{MeV}$, the charged tracks cannot be resolved, and the $\chi^\pm$ only appear as $\not{E}_T$. Applying to the various LSP scenarios identified above, we note that in the Wino-like LSP case, arising for example in the anomaly mediated SUSY breaking (AMSB) scenario, the mass splitting is around 160 MeV [34] for large $|\mu| \gtrsim \frac{4\text{TeV}}{\tan\beta}$. Wino masses less than about 270 GeV with this level of degeneracy have been excluded. Smaller values of $|\mu|$, however, increase Δm in the Wino-like LSP case. For the Higgsino-LSP, the mass splittings are typically on the order of a few GeV. Both cases avoid the disappearing-track limits given the relatively large mass splittings. Therefore, in our analysis below, we focus on the scenarios in which the nearly degenerate $\chi_1^\pm$ (and χ_2^0 in the Higgsino-like LSP case) all appear solely as $\not{E}_T$ at the LHC.

In our discussion below, we assume the slepton decays directly to the χ_1^0 LSP (and neutralino/chargino states that are degenerate with the LSP for the Wino- or Higgsino-like LSP cases) plus one lepton, a mode that is most likely to occur when the slepton is lighter than all other heavier neutralinos and charginos. In cases when sleptons are heavier than charginos and neutralinos other than the LSP (and its nearly degenerate neutralino/chargino states), sleptons may decay into those neutralino/chargino states, which subsequently cascade decay to the LSP. The final states from such processes are typically more complicated, involving multi-leptons, multi-jets and $\not{E}_T$. While a slepton search relying on such slepton cascade decays is complementary to the one assuming direct decay of the slepton to the LSP plus a lepton, an analysis of the cascade decay scenario goes beyond the scope of our current study, and we leave it for future work.

2.2 Slepton decays

We now turn to the slepton branching fractions for the three different LSP cases. For the Bino-like LSP, $\tilde{\ell}_L$ and $\tilde{\ell}_R$ both decay to $\ell\chi_1^0$, and $\tilde{\nu}$ decays to $\nu\chi_1^0$ with 100% branching

JHEP11(2014)117

fraction. For the Wino-like LSP, $\tilde{\ell}_L$ decays to $\ell\chi_1^0, \nu\chi_1^\pm$ ($\tilde{\nu}_L$ decays to $\nu\chi_1^0, \ell\chi_1^\pm$) with branching fractions of 33% and 67%, respectively. These branching fractions are set by the $\sqrt{2}$ enhancement of charged current coupling relative to that of the neutral current. The $\tilde{\ell}_R$ decays to $\ell\chi_1^0$ with a branching fraction of nearly 100% via a small Wino−Bino mixing. The decay of $\tilde{\ell}_R$ to $\nu\chi_1^\pm$ is highly suppressed by the small lepton Yukawa couplings.

For the Higgsino-like LSP case, due to the strong suppression of the small lepton Yukawa coupling, $\tilde{\ell}_L$ and $\tilde{\nu}_L$ decay to $\chi_{1,2}^0$ and $\chi_1^\pm$ via the Bino- and Wino-components of $\chi_{1,2}^0$ and $\chi_1^\pm$. The branching fractions to $\chi_{1,2}^0$ depend on the relative Bino and Wino fractions of the $\chi_{1,2}^0$: $|N_{i\tilde{B}}|^2$ and $|N_{i\tilde{W}}|^2$ ($i = 1, 2$), respectively, which are given to leading order in $m_Z/(M_{1,2} \pm \mu)$ by:

$$N_{1\tilde{B}} = (s_\beta + c_\beta)\frac{s_W m_Z}{\sqrt{2}(M_1 - \mu)} \qquad N_{2\tilde{B}} = -(s_\beta - c_\beta)\frac{s_W m_Z}{\sqrt{2}(M_1 + \mu)} \tag{2.1}$$

$$N_{1\tilde{W}} = -(s_\beta + c_\beta)\frac{c_W m_Z}{\sqrt{2}(M_2 - \mu)} \qquad N_{2\tilde{W}} = (s_\beta - c_\beta)\frac{c_W m_Z}{\sqrt{2}(M_2 + \mu)} \tag{2.2}$$

where $s_W = \sin\theta_W$, $c_W = \cos\theta_W$ for θ_W being the weak mixing angle; $s_\beta = \sin\beta$ and $c_\beta = \cos\beta$. In arriving at these expressions, we have assumed that $|M_{1,2} - \mu| \gg m_Z$. Note that the relative sign between the Bino and Wino components of the neutralinos is physical, and has interesting consequences. Similarly, the Wino fractions of $\chi_1^\pm$ are given by the absolute squares of

$$U_{1\tilde{W}^-} = \left(c_\beta + s_\beta \frac{\mu}{M_2}\right)\frac{\sqrt{2}c_W m_Z}{M_2}, \qquad V_{1\tilde{W}^+} = \left(s_\beta + c_\beta \frac{\mu}{M_2}\right)\frac{\sqrt{2}c_W m_Z}{M_2}. \tag{2.3}$$

Note that we have explicitly kept the sub-leading term μ/M_2 in the mixing coefficient since it can be important for the case of large $\tan\beta$ (as c_β goes to zero) in $U_{1\tilde{W}^-}$, which is relevant for $\tilde{\ell}_L$ decays.

The partial decay widths for the charged slepton and sneutrino decays into Higgsino-like LSPs are given approximately by

$$\Gamma(\tilde{\ell} \to \ell\chi_{1,2}^0) = C\ (s_\beta \pm c_\beta)^2 \left(m_Z \frac{s_W^2}{M_1 \mp \mu} - m_Z \frac{c_W^2}{M_2 \mp \mu}\right)^2, \tag{2.4}$$

$$\Gamma(\tilde{\ell} \to \nu_\ell\chi_1^\pm) = C\ 8c_W^4 \left(c_\beta + s_\beta \frac{\mu}{M_2}\right)^2 \left(\frac{m_Z}{M_2}\right)^2, \tag{2.5}$$

$$\Gamma(\tilde{\nu}_\ell \to \nu_\ell\chi_{1,2}^0) = C\ (s_\beta \pm c_\beta)^2 \left(m_Z \frac{s_W^2}{M_1 \mp \mu} + m_Z \frac{c_W^2}{M_2 \mp \mu}\right)^2, \tag{2.6}$$

$$\Gamma(\tilde{\nu}_\ell \to \ell\chi_1^\pm) = C\ 8c_W^4 \left(s_\beta + c_\beta \frac{\mu}{M_2}\right)^2 \left(\frac{m_Z}{M_2}\right)^2, \tag{2.7}$$

where

$$C = \frac{1}{16\pi}\frac{e^2}{4s_W^2 c_W^2}\frac{(m_\mathcal{P}^2 - m_\mathcal{D}^2)^2}{m_\mathcal{P}^3} \tag{2.8}$$

for $m_\mathcal{P}$ and $m_\mathcal{D}$ being the the parent slepton mass and daughter neutralino/chargino mass, respectively. The "±" in eqs. (2.4) and (2.6) correspond to χ_1^0 and χ_2^0, respectively. Given the near degeneracy of $\chi_{1,2}^0$ for the Higgsino states, the rates for decays to these two

JHEP11(2014)117

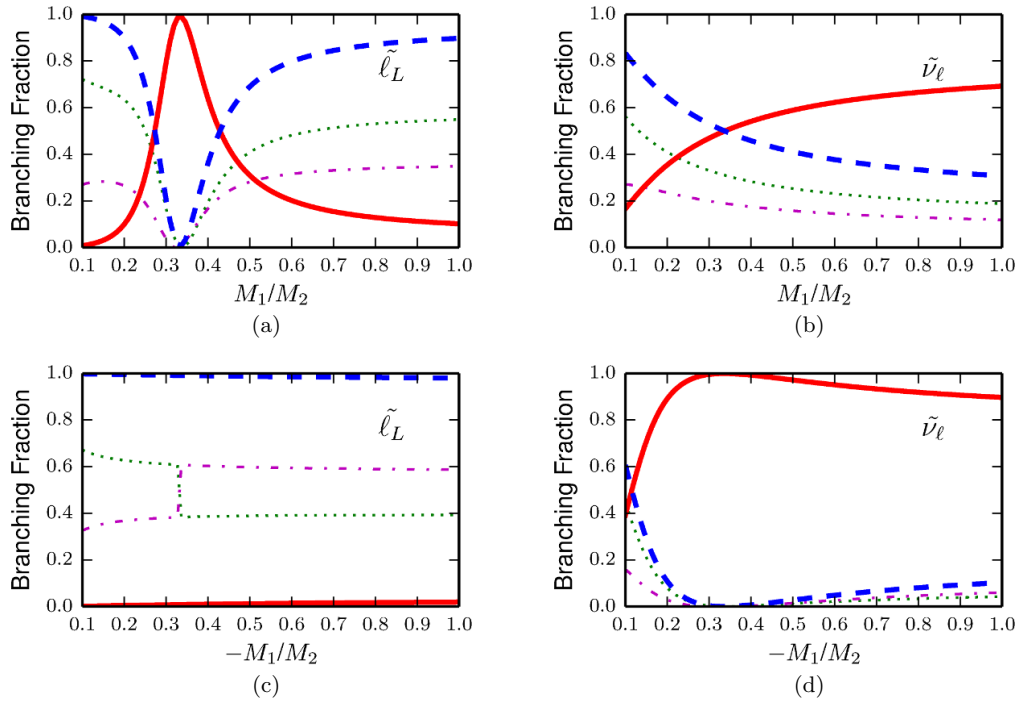

Figure 1. Branching fractions for $\tilde{\ell}_L \to \ell\chi^0_{1,2}, \nu\chi^\pm_1$ (left panels) and $\tilde{\nu} \to \nu\chi^0_{1,2}, \ell\chi^\pm_1$ (right panels) as a function of M_1/M_2. We have fixed $M_1/M_2 > 0$ in (a) and (b) and $M_1/M_2 < 0$ in (c) and (d). Other parameters are chosen as $m_{SL} = 500\,\text{GeV}$, $|M_2| = 10\,\text{TeV}$, $\mu = 100\,\text{GeV}$ and $\tan\beta = 10$. The thick solid red and dashed blue curves are the branching fractions to charginos and neutralinos $(\chi^0_1+\chi^0_2)$, respectively. Also shown in dotted green and dot-dashed magenta lines are the individual decay branching fraction to χ^0_1 and χ^0_2.

channels are usually added together since $\chi^0_{1,2}$ both appear as $\not{E}_T$ at hadron colliders. In the limit of $|\mu| \ll |M_{1,2}|$,

$$\Gamma(\tilde{\ell} \to \ell\chi^0_1 + \ell\chi^0_2) = C\ 2\left(m_Z \frac{s_W^2}{M_1} - m_Z \frac{c_W^2}{M_2}\right)^2, \tag{2.9}$$

$$\Gamma(\tilde{\nu}_\ell \to \nu_\ell\chi^0_1 + \nu_\ell\chi^0_2) = C\ 2\left(m_Z \frac{s_W^2}{M_1} + m_Z \frac{c_W^2}{M_2}\right)^2, \tag{2.10}$$

with no dependence on $\tan\beta$. Decays to charginos, however, show a different $\tan\beta$ dependence for $\tilde{\ell}$ and $\tilde{\nu}_\ell$. The decay $\tilde{\ell} \to \nu_\ell\chi^\pm_1$ depends on $(c_\beta + s_\beta \frac{\mu}{M_2})^2$, which decreases with increasing $\tan\beta$ until $\tan\beta \sim |M_2/\mu|$, when the decay branching fraction stabilizes. On the other hand, $\Gamma(\tilde{\nu}_\ell \to \ell\chi^\pm_1)$ depends only weakly on $\tan\beta$, since $c_\beta\mu/M_2$ is always small compared to s_β, which changes little for large $\tan\beta$. As a result, the branching fractions for $\tilde{\ell}_L$ show a strong $\tan\beta$ dependence since the total decay width varies with $\tan\beta$ because of $\tilde{\ell} \to \nu_\ell\chi^\pm_1$, while the branching fractions for $\tilde{\nu}_\ell$ vary little with respect to $\tan\beta$.

In figure 1, we show the branching fractions for charged slepton and sneutrino decays into Higgsino-like LSP χ^0_1, as well as nearly degenerate Higgsino neutralino χ^0_2 and chargino $\chi^\pm_1$. Other parameters are chosen to be $\tan\beta = 10$, $m_{SL} = 500\,\text{GeV}$, $\mu = 100\,\text{GeV}$ and $|M_2| = 10\,\text{TeV}$. In this paper, we always use $M_1 > 0$ as our convention. In general,

JHEP11(2014)117

there exist only two physical phases involving the electroweak gaugino and Higgsino mass parameters. We assume the gaugino/Higgsino sector introduces no new CP-violation, so these phases simply amount to relative signs. We chose them to be the relative signs of M_1 and M_2 and the relative sign of μ and M_2. As we discuss below, the choice of these phases can have a significant impact on the slepton decay branching fractions. On the other hand, the dependence of the branching fractions on the charged slepton/sneutrino mass or the Higgsino-like LSP mass is weak since the Higgsino-like neutralinos and charginos are almost degenerate and phase space effects cancel out. Note that, within this Higgsino-like LSP regime, when M_1 or M_2 is less than $m_{\tilde{\ell}_L}$ and $m_{\tilde{\nu}_\ell}$, the $\tilde{\ell}_L$ or $\tilde{\nu}_\ell$ first decay into the Bino or Wino-like states that subsequently cascade decay down to the Higgsino LSP. The collider signature would be very different for such a case, which lies beyond the scope of the current study.

Figure 1 (a) shows the M_1/M_2 dependence of branching fractions for $\tilde{\ell}_L$ to $\ell\chi_1^0$ (dotted green curve), $\ell\chi_2^0$ (dot-dashed magenta curve), as well as $\nu_\ell\chi_1^\pm$ (thick solid red curve), for $M_1/M_2 > 0$. The sum of the $\ell\chi_1^0$ and $\ell\chi_2^0$ branching fractions is also given by the thick dashed blue line since these two final states can not be distinguished at the LHC. The curves show the limiting behavior for $M_1 \ll M_2$ where the decays are dominated by the Bino component; for $M_1 \gtrsim M_2$ where the decays are dominated by the Wino component; and behavior in between. For $M_1 \ll M_2$, the branching fractions for decays to neutralinos reach almost 100% since the decay to charginos is suppressed by the relatively small Wino fraction in $\chi_1^\pm$. For $M_1 \gtrsim M_2$, the branching fraction for decays to neutralinos is about 90% since the decay to $\nu_\ell\chi_1^\pm$ is suppressed by either $\cos\beta$ or μ/M_2 compared to decay to neutralinos, as given in eq. (2.5).

There is a notable point at $M_1/M_2 \sim \tan^2\theta_W \approx 0.3$ where the decays to neutralinos vanish due to the cancellation between the contributions of the Bino and Wino fractions in the Higgsino-like neutralinos for $M_1/M_2 > 0$. In this region, decay to charginos, being all that remains, is dominant.

The branching fractions for $\tilde{\nu}_\ell$ decay are shown in figure 1 (b). For sneutrino decays to the chargino, the Wino-Higgsino mixing scales with $\sin\beta$ and so is generically more important than that for the charged slepton decays, unless the Bino component in $\chi_{1,2}^0$ dominates for small M_1/M_2. No minimum for the decays to $\chi_{1,2}^0$ occurs since there is no cancellation between the Bino- and Wino- contribution for $M_1/M_2 > 0$. Decay to neutralinos is dominant for $M_1 \ll M_2$, reaching about 80% for $M_1/M_2 = 0.1$, while decays to charginos dominate for $M_1 \gtrsim M_2$, reaching about 70% for $M_1/M_2 = 1$.

Figure 1 (c) and (d) show the the decays of the charged slepton and sneutrino for $M_1/M_2 < 0$. The $\tilde{\ell}_L \to \chi_{1,2}^0$ branching fraction will not have a minimum in its decay branching fraction since the Bino- and Wino-component interfere constructively in this case. The step in the neutralino branching fraction curves near $M_1/M_2 \sim 0.3$ is due to a switchover between $\frac{1}{\sqrt{2}}(\tilde{H}_u \pm \tilde{H}_d)$ as being the LSP. The branching fractions for $\tilde{\ell}_L \to \ell\chi_{1,2}^0$ almost reaches 100%, due to the relative smallness of the partial decay width for $\tilde{\ell}_L \to \nu_\ell\chi_1^\pm$. $\Gamma(\tilde{\nu}_\ell \to \nu_\ell\chi_{1,2}^0)$, on the other hand, will experience a suppression for $M_1/M_2 \sim -\tan^2\theta_W$, as shown in eq. (2.10).

JHEP11(2014)117

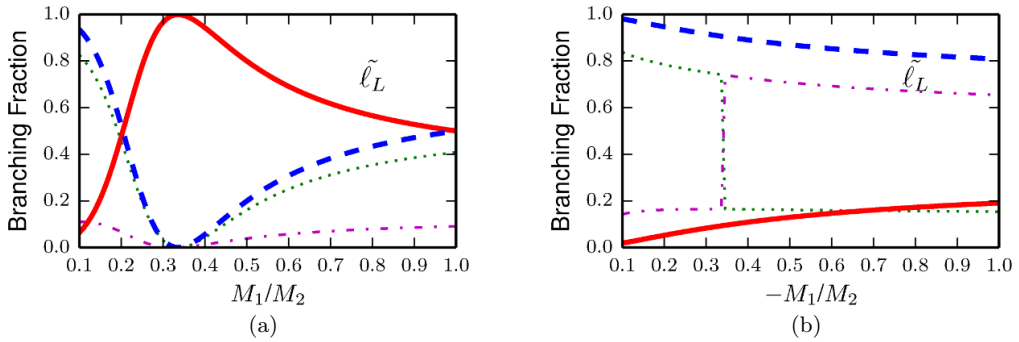

Figure 2. Branching fraction of $\tilde{\ell}_L \to \ell\chi^0_{1,2}, \nu\chi^\pm_1$ as a function of M_1/M_2 for (a) $M_1/M_2 > 0$ and (b) $M_1/M_2 < 0$ with $\tan\beta = 3$. The other parameter choices and color coding are the same as in figure 1.

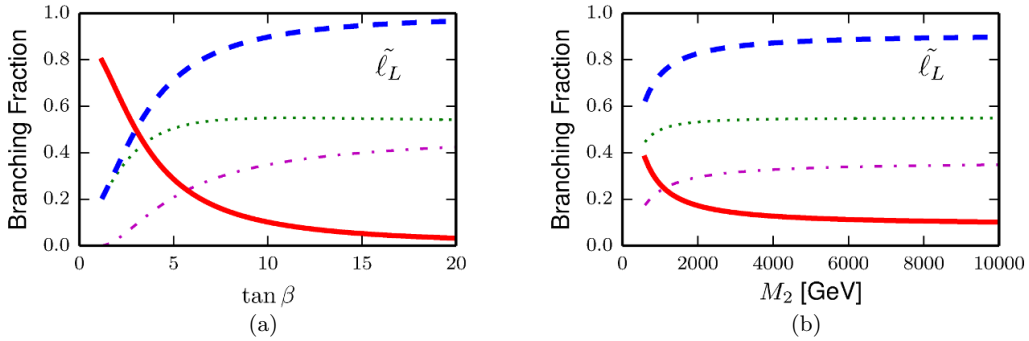

Figure 3. Branching fraction of $\tilde{\ell}_L \to \ell\chi^0_{1,2}, \nu\chi^\pm_1$ as a function of (a) $\tan\beta$ for $M_2 = 10\,\text{TeV}$ and (b) M_2 for $\tan\beta = 10$. We have chosen the other parameters to be $m_{SL} = 500\,\text{GeV}$, $\mu = 100\,\text{GeV}$, $M_1/M_2 = 1$.

Figure 2 shows the dependence of charged slepton branching fractions on M_1/M_2 for $\tan\beta = 3$. While the generic features are the same as figure 1 for $\tan\beta = 10$, the decay fraction for $\tilde{\ell} \to \nu_\ell\chi^\pm_1$ is relatively larger due to the enhancement of $\Gamma(\tilde{\ell} \to \nu_\ell\chi^\pm_1)$ arising from the larger value of $\cos\beta$. For $M_1/M_2 = 1$, decay branching fractions to $\ell\chi^0_{1,2}$ and $\nu_\ell\chi^0_{1,2}$ are about 50% each. Similarly, for $M_1/M_2 < 0$, the branching fraction of decays to neutralinos is about 80% to 100%, while the decays to charginos could be as large as 20%.

Figure 3 (a) shows the $\tan\beta$ dependence for the $\tilde{\ell}_L \to \ell\chi^0_{1,2}, \nu\chi^\pm_1$ branching fractions for $m_{SL} = 500\,\text{GeV}$, $\mu = 100\,\text{GeV}$, $M_1/M_2 = 1$ and $M_2 = 10\,\text{TeV}$. For $\tan\beta < M_2/\mu$ such that $\cos\beta$ is much greater than $s_\beta\mu/M_2$, the $\tilde{\ell}_L \to \nu_\ell\chi^\pm_1$ branching fraction always decreases as $\tan\beta$ increases, with $\tilde{\ell}_L \to \ell\chi^0_{1,2}$ becoming dominant for $\tan\beta \gtrsim 10$. Figure 3 (b) shows the M_2 dependence of charged slepton decay branching fraction for $\tan\beta = 10$. The dependence of charged slepton decay branching fractions on M_2 is also weak unless $\tan\beta > M_2/\mu$, when $\Gamma(\tilde{\ell} \to \nu_\ell\chi^\pm_1)$ could have an explicit M_2 dependence. The $\tilde{\ell}_L \to \nu_\ell\chi^\pm_1$ branching fraction decreases as M_2 increases, saturating when $M_2/\mu > \tan\beta$. The sneutrino decay branching fraction, on the other hand, depends mildly on $\tan\beta$ and M_2.

JHEP11(2014)117

	$\tilde{\ell}_L \to \ell\chi^0_{1(2)}$	$\tilde{\ell}_L \to \nu\chi^\pm_1$	$\tilde{\nu} \to \nu\chi^0_{1(2)}$	$\tilde{\nu} \to \ell\chi^\pm_1$	$\tilde{\ell}_R \to \ell\chi^0_{1(2)}$
Bino-like LSP	100%		100%		100%
Wino-like LSP	33.3%	66.7%	33.3%	66.7%	100%
Higgsino-like LSP (I)	0.8%	99.2%	50.3%	49.7%	100%
Higgsino-like LSP (II)	99.1%	0.9%	0.0%	100.0%	100%

Table 1. Branching fractions of charged sleptons and sneutrinos into Bino-, Wino- and Higgsino-like LSPs. We have set $m_{SL} = 500\,\text{GeV}$, $\tan\beta = 10$, and used an LSP mass parameter of 100 GeV. For the Higgsino-like LSP case, we presented the results for two representative benchmark values: (I) $M_1/M_2 = 1/3$ and (II) $M_1/M_2 = -1/3$ with $|M_2| = 10\,\text{TeV}$.

Note that in the foregoing discussion of the $\tilde{\ell}_L$ and $\tilde{\nu}_\ell$ decays to Higgsino-like LSPs, we have considered the case of $M_1 > 0$ and $\mu > 0$, with two different signs for M_2. The relative sign between these three mass parameters is physical, and the behavior of the branching fractions will change when one of these parameters flips sign. For $\mu/M_2 < 0$, decays to charginos will be relatively suppressed compared to the $\mu/M_2 > 0$ case, in particular for $\tilde{\ell}_L$, as shown in eq. (2.5).

For the $\tilde{\ell}_R$, it again decays to $\ell\chi^0_{1,2}$ 100% via the Bino-component of $\chi^0_{1,2}$ since the decay to $\chi^\pm_1$ is suppressed by the small lepton Yukawa couplings.

Given the branching fraction dependence on M_1/M_2, as well as $\tan\beta$, for the Higgsino-like LSP case, we consider two benchmark choices for M_1/M_2 to represent two extreme cases: (I) $M_1/M_2 = 1/3$ with suppressed $\Gamma(\tilde{\ell}_L \to \ell\chi^0_{1,2})$ and (II) $M_1/M_2 = -1/3$ with suppressed $\Gamma(\tilde{\nu}_\ell \to \nu_\ell\chi^0_{1,2})$ (therefore enhanced decays to charged leptons). The corresponding branching fractions are given in table. 1. Case (I) leads to a suppressed overall cross section for dilepton plus $\not{E}_T$ final states, while case (II) leads to an enhancement. These cases are the upper and lower boundaries of the envelope of possible signal rates in the Higgsino-like LSP scenario.

2.3 Slepton production and signatures

For Drell-Yan pair production of sleptons $\tilde{\ell}_L\tilde{\ell}_L$, $\tilde{\ell}_L\tilde{\nu}_\ell$, $\tilde{\nu}_\ell\tilde{\nu}_\ell$ and $\tilde{\ell}_R\tilde{\ell}_R$ with dominant direct decay of sleptons into χ^0_1 (and $\chi^\pm_1$, χ^0_2 for Wino-like and Higgsino-like LSP cases), the collider signatures are dilepton plus $\not{E}_T$, single lepton plus $\not{E}_T$, and $\not{E}_T$ only. The single lepton channel suffers from large SM backgrounds, mainly driven by W boson production. The $\not{E}_T$ only signature requires an extra jet or lepton from initial or final state radiation, which leads to more suppressed cross sections. Current collider searches for slepton Drell-Yan production focus on the final state of two isolated energetic leptons plus $\not{E}_T$ [27, 28]. The SM backgrounds are typically large, dominantly from WW or $t\bar{t}$. In our analyses below, we focus on the dilepton plus $\not{E}_T$ channel and reinterpret the current 8 TeV LHC slepton search limits for various LSP scenarios, as well as project the reach of the LHC at 14 TeV. In particular, we include contributions from the presence of sneutrinos for the case of left-handed sleptons, as their mass is related to the left-handed slepton mass and they can contribute to the dilepton and missing energy signature for non-Bino-like LSPs.

JHEP11(2014)117

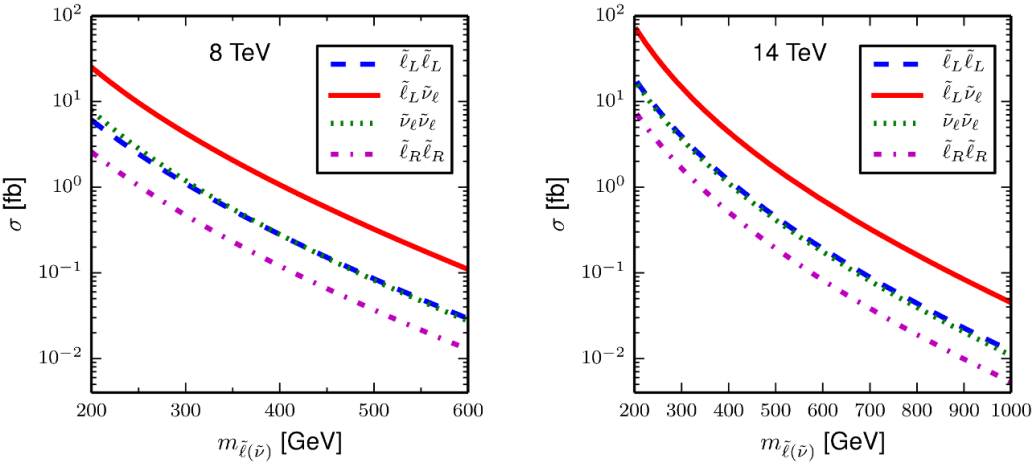

(a) (b)

Figure 4. Leading-order cross sections for the Drell-Yan pair production of $\tilde{\ell}_L\tilde{\ell}_L$ (dashed blue), $\tilde{\ell}_L\tilde{\nu}_\ell$ (solid red), $\tilde{\nu}_\ell\tilde{\nu}_\ell$ (dotted green) and $\tilde{\ell}_R\tilde{\ell}_R$ (dot-dashed magenta) for the (a) 8 TeV and (b) 14 TeV LHC.

In figure 4, we show the individual leading order Drell-Yan pair production cross sections for $\tilde{\ell}_L\tilde{\ell}_L$, $\tilde{\ell}_L\tilde{\nu}_\ell$, $\tilde{\nu}_\ell\tilde{\nu}_\ell$ and $\tilde{\ell}_R\tilde{\ell}_R$ at the LHC with $\sqrt{s} = 8$ TeV and 14 TeV. The production of $\tilde{\ell}_L\tilde{\nu}_\ell$ is markedly larger than the other cross sections, ranging from 25 to 0.1 fb for $\sqrt{s} = 8$ TeV for masses from 200 to 600 GeV and from 70 to 0.04 fb for $\sqrt{s} = 14$ TeV for masses from 200 GeV to 1 TeV. Sneutrino and left-handed charged slepton pair production are comparable in size and smaller than the production by about a factor of 3, while right-handed slepton pair production, due to a cancellation between the Z and γ s-channel graphs, is smaller still, about an order of magnitude less than the associated production cross section. The NLO K-factors are approximately 1.18 [43], independent of which particular pair production considered, as the QCD structure of the graphs is identical in all four cases.

In figure 5, we show the signal cross section, the sum of all possible slepton production cross sections multiplied by the branching fraction leading to dilepton plus $\not{E}_T$ final states as a function of slepton mass for the (a) 8 TeV and (b) 14 TeV LHC. For the left-handed slepton, we have included the contributions from $\tilde{\ell}_L\tilde{\ell}_L$, $\tilde{\nu}_L\tilde{\nu}_L$ and $\tilde{\ell}_L\tilde{\nu}_L$. The Higgsino-like LSP benchmark (II) for light $\tilde{\ell}_L$ with $M_1/M_2 = -1/3$ represents the most promising scenario since sleptons decay dominantly to $\ell\chi^0_{1,2}$ while sneutrinos decay dominantly to $\ell\chi^\pm_1$. The cross sections range from about 70 fb to 0.3 fb for slepton masses from 200 to 600 GeV at the 8 TeV LHC, and from 200 fb to 0.1 fb at the 14 TeV LHC for slepton masses from 200 GeV to 1 TeV. The Higgsino-like LSP benchmark (I) for light $\tilde{\ell}_L$ with $M_1/M_2 = 1/3$ represents the worst-case scenario with a strong suppression of slepton decays to leptons. For the Bino- and Wino-like LSP scenarios, the signal cross sections range from 40 fb to about 0.01 fb for slepton mass between 200 GeV to 1 TeV at the 14 TeV LHC. Right-handed sleptons are less promising than all the left-handed cases except for the highly pessimistic

JHEP11(2014)117

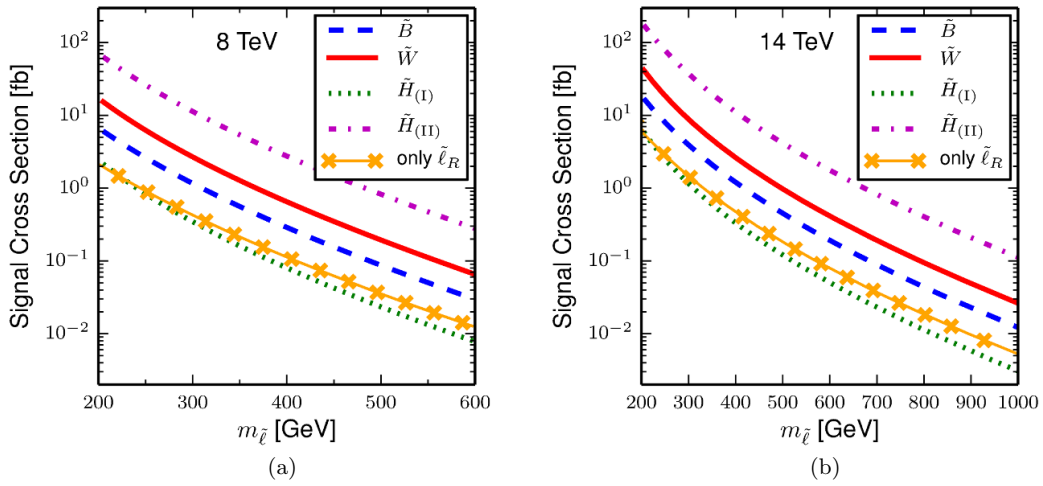

Figure 5. Sum of all possible production mechanisms weighted by branching fraction for dilepton plus $\not{E}_T$ final states as a function of slepton mass for the (a) 8 TeV and (b) 14 TeV LHC.

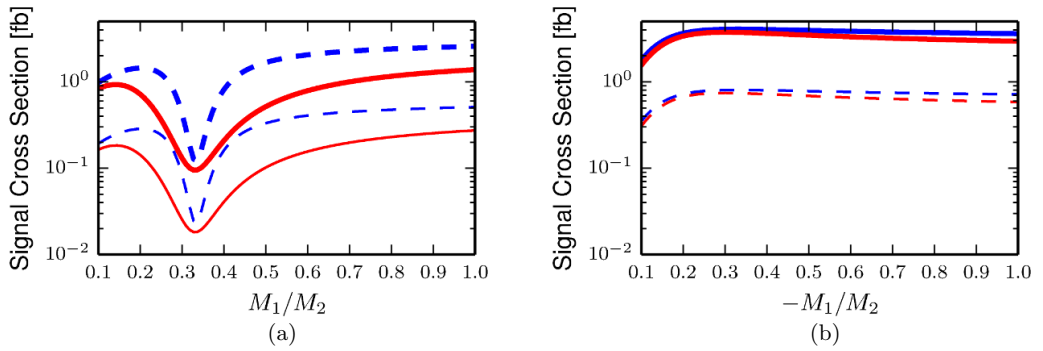

Figure 6. $\sigma \times \mathrm{Br}$ for dilepton plus $\not{E}_T$ final states in a Higgsino-like LSP scenario as a function of M_1/M_2 for (a) $M_1/M_2 > 0$ and (b) $M_1/M_2 < 0$. Thick curves and thin curves are for 14 TeV and 8 TeV, respectively. Dashed blue curves are for $\tan\beta = 10$ and solid red curves are for $\tan\beta = 3$. Other parameters are chosen as $m_{SL} = 500\,\mathrm{GeV}$ and $|M_2| = 10\,\mathrm{TeV}$.

Higgsino benchmark (I), ranging in signal cross section from 7 fb to 0.005 fb at the 14 TeV LHC.

To show the strong dependence of $\tilde{\ell}_L$, $\tilde{\nu}$ decay branching fractions on the sign and value of M_1/M_2, in figure 6 we plot the $\sigma \times \mathrm{Br}$ for dilepton plus $\not{E}_T$ final states for the Higgsino-like LSP case with a light $\tilde{\ell}_L$ as a function of M_1/M_2 at the 14 (8) TeV LHC, which are indicated by thick (thin) curves. The dip in the positive M_1/M_2 case results from the suppressed charged slepton decay branching fractions to leptons at $M_1/M_2 \sim \tan^2\theta_W$, with an overall cross section of about 0.1 fb at the 14 TeV LHC with $\tan\beta = 10$. The maximum value for $\sigma \times \mathrm{Br}$ appears at $M_1/M_2 \sim -\tan^2\theta_W$ due to the enhanced sneutrino decay branching fractions to leptons, with an overall cross section of about 4.0 fb. For

JHEP11(2014)117

$|M_1/M_2| \ll 1$, the Bino component in the Higgsino states $\chi^0_{1,2}$ is dominant and the cross section is about 1 fb at the 14 TeV LHC, while the cross section reaches about $2.6 - 3.6$ fb for $|M_1/M_2| \gtrsim 1$. Smaller values of $\tan\beta$ typically lead to smaller signal cross sections.

3 Current searches and studies

The least model-dependent bounds on sleptons are obtained from LEP searches for dilepton plus missing energy signatures [35] with $\sqrt{s}$ up to 208 GeV. For a slepton-neutralino LSP mass splitting greater than 15 GeV, the right-handed slepton mass limits are: $m_{\tilde{e}_R} > 99.6$ GeV, $m_{\tilde{\mu}_R} > 94.9$ GeV and $m_{\tilde{\tau}_R} > 85.9$ GeV. For left-handed sleptons with a Bino-like LSP, the bounds are stronger due to the larger production cross section. For tau sleptons, on the other hand, the presence of significant left-right mixing can decrease the production cross section for the lightest stau pair, leading to more relaxed limits. A lower limit of $m_{\tilde{\tau}} > 85.0$ GeV can be obtained when the production cross section for the lightest stau is minimized. It should be noted that the slepton mass limits are obtained with $\mu = -200$ GeV and $\tan\beta = 1.5$, a point at which the neutralino mass limit based on the LEP neutralino and chargino searches is the weakest, and the selectron cross section is relatively small.

The foregoing bounds also assume the gaugino mass unification relation $M_1 = (5/3)\tan^2\theta_W M_2$, which is relevant in fixing the neutralino mass and field content, with the neutralino LSP being mostly Bino-like. Slepton mass limits would change for a non-unified mass relation between M_1 and M_2. In the case where the $\tilde{e}_R - \chi^0_1$ mass splitting is small and the usual dilepton search is insensitive, a single lepton plus missing energy search yields a lower limit on $m_{\tilde{e}_R}$ of 73 GeV, independent of $m_{\chi^0_1}$ [36, 37]. For sneutrinos, a mass limit of 45 GeV can be deduced from the invisible Z decay width [38]. An indirect mass limit on sneutrinos can also be derived from the direct search limits on the charged slepton masses, but for LEP searches it is not competitive with the invisible width constraint.

Searches for first and second generation charged sleptons have been performed by both the ATLAS [25, 27] and CMS collaborations [26]. With about 20 fb^{-1} luminosity collected at 8 TeV, both collaborations studied the signal of opposite-sign (OS) same flavor (SF) dilepton plus missing E_T from the electroweak pair production of sleptons assuming a 100% decay branching fraction for $\tilde{\ell}^{\pm} \to \ell^{\pm} + \chi^0_1$. The most stringent bounds come from the ATLAS results, which exclude left-handed (right-handed) slepton masses between 95 and 310 GeV (235 GeV) at 95% C.L. for a Bino-like LSP with $m_{\chi^0_1} = 0$ GeV. For larger χ^0_1 masses, the upper range of the exclusion reach does not change while the lower bound shifts approximately as 80 GeV $+m_{\chi^0_1}$.

4 Recasting LHC 8 TeV search limits

We consider the signal consisting of two same flavor, opposite sign energetic leptons (electrons or muons) plus significant missing energy at the 8 TeV LHC. The dominant SM backgrounds arise from $t\bar{t}$ and di-boson production. We use Madgraph 5 version v1.4.7 and Madevent v5.1.4.7 [39] to generate our signal events. These events are passed to Pythia v6.426 [40] to simulate initial state radiation, final state radiation, showering and

JHEP11(2014)117

hadronization. Additionally we use Delphes v3.0.10 [41] with the Snowmass card [42] to simulate detector effects. We chose not to simulate pile-up to increase computational speed because we are considering a clean leptonic final state which should not be sensitive to pile-up. The event generation procedure produces events at leading order. NLO effects are taken into account by scaling our events by an appropriate K-factor [43]. We additionally take into account various experimental efficiencies that may be poorly modeled by our crude detector simulation by scaling our signal yields to match the expected yields quoted in the experimental search [25].

Following the 8 TeV dilepton search technique at the ATLAS [25, 27], we apply the following cuts:

- Exactly two leptons (electron or muon) with $p_T^\ell > 10\,\text{GeV}$ and $|\eta^\ell| < 2.5$. The invariant mass of the lepton pair is required to be greater than 20 GeV and to be away from the Z-pole: $|m_{\ell\ell} - m_Z| > 10\,\text{GeV}$.

- Jet veto with $p_T^j < 20\,\text{GeV}$ for central jets with $|\eta^j| < 2.4$; $p_T^j < 30\,\text{GeV}$ for forward jets with $2.4 < |\eta^j| < 4.5$.

- $\not{E}_T{}^{\text{rel}} > 40\,\text{GeV}$, with

$$\not{E}_T{}^{\text{rel}} = \begin{cases} \not{E}_T \sin\left(\Delta\phi^{\ell,j}\right) & \text{for } \Delta\phi^{\ell,j} < \pi/2 \\ \not{E}_T & \text{otherwise} \end{cases}, \tag{4.1}$$

  where $\Delta\phi^{\ell,j}$ is the azimuthal angle between the direction of p_T^{miss} and the nearest lepton or central jet.

- $M_{T2} > 90$ or 110 GeV where M_{T2} is the stransverse mass variable [44–46]. We choose the optimized cut to give the higher value of $S/\sqrt{B}$ for each point in signal parameter space, where S (B) is the number of signal (background) events.

For the signal process, our simulation matches well with the ATLAS distributions for the given benchmark points after a scaling by factor of 1.25 for both di-electron and di-muon channels that accounts for both a K-factor expected to be 1.18 and differences in reconstruction efficiencies. We use this scaling factor in all subsequent calculations for 8 TeV.

To reproduce the exclusion plot from the ATLAS paper we utilized the CL_s method discussed in [47, 48]. We generate signal events using Monte-Carlo to determine the signal strength over the range of parameters $90 < m_{\tilde{\ell}} < 600\,\text{GeV}$ and $25 < m_{\chi_1^0} < m_{\tilde{\ell}} - 30\,\text{GeV}$. For our SM backgrounds, we simply use the number of events predicted by the ATLAS experiment for each cut scenario [25]. We follow the method in the ATLAS paper where we choose the M_{T2} cut that maximizes $S/\sqrt{B}$. We also demand that the signal to background is greater than a minimal threshold: $S/B > 0.1$. We reproduced the exclusion limits for the Bino-like LSP for left- and right-handed sleptons, indicated by the dashed blue line and orange line with crosses, respectively, in figure 7 (a). Our bounds reproduce the ATLAS search results well with slight discrepancy at low masses.

JHEP11(2014)117

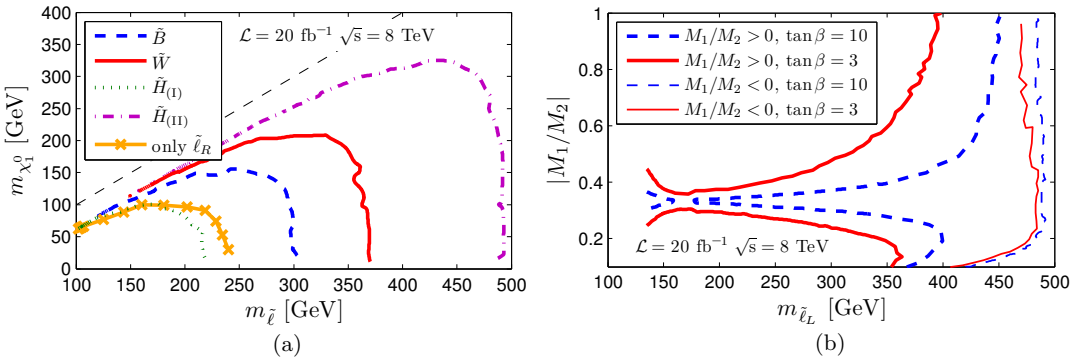

Figure 7. Recast of ATLAS dilepton plus $\not{E}_T$ search results [25] with 20 fb^{-1} luminosity data collected at the 8 TeV LHC. The left panel shows the 95% C.L. exclusion limits in the $m_{\tilde{\ell}} - m_{\tilde{\chi}_1^0}$ plane for the left-handed slepton with Bino-like LSP (dashed blue line), Wino-like LSP (solid red line), Higgsino-like LSP with $M_1/M_2 = 1/3$ (dotted green line), $M_1/M_2 = -1/3$ (dot-dashed magenta line), as well as for the right-handed slepton (orange line with crosses). The right panel shows the 95% C.L. exclusion bounds in the $m_{\tilde{\ell}_L} - |M_1/M_2|$ plane for the left-handed slepton with a Higgsino-like LSP, for $M_1/M_2 > 0$ (thick lines) with $\tan\beta = 10$ (dashed blue), 3 (solid red), and $M_1/M_2 < 0$ (thin lines). All other parameters are fixed to be $\mu = 100$ GeV and $|M_2| = 10$ TeV.

As discussed in detail in section 2, the decay branching fractions of left-handed charged sleptons and sneutrinos depend strongly on the composition of the neutralino LSP, and in particular on the sign and value of M_1/M_2 in the Higgsino-like LSP scenario. For a given slepton mass, the resulting dilepton $+\not{E}_T$ final states cross section, therefore, varies with the choice of LSP scenario. In figure 7 (a), we recast the current 8 TeV ATLAS slepton search results in the dilepton $+\not{E}_T$ channel for the various benchmark scenarios given in table 1. For cases where $m_{\tilde{\ell}} \gtrsim m_{\tilde{\chi}} + 50$ GeV , we find that the Wino-like LSP scenario is excluded for slepton masses below approximately 365 GeV, while the pessimistic and optimistic Higgsino-like LSP scenarios imply exclusion of sleptons lighter than about 220 GeV and 495 GeV, respectively.

To show the dependence of limits on M_1/M_2 in the Higgsino-like LSP scenario, we plot in figure 7 (b) the 95% C.L. limits in the parameter space of $|M_1/M_2|$ versus $m_{\tilde{\ell}_L}$ with the Higgsino-like LSP mass set to be 100 GeV. The thick curves are for $M_1/M_2 > 0$ whereas the thin curves are for $M_1/M_2 < 0$. Regions to the left of the curves are excluded (excepting the small blue wedge of unconstrained light sleptons on the left edge of the plot). The suppression of signal for positive $M_1/M_2 \sim \tan^2\theta_W$ is clearly visible in the blue curves, where sensitivity drops precipitously to much lower masses. We also note that the low mass region of $m_{\tilde{\ell}} \lesssim 150$ GeV for $\tan\beta = 10$ cannot be excluded for this LSP mass due to the loss of sensitivity for small mass splitting between the slepton and the LSP. The exclusion region for $\tan\beta = 3$ is even weaker due to the suppression of the signal cross sections, with no sensitivity for any slepton masses when $0.3 < M_1/M_2 < 0.35$. In the negative M_1/M_2 case, by comparison, the slepton mass exclusion is significantly stronger ($m_{\tilde{\ell}} \gtrsim 470 - 490$ GeV) and relatively insensitive to $|M_1/M_2|$ until it gets fairly small, when the $m_{\tilde{\ell}}$ reach is reduced due to the suppression of $\Gamma(\tilde{\nu}_L \to \ell\chi_1^{\pm})$.

JHEP11(2014)117

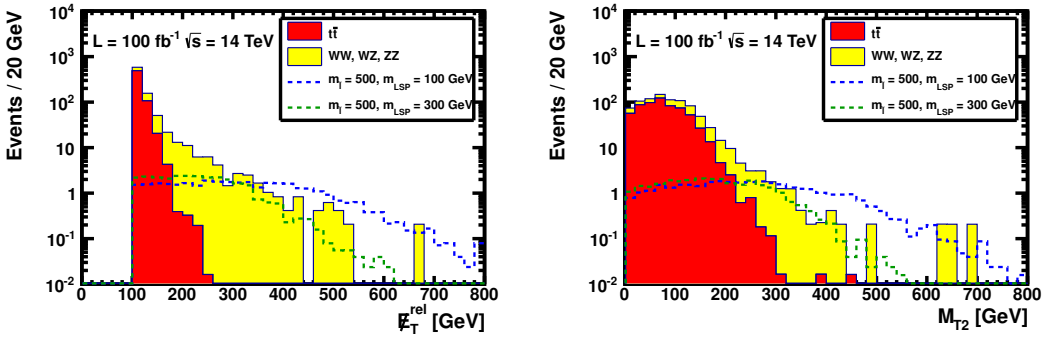

(a) (b)

Figure 8. Signal and background distributions for (a) $\not{E}_T{}^{\rm rel}$ and (b) M_{T2} for 100 fb^{-1} integrated luminosity at the 14 TeV LHC. Selection cuts, jet veto, Z veto, and $\not{E}_T{}^{\rm rel}$ cut of 100 GeV have been imposed. The signal distributions are shown for two benchmark points of $(m_{\tilde{\ell}_L}, m_{\tilde{\chi}_1^0}) = (500, 100)$ GeV and $(m_{\tilde{\ell}_L}, m_{\tilde{\chi}_1^0}) = (500, 300)$ GeV with a Bino-like LSP.

5 14 TeV exclusion and discovery reach

We now turn to projections for Run II at the LHC, with 14 TeV center-of-mass energy. As with the 8 TeV LHC analysis, we consider the dilepton $+\not{E}_T$ channel and generate the signal and background Monte-Carlo events in the same manner as in section 4. For the signal process, we used the next-to-leading order production cross section for sleptons as given in ref. [43]. Background processes are scaled with K-factors from ref. [49]. We generate the signal over the range of parameters $200 < m_{\tilde{\ell}} < 1000$ GeV and $25 < m_{\chi_1^0} < m_{\tilde{\ell}} - 30$ GeV. We also demand $S > 2$, $B > 2$, and $S/B > 0.1$.

For the 14 TeV analysis, we adopted the following cuts:

- 2 isolated leptons (electron or muon) with $p_T^\ell > 50$ GeV, $|\eta^\ell| < 2.5$, and $m_{\ell\ell} > 20$ GeV.
- No jets with $p_T^j > 50$ GeV and $|\eta^j| < 4.5$.
- Z veto with $|m_{\ell\ell} - m_Z| > 10$ GeV.
- Optimized cuts on $\not{E}_T{}^{\rm rel}$ and M_{T2}. Cuts range from $100 < \not{E}_T{}^{\rm rel} < 200$ GeV and $0 < M_{T2} < 200$ GeV in increments of 50 GeV.

In figure 8, we show the $\not{E}_T{}^{\rm rel}$ and M_{T2} distributions for both the backgrounds and two signal benchmark points of $(m_{\tilde{\ell}_L}, m_{\tilde{\chi}_1^0}) = (500, 100)$ GeV and $(m_{\tilde{\ell}_L}, m_{\tilde{\chi}_1^0}) = (500, 300)$ GeV with a Bino-like LSP after imposing the selection cuts, jet and Z vetoes, and minimum $\not{E}_T{}^{\rm rel}$ cut of 100 GeV. We observe that the backgrounds and signal (for the larger slepton-LSP mass splitting) become comparable at $\not{E}_T{}^{\rm rel}$ and M_{T2} on the order of 300 GeV, naïvely suggesting imposing cuts in the vicinity of this region. However, the background distributions tend to fall quickly at higher $\not{E}_T{}^{\rm rel}$ and M_{T2}, so to obtain sufficient statistics we impose somewhat looser cuts, with the requirements on B, S and S/B listed above.

JHEP11(2014)117

	Signal		$t\bar{t}$		Di-boson	
	ee	$\mu\mu$	ee	$\mu\mu$	ee	$\mu\mu$
CS [fb]	3.2×10^{-1}	3.2×10^{-1}	4.0×10^{3}	4.0×10^{3}	8.3×10^{2}	8.3×10^{2}
Selection Cuts	80%	82%	14%	16%	12%	14%
Jet Veto	64%	66%	4%	4%	10%	11%
Z Veto	64%	65%	4%	4%	9%	10%
$M_{T2} > 50$ GeV	51%	52%	1%	1%	2%	2%
$\not{E}_T^{\rm rel} > 150$ GeV	33%	34%	$< 0.01\%$	$< 0.01\%$	0.03%	0.02%
CS after cuts [fb]	1.1×10^{-1}	1.1×10^{-1}	1.0×10^{-5}	1.7×10^{-5}	2.2×10^{-1}	1.6×10^{-1}
$S/\sqrt{B}$ @ 100 fb^{-1}		combined:	3.5			

Table 2. Cut efficiency for benchmark point of $(m_{\tilde{\ell}_L}, m_{\tilde{\chi}_1^0}) = (500, 100)$ GeV with a Bino-like LSP, using cuts specified above. Signal significance is shown for the combined ee and $\mu\mu$ channels using 100 fb^{-1} of data at the 14 TeV LHC. The $t\bar{t}$ cross section before the selection cuts already include a precut of $p_T^j < 100$ GeV.

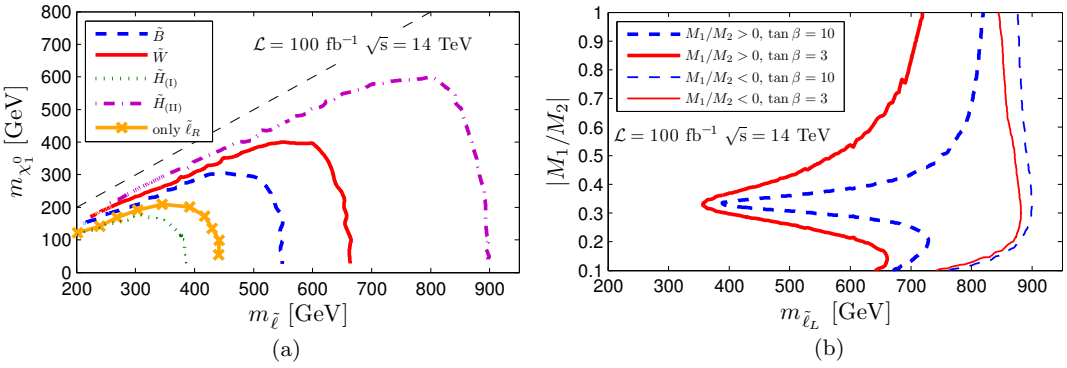

Figure 9. Prospective 95% C.L. exclusion limits in the (a) $m_{\tilde{\ell}} - m_{\chi_1^0}$ plane, (b) $m_{\tilde{\ell}_L} - |M_1/M_2|$ plane for slepton pair production with dilepton $+\not{E}_T$ final states, with 100 fb^{-1} luminosity at the 14 TeV LHC for various LSP scenarios. The color coding and parameter choices are the same as in figure 7.

The resulting, illustrative cut efficiencies are listed in table 2 for the benchmark point of $(m_{\tilde{\ell}_L}, m_{\tilde{\chi}_1^0}) = (500, 100)$ GeV with a Bino-like LSP.

The resulting, prospective 95% C.L. expected exclusion limits in the $m_{\tilde{\ell}} - m_{\chi_1^0}$ plane are given in figure 9 (a) for the 14 TeV LHC with 100 fb^{-1} integrated luminosity for various slepton and neutralino LSP scenarios. For the right-handed slepton, the reach is about 430 GeV for small LSP masses. For the left-handed sleptons, the reach is 550 GeV (670 GeV) for the Bino-like (Wino-like) LSP case, and about 400 GeV and 900 GeV for the Higgsino-like LSP cases (I) and (II), respectively. We find the reach with 300 fb^{-1} is typically about $50 - 100$ GeV better. A 5% systematic error has been included in our limits to give a reasonably realistic reach for the LHC.

The prospective 14 TeV exclusion reach in the $m_{\tilde{\ell}} - |M_1/M_2|$ plane for the Higgsino-like LSP case is shown in figure 9 (b) for 100 fb^{-1} integrated luminosity. Regions to the left-side of the curves are excluded. The weakest reach is for the $M_1/M_2 > 0$ case with

JHEP11(2014)117

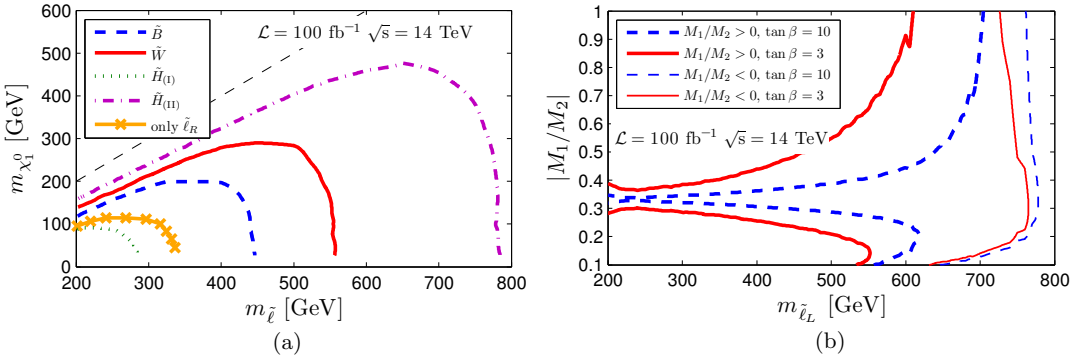

Figure 10. 5σ discovery reach at the 14 TeV LHC in the (a) $m_{\tilde{\ell}} - m_{\chi_1^0}$ plane, (b) $m_{\tilde{\ell}_L} - |M_1/M_2|$ plane for slepton pair production with dilepton $+\not{E}_T$ final states, with 100 fb^{-1} integrated luminosity for various LSP scenarios. The color coding and parameter choices are the same as in figure 7.

small $\tan\beta$. In particular, for $M_1/M_2 \sim \tan^2\theta_W$, the slepton mass reach is only about 350 GeV for $\tan\beta = 3$ with 100 fb^{-1} luminosity. The slepton mass reach increases when M_1/M_2 deviates from $\tan^2\theta_W$, approaching about 650 GeV for small M_1/M_2 and 710 GeV for large M_1/M_2. The slepton mass reach for negative M_1/M_2 is typically better, around $800 - 900$ GeV, a pattern similar to that found in the 8 TeV analysis. Comparing with figure 7 (b) we observe that the presently allowed region for small $m_{\tilde{\ell}}$ in the Higgsino-like LSP scenario with $M_1/M_2 > 0$ could be excluded with the higher energy run. For $M_1/M_2 < 0$, the exclusion reach becomes as much as a factor of two stronger than at present with 300 fb^{-1} integrated luminosity.

In figure 10 (a) we show the 5σ discovery reach for the various LSP benchmark scenarios we have considered previously. The maximum reach occurs for the Higgsino-like LSP with $M_1/M_2 = -1/3$, for which sleptons as heavy as ~ 800 GeV could be discovered with 100 fb^{-1} integrated luminosity. For a very light LSP, the reach is roughly three times weaker for $M_1/M_2 = 1/3$ case, while the reach for the Wino- and Bino-like LSP scenarios fall in between. Figure 10 (b) gives the corresponding discovery potential in the $m_{\tilde{\ell}_L} - |M_1/M_2|$ plane for a Higgsino-like LSP. While no sensitivity for slepton could be achieved for the worse case scenario of $M_1/M_2 \sim \tan^2\theta_W$, reaches in $m_{\tilde{\ell}}$ increases when M_1/M_2 deviates from this value. For $M_1/M_2 < 0$, 5σ reach can be as large as 800 GeV. With 300 fb^{-1} at the 14 TeV LHC, the reach is improved by about $50 - 100$ GeV.

6 Summary and conclusion

With the absence thus far of any superpartner signals at the LHC, the attention for LHC Run-II (14 TeV) will clearly require emphasis on more difficult-to-observe signatures. Among the most challenging are those associated with sleptons, given the $\mathcal{O}$(fb) electroweak production cross sections. In this work, we studied the dependence of slepton decay branching fractions on the nature of the LSP. In particular, in the Higgsino-like LSP scenarios, both decay branching fractions of $\tilde{\ell}_L$ and $\tilde{\nu}_\ell$ exhibit strong dependence on the

JHEP11(2014)117

sign and value of M_1/M_2: $\tilde{\ell}_L \to \ell\chi^0_{1,2}$ is minimized for $M_1/M_2 \sim \tan^2\theta_W$, while $\tilde{\nu}_\ell \to \ell\chi^\pm_1$ is maximized for $M_1/M_2 \sim -\tan^2\theta_W$. Combined with the slepton pair production, we analyzed the prospective reach for the OS dilepton plus $\not{E}_T$ final state at the 8 and 14 TeV LHC.

We recasted the existing 8 TeV results of dilepton plus $\not{E}_T$ signal, reported by the LHC collaborations assuming a Bino-like LSP, in various LSP scenarios. We find that the LHC slepton reach is strongly enhanced for a non-Bino-like LSP: the 95% C.L. limit for m_{ℓ_L} extends from 300 GeV for Bino-like LSP to about 370 GeV for Wino-like LSP. More interestingly, the reach in the Higgsino-like LSP scenario sensitively depends on the value and sign of M_1/M_2. The 95% C.L. reach for $\tilde{\ell}_L$ is the strongest ($\sim$ 490 GeV) for $M_1/M_2 \sim -\tan^2\theta_W$ and is the weakest ($\sim$ 220 GeV) for $M_1/M_2 \sim \tan^2\theta_W$.

We also studied the 95% C.L. exclusion and 5σ discovery reach of slepton at the 14 TeV LHC with 100 fb^{-1} luminosity. The projected 95% C.L. mass limits for the left-handed slepton varies from 550 (670) GeV for a Bino-like (Wino-like) LSP to 900 (390) GeV for a Higgsino-like LSP under the most optimistic (pessimistic) scenario. The reach for the right-handed slepton is about 440 GeV. The corresponding 5σ discovery is about 100 GeV smaller. For 300 fb^{-1} integrated luminosity, the reach is about 50 $-$ 100 GeV higher.

Interestingly, relatively light leptons with moderate $\tan\beta$ are needed to explain the present difference between the muon anomalous magnetic moment experimental result and the SM prediction. The LHC Run-II should, thus, be able to probe this possibility for the Wino-like and Higgsino-like LSP. The observation of a signal in this case could be consistent with a supersymmetric explanation for the $g_\mu - 2$ result.[1] In addition, one may also expect signatures in other low-energy electroweak processes, such as tests of lepton universality with pion leptonic decays or deviations from first row CKM unitarity as probed by β-decay and kaon leptonic decays. On the other hand, the non-observation of dilepton plus $\not{E}_T$ signal for slepton Drell-Yan pair production would not generally preclude light sleptons, as the rates for the right-handed sleptons and for the left-handed sleptons with a Higgsino-like LSP and $M_1/M_2 \sim \tan^2\theta_W$ are considerably suppressed. Probing these MSSM scenarios would require alternate avenues, such as the production of sleptons via the cascade decays from electroweak gaugino production or future studies at a high energy e^+e^- collider.

Note also that our analyses of the dilepton plus $\not{E}_T$ signal have assumed that in the Wino-like LSP and Higgsino-like LSP cases, $\chi^\pm_1$ (and χ^0_2 in the Higgsino-like LSP case) appear solely as $\not{E}_T$ at the LHC. For small mass splitting $\Delta m = m_{\chi^\pm_1} - m_{\chi^0_1} \lesssim 200$ MeV, however, the $\chi^\pm_1$ may appear as a disappearing track or even as a stable track inside the detector, resulting in distinctive collider signatures. The current ATLAS analysis of the disappearing-track search has imposed very strong limits on the degenerate chargino mass for relatively small mass splittings [33]. The signature for slepton pair production

[1] The various one-loop contributions to the anomalous magnetic moment are proportional to sign(μM_j) for $j = 1, 2$, depending on which neutralino or chargino appears in the loop [18]. Thus, knowing the relative sign of M_1 and M_2, as well as the values of the superpartner masses, will allow for a precise determination of the MSSM contribution to the anomalous magnetic moment.

JHEP11(2014)117

in such a highly degenerate scenario could include disappearing tracks, single hard lepton plus disappearing tracks, or dilepton plus disappearing tracks. The behavior of the decay branching fractions of the slepton analyzed in this paper can be applied to such searches as well.

Acknowledgments

The work was supported in part under U.S. Department of Energy contracts DE-FG02-04ER-41298 (S.S. and J.E.), DE-FG02-04ER-41268 (W.S.), DE-FG02-08ER41531 (M.J.R-M) and DE-SC0011095 (M.J.R-M) as well as by the Wisconsin Alumni Research Foundation (M.J.R-M).

References

[1] ATLAS collaboration, *Observation of a new particle in the search for the Standard Model Higgs boson with the ATLAS detector at the LHC*, *Phys. Lett.* **B 716** (2012) 1 [arXiv:1207.7214] [INSPIRE].

[2] CMS collaboration, *Observation of a new boson at a mass of 125 GeV with the CMS experiment at the LHC*, *Phys. Lett.* **B 716** (2012) 30 [arXiv:1207.7235] [INSPIRE].

[3] ATLAS collaboration, *Search for squarks and gluinos with the ATLAS detector in final states with jets and missing transverse momentum and 20.3 fb^{-1} of $\sqrt{s} = 8$ TeV proton-proton collision data*, ATLAS-CONF-2013-047.

[4] CMS Collaboration, *Search for New Physics in the Multijets and Missing Momentum Final State in Proton-Proton Collisions at 8 TeV*, CMS-PAS-SUS-13-012.

[5] G.F. Giudice and R. Rattazzi, *Theories with gauge mediated supersymmetry breaking*, *Phys. Rept.* **322** (1999) 419 [hep-ph/9801271] [INSPIRE].

[6] L. Randall and R. Sundrum, *Out of this world supersymmetry breaking*, *Nucl. Phys.* **B 557** (1999) 79 [hep-th/9810155] [INSPIRE].

[7] G.F. Giudice, M.A. Luty, H. Murayama and R. Rattazzi, *Gaugino mass without singlets*, *JHEP* **12** (1998) 027 [hep-ph/9810442] [INSPIRE].

[8] T. Gherghetta, G.F. Giudice and J.D. Wells, *Phenomenological consequences of supersymmetry with anomaly induced masses*, *Nucl. Phys.* **B 559** (1999) 27 [hep-ph/9904378] [INSPIRE].

[9] A.B. Lahanas and D.V. Nanopoulos, *The Road to No Scale Supergravity*, *Phys. Rept.* **145** (1987) 1 [INSPIRE].

[10] H. Goldberg, *Constraint on the Photino Mass from Cosmology*, *Phys. Rev. Lett.* **50** (1983) 1419 [*Erratum ibid.* **103** (2009) 099905] [INSPIRE].

[11] J.R. Ellis, J.S. Hagelin, D.V. Nanopoulos, K.A. Olive and M. Srednicki, *Supersymmetric Relics from the Big Bang*, *Nucl. Phys.* **B 238** (1984) 453 [INSPIRE].

JHEP11(2014)117

[12] M. Drees and M.M. Nojiri, *The Neutralino relic density in minimal $N = 1$ supergravity*, *Phys. Rev.* **D 47** (1993) 376 [hep-ph/9207234] [INSPIRE].

[13] T. Nihei, L. Roszkowski and R. Ruiz de Austri, *Exact cross-sections for the neutralino WIMP pair annihilation*, *JHEP* **03** (2002) 031 [hep-ph/0202009] [INSPIRE].

[14] A. Birkedal-Hansen and E.-h. Jeong, *Gaugino and Higgsino coannihilations. 1. Neutralino neutralino interactions*, *JHEP* **02** (2003) 047 [hep-ph/0210041] [INSPIRE].

[15] K. Griest and D. Seckel, *Three exceptions in the calculation of relic abundances*, *Phys. Rev.* **D 43** (1991) 3191 [INSPIRE].

[16] MOLLER collaboration, J. Mammei, *The MOLLER Experiment*, *Nuovo Cim.* **C 035N04** (2012) 203 [arXiv:1208.1260] [INSPIRE].

[17] QWEAK collaboration, D. Androic et al., *First Determination of the Weak Charge of the Proton*, *Phys. Rev. Lett.* **111** (2013) 141803 [arXiv:1307.5275] [INSPIRE].

[18] T. Moroi, *The Muon anomalous magnetic dipole moment in the minimal supersymmetric standard model*, *Phys. Rev.* **D 53** (1996) 6565 [*Erratum ibid.* **D 56** (1997) 4424] [hep-ph/9512396] [INSPIRE].

[19] V. Cirigliano, J. Jenkins and M. Gonzalez-Alonso, *Semileptonic decays of light quarks beyond the Standard Model*, *Nucl. Phys.* **B 830** (2010) 95 [arXiv:0908.1754] [INSPIRE].

[20] K. Kumar, Z.-T. Lu and M.J. Ramsey-Musolf, *Working Group Report: Nucleons, Nuclei and Atoms*, arXiv:1312.5416 [INSPIRE].

[21] INTENSITY FRONTIER CHARGED LEPTON WORKING GROUP collaboration, J. Albrecht et al., *Working Group Report: Charged Leptons*, arXiv:1311.5278 [INSPIRE].

[22] F. del Aguila and L. Ametller, *On the detectability of sleptons at large hadron colliders*, *Phys. Lett.* **B 261** (1991) 326 [INSPIRE].

[23] H. Baer, C.-h. Chen, F. Paige and X. Tata, *Detecting Sleptons at Hadron Colliders and Supercolliders*, *Phys. Rev.* **D 49** (1994) 3283 [hep-ph/9311248] [INSPIRE].

[24] Y. Andreev, S.I. Bityukov and N.V. Krasnikov, *Sleptons at post-WMAP benchmark points at LHC(CMS)*, *Phys. Atom. Nucl.* **68** (2005) 340 [hep-ph/0402229] [INSPIRE].

[25] ATLAS collaboration, *Search for direct-slepton and direct-chargino production in final states with two opposite-sign leptons, missing transverse momentum and no jets in 20/fb of pp collisions at $\sqrt{s} = 8$ TeV with the ATLAS detector*, ATLAS-CONF-2013-049.

[26] CMS Collaboration, *Search for electroweak production of charginos, neutralinos and sleptons using leptonic final states in pp collisions at 8 TeV*, CMS-PAS-SUS-13-006.

[27] ATLAS collaboration, *Search for direct production of charginos, neutralinos and sleptons in final states with two leptons and missing transverse momentum in pp collisions at $\sqrt{s} = 8$ TeV with the ATLAS detector*, *JHEP* **05** (2014) 071 [arXiv:1403.5294] [INSPIRE].

[28] CMS collaboration, *Searches for electroweak production of charginos, neutralinos and sleptons decaying to leptons and W, Z and Higgs bosons in pp collisions at 8 TeV*, *Eur. Phys. J.* **C 74** (2014) 3036 [arXiv:1405.7570] [INSPIRE].

[29] J. Eckel, W. Shepherd and S.-F. Su, *Slepton Discovery in Electroweak Cascade Decay*, *JHEP* **05** (2012) 081 [arXiv:1111.2615] [INSPIRE].

[30] J.L. Feng, S.T. French, I. Galon, C.G. Lester, Y. Nir et al., *Measuring Slepton Masses and Mixings at the LHC*, *JHEP* **01** (2010) 047 [arXiv:0910.1618] [INSPIRE].

JHEP11(2014)117

[31] J.L. Feng, S.T. French, C.G. Lester, Y. Nir and Y. Shadmi, *The Shifted Peak: Resolving Nearly Degenerate Particles at the LHC*, *Phys. Rev.* **D 80** (2009) 114004 [arXiv:0906.4215] [INSPIRE].

[32] N.V. Krasnikov, *Search for flavor lepton number violation in slepton decays at LHC*, *JETP Lett.* **65** (1997) 148 [hep-ph/9611282] [INSPIRE].

[33] ATLAS collaboration, *Search for charginos nearly mass degenerate with the lightest neutralino based on a disappearing-track signature in pp collisions at $\sqrt{s}$=8 TeV with the ATLAS detector*, *Phys. Rev.* **D 88** (2013) 112006 [arXiv:1310.3675] [INSPIRE].

[34] M. Ibe, S. Matsumoto and R. Sato, *Mass Splitting between Charged and Neutral Winos at Two-Loop Level*, *Phys. Lett.* **B 721** (2013) 252 [arXiv:1212.5989] [INSPIRE].

[35] LEP2 SUSY WORKING group, *Combined LEP Selectron/Smuon/Stau Results, 183-208 GeV*, 2004, LEPSUSYWG/04-01.1, http://lepsusy.web.cern.ch/lepsusy/.

[36] L3 collaboration, P. Achard et al., *Search for scalar leptons and scalar quarks at LEP*, *Phys. Lett.* **B 580** (2004) 37 [hep-ex/0310007] [INSPIRE].

[37] ALEPH collaboration, A. Heister et al., *Absolute lower limits on the masses of selectrons and sneutrinos in the MSSM*, *Phys. Lett.* **B 544** (2002) 73 [hep-ex/0207056] [INSPIRE].

[38] ALEPH COLLABORATION, DELPHI COLLABORATION, L3 COLLABORATION, OPAL COLLABORATION, SLD COLLABORATION, LEP ELECTROWEAK WORKING GROUP, SLD ELECTROWEAK GROUP, SLD HEAVY FLAVOUR GROUP collaboration, S. Schael et al., *Precision electroweak measurements on the Z resonance*, *Phys. Rept.* **427** (2006) 257 [hep-ex/0509008] [INSPIRE].

[39] J. Alwall, M. Herquet, F. Maltoni, O. Mattelaer and T. Stelzer, *MadGraph 5 : Going Beyond*, *JHEP* **06** (2011) 128 [arXiv:1106.0522] [INSPIRE].

[40] T. Sjöstrand, S. Mrenna and P.Z. Skands, *PYTHIA 6.4 Physics and Manual*, *JHEP* **05** (2006) 026 [hep-ph/0603175] [INSPIRE].

[41] DELPHES 3 collaboration, J. de Favereau et al., *DELPHES 3, A modular framework for fast simulation of a generic collider experiment*, *JHEP* **02** (2014) 057 [arXiv:1307.6346] [INSPIRE].

[42] http://www.snowmass2013.org/tiki-index.php?page=Energy_Frontier_FastSimulation.

[43] B. Fuks, M. Klasen, D.R. Lamprea and M. Rothering, *Revisiting slepton pair production at the Large Hadron Collider*, *JHEP* **01** (2014) 168 [arXiv:1310.2621] [INSPIRE].

[44] C.G. Lester and D.J. Summers, *Measuring masses of semiinvisibly decaying particles pair produced at hadron colliders*, *Phys. Lett.* **B 463** (1999) 99 [hep-ph/9906349] [INSPIRE].

[45] A. Barr, C. Lester and P. Stephens, *m(T2): The Truth behind the glamour*, *J. Phys.* **G 29** (2003) 2343 [hep-ph/0304226] [INSPIRE].

[46] H.-C. Cheng and Z. Han, *Minimal Kinematic Constraints and m(T2)*, *JHEP* **12** (2008) 063 [arXiv:0810.5178] [INSPIRE].

[47] T. Junk, *Confidence level computation for combining searches with small statistics*, *Nucl. Instrum. Meth.* **A 434** (1999) 435 [hep-ex/9902006] [INSPIRE].

[48] A.L. Read, *Modified frequentist analysis of search results (The CL(s) method)*, in *Geneva 2000, Confidence limits*, pg. 81.

[49] NLO MULTILEG WORKING GROUP collaboration, Z. Bern et al., *The NLO multileg working group: Summary report*, arXiv:0803.0494 [INSPIRE].

JHEP11(2014)117

APPENDIX C

Exotic Stop and Sbottom Decay at the LHC

The following manuscript was submitted to the arXiv and also submitted for publication in the Journal of High Energy Physics. Original reference: J. Eckel, S. Su, H. Zhang, "*Exotic Stop Decay at the LHC*", arXiv:1411.1061.

Exotic Stop Decay at the LHC

Jonathan Eckel[1*], Shufang Su[1†], Huanian Zhang[1‡]

[1] *Department of Physics, University of Arizona, Tucson, Arizona 85721*

Abstract

Current searches for the stop focus on the decay channels of $\tilde{t} \to t\chi_1^0$ or $\tilde{t} \to b\chi_1^\pm \to bW\chi_1^0$, leading to $tt/bbWW + \not{E}_T$ final states for stop pair production at the LHC. In supersymmetric scenarios with light gauginos other than the neutralino lightest supersymmetric particle (LSP), different decay modes of the stop could be dominant, which significantly weaken the current stop search limits at the LHC. Additionally, new decay modes offer alternative discovery channels for stop searches. In this paper, we study the stop decay in the Bino-like LSP case with light Wino or Higgsino next-to-LSPs (NLSPs), and identify cases in which additional decay modes become dominant. We also perform a detailed collider analysis for stop pair production with one stop decaying via $\tilde{t}_1 \to t\chi_2^0 \to th\chi_1^0$, and the other stop decaying via $\tilde{t}_1 \to b\chi_1^\pm \to bW\chi_1^0$, leading to the $bbbbjj\ell + \not{E}_T$ collider signature. At the 14 TeV LHC with 300 fb^{-1} integrated luminosity, the stop can be excluded up to about 1040 GeV at the 95% C.L., or be discovered up to 940 GeV at 5σ significance.

* eckel@physics.arizona.edu

† shufang@email.arizona.edu

‡ fantasyzhn@email.arizona.edu

I. INTRODUCTION

100

The discovery of a 125 GeV Higgs at the Large Hadron Collider (LHC) [1, 2] motivates the consideration of new physics beyond the Standard Model (SM). In the SM, the Higgs receives unstable quadratically divergent radiative corrections to its mass from the top quark loop. An unnatural cancellation is needed to recover the light physical Higgs mass, which is the so called "naturalness problem" [3]. Supersymmetry (SUSY) provides a solution to the naturalness problem by introducing superpartners to the SM particles, with interactions following the SUSY relations. The quadratic divergence from the superpartners cancels that of the SM particles, with the remnant contributions being only logarithmically divergent. Given the large top Yukawa coupling, the top and stop sectors of the Minimal Supersymmetric Standard Model (MSSM) provide the largest radiative corrections to the Higgs mass. Stop masses can not be too heavy in order to avoid excessive fine tuning of the Higgs mass. A TeV scale stop typically leads to fine tuning of about 1% [4]. Given the tight connection between the stop and Higgs sectors, it is important to fully explore the discovery potential of the stop at the LHC.

Most of the current searches for the light stop focus on the decay $\tilde{t} \to t\chi_1^0$ or $\tilde{t} \to b\chi_1^\pm \to bW\chi_1^0$, leading to $tt + \not{E}_T$ or $bbWW + \not{E}_T$ final states for stop pair production at the LHC. However, due to the large SM background from $t\bar{t}$, searches for the stop can be very challenging. The current limits from ATLAS and CMS experiments exclude stops with masses up to about 645 GeV for a light neutralino LSP [5–15]. At energy of 14 TeV with 100 fb^{-1} of integrated luminosity, the expected discovery sensitivity for stops at the LHC is about 1 TeV [16].

The current stop search limits, however, always assume the dominance of the stop decay channels mentioned above. The current limits could be significantly weakened when other stop decay modes open, which could occur in many regions of MSSM parameter space. On the other hand, the opening of new channels offers alternative discovery potential for stops at the LHC. Therefore, it is timely to study the non-minimal stop decay pattern as well as assess the stop discovery potential at the 14 TeV LHC.

Even under the usual assumption of a Bino-like LSP, the existence of other light neutralino states, for example, Wino-like or Higgsino-like next-to-LSPs (NLSPs) could lead to new decay channels for the stop. For instance, $\tilde{t}$ could decay to $t\chi_{2,3}^0$, with $\chi_{2,3}^0$ further

decaying to $Z\chi_1^0, h\chi_1^0$. Given the relatively large $\mathrm{SU}(2)_L$ coupling and top Yukawa coupling, compared to the $\mathrm{U}(1)_Y$ coupling relevant for the Bino-like LSP, decays to $t\chi_{2,3}^0$ could even be dominant despite the phase space suppression. In this paper, we study the stop decay branching fractions for the Wino- or Higgsino-like NLSP case, considering the minimal mixing and the maximal mixing scenarios in the stop sector, and outline the main search channels for the stops at the LHC. 101

Similarly, the current sbottom searches focus on $\tilde{b} \to b\chi_1^0$, with $bb + \not{E}_T$ being the dominant search channel. Given data collected at the LHC 7/8 TeV, sbottoms with masses up to 700 GeV are excluded [17]. Even in parameter space with highly degenerate sbottom and LSP masses, the sbottom is excluded with mass up to about 400 GeV [18]. The left-handed sbottom mass is related to the left-handed stop mass since they are controlled by the same soft SUSY breaking mass parameter. In this paper, we also study the left-handed sbottom decay pattern for various scenarios, as well as its collider signatures.

Given the discovery of the SM-like Higgs boson at the LHC, we can now use final states with a Higgs boson to search for new physics beyond the SM. To explore the 14 TeV LHC reach for the exotic stop decay channels, we performed a detailed collider analysis with a Higgs in the final state: $pp \to \tilde{t_1}\tilde{t_1}^*$ with one stop decaying via $\tilde{t}_1 \to t\chi_2^0 \to th\chi_1^0$, and other stop decaying via $\tilde{t}_1 \to b\chi_1^\pm \to bW\chi_1^0$, leading to $bbbbjj\ell + \not{E}_T$ signature. By designing cuts to identify the signal while suppressing SM backgrounds, we obtained the 95% C.L. exclusion limit as well as the 5σ discovery reach at the 14 TeV LHC with 300 fb^{-1} integrated luminosity. Final states with $\chi_2^0 \to Z\chi_1^0$ are left for future studies.

The rest of the paper is organized as the following. In Sec. II, we present the third generation squark sector in the MSSM and discuss its connection to the Higgs sector. In Sec. III, we discuss the stop and sbottom decays for various scenarios, as well as the collider signatures for stop/sbottom pair production. In Sec. IV, we summarize the current LHC stop and sbottom search results from both ATLAS and CMS. In Sec. V, we investigate the 14 TeV reach of the stop via final states with a Higgs. In Sec. VI, we conclude.

II. MSSM STOP SECTOR

In this study, we work in the MSSM and focus primarily on the third generation squark sector. We decouple other SUSY particles: the gluino, sleptons, and the first and second

generation squarks. We also decouple the non-SM Higgs particles by setting M_A large. The remaining SUSY particles in the model are the third generation squarks, the neutralinos and charginos. 102

The gauge eigenstates for the superpartners of the top and bottom quarks are $(\tilde{t}_L, \tilde{b}_L), \tilde{t}_R$ and $\tilde{b}_R$, with the left-handed states grouped as an $\mathrm{SU}(2)_L$ doublet and the right-handed states as singlets. The mass matrix for the stop sector is

$$\mathbf{m}_{\tilde{\mathbf{t}}}^{\mathbf{2}} = \begin{pmatrix} M_{3SQ}^2 + m_t^2 + \Delta_{\tilde{u}_L} & m_t \tilde{A}_t \\ m_t \tilde{A}_t & M_{3SU}^2 + m_t^2 + \Delta_{\tilde{u}_R} \end{pmatrix}, \tag{1}$$

with M_{3SQ}^2 and M_{3SU}^2 representing the soft SUSY breaking masses for $\tilde{t}_L$ and $\tilde{t}_R$, m_t^2 term coming from the F-term contribution in the SUSY Lagrangian and the Δ terms coming from the D-term contribution. The off-diagonal term $\tilde{A}_t$ is given by:

$$\tilde{A}_t = A_t - \mu \cot \beta, \tag{2}$$

for A_t representing the trilinear coupling and μ representing the supersymmetric bilinear mass term in the Higgs sector.

The stop mass matrix can be diagonalized with a stop mixing angle θ_t:

$$\begin{pmatrix} \tilde{t}_1 \\ \tilde{t}_2 \end{pmatrix} = \begin{pmatrix} \cos\theta_t & -\sin\theta_t \\ \sin\theta_t & \cos\theta_t \end{pmatrix} \begin{pmatrix} \tilde{t}_L \\ \tilde{t}_R \end{pmatrix}, \tag{3}$$

with mass eigenstates $\tilde{t}_1$, $\tilde{t}_2$: $m_{\tilde{t}_1} < m_{\tilde{t}_2}$. For $M_{3SQ} < (>) M_{3SU}$, $\tilde{t}_1$ is mostly left-handed (right-handed), while for $M_{3SQ}^2 \sim M_{3SU}^2$, $\tilde{t}_{1,2}$ could be a mixture of the left- and right-handed states.

Given the large top Yukawa coupling, the stop sector provides the dominant contribution to the radiative corrections of the SM-like Higgs mass in the MSSM. For $M_{3SQ} = M_{3SU} = M_{SUSY}$, the correction to the SM-like Higgs mass squared is [19]:

$$\delta m_h^2 = \frac{3}{4\pi^2} y_t^2 m_t^2 \sin^2\beta \left(\log \frac{M_{SUSY}^2}{m_t^2} + \frac{\tilde{A}_t^2}{M_{SUSY}^2} \left(1 - \frac{\tilde{A}_t^2}{12 M_{SUSY}^2} \right) \right). \tag{4}$$

In the minimal mixing case with $\tilde{A}_t = 0$, a large M_{SUSY} is needed to provide a SM-like Higgs mass of 125 GeV. In the maximal mixing case with $\tilde{A}_t = \sqrt{6} M_{SUSY}$, a relatively small M_{SUSY} can be accommodated given the additional contribution from the $\tilde{A}_t$ term. In the general MSSM when $M_{3SQ}^2 \neq M_{3SU}^2$, to provide a SM-like Higgs mass of 125 GeV,

the light stop $\tilde{t}_1$ can still be as light as 200 GeV. A large mass splitting between the stop mass eigenstates (and a large $\tilde{A}_t$ term), however, is typically needed, resulting in $m_{\tilde{t}_2} \gtrsim 500$ GeV in general [20, 21]. 103

Similarly, the mass matrix for the sbottom is given as:

$$\mathbf{m}^{\mathbf{2}}_{\tilde{\mathbf{b}}} = \begin{pmatrix} M^2_{3SQ} + m^2_b + \Delta_{\tilde{d}_L} & m_b \tilde{A}_b \\ m_b \tilde{A}_b & M^2_{3SD} + m^2_b + \Delta_{\tilde{d}_R} \end{pmatrix}, \tag{5}$$

with

$$\tilde{A}_b = A_b - \mu \tan\beta. \tag{6}$$

Given the suppression of the off-diagonal terms by the small bottom mass, large mixing among the sbottom mass eigenstates is less common.

Since the stop sector provides the dominant contribution to the Higgs mass corrections, we decouple the right-handed sbottom in our analysis. The left-handed sbottom mass, however, is determined by M_{3SQ} and could be relatively light. Given $m_b \tilde{A}_b, M^2_{3SQ} << M^2_{3SD}$, the light sbottom mass eigenstate is mostly left-handed: $\tilde{b}_1 \sim \tilde{b}_L$. Although the sbottom corrections to the Higgs mass are small compared to the stop corrections, there can be significant modifications to the Higgs couplings, especially the bottom Yukawa coupling [22].

III. STOP DECAY

We consider the neutralino/chargino spectrum with a Bino-like LSP. For simplicity, we consider three representative scenarios:

- Case I, Bino-like LSP with decoupled Winos and Higgsinos: $M_1 < m_{\tilde{t},\tilde{b}_1} \ll |\mu|, M_2$.
- Case IA, Bino-like LSP with Wino-like NLSPs: $M_1 < M_2 < m_{\tilde{t},\tilde{b}_1} \ll |\mu|$.
- Case IB, Bino-like LSP with Higgsino-like NLSPs: $M_1 < |\mu| < m_{\tilde{t},\tilde{b}_1} \ll M_2$.

The decays of the light stop or sbottom highly depend on the low-lying neutralino/chargino spectrum, as well as the composition of the light stop and sbottom.

In each scenario, we consider two limiting cases with different stop left-right mixing. In the minimal mixing case, $\tilde{A}_t = A_t - \mu \cot\beta = 0$, the lightest stop mass eigenstate $\tilde{t}_1$ is either

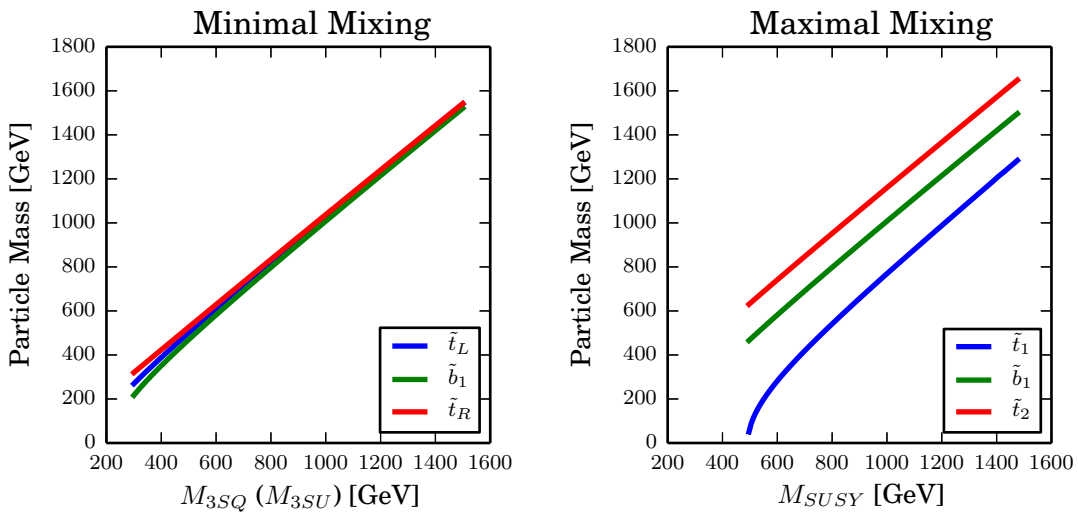

FIG. 1: The mass spectra for stops and sbottom for the minimal mixing case (left panel) and the maximal mixing case with $M_{3SQ} = M_{3SU} = M_{SUSY}$ (right panel).

purely $\tilde{t}_L$ ($M_{3SQ} < M_{3SU}$) or purely $\tilde{t}_R$ ($M_{3SQ} > M_{3SU}$). We decouple $\tilde{t}_2$ for simplicity. In the maximal mixing case with $M_{3SQ} = M_{3SU} = M_{SUSY}$ and $|\tilde{A}_t| = \sqrt{6}M_{SUSY}$, both $\tilde{t}_{1,2}$ are a mixture of $\tilde{t}_L$ and $\tilde{t}_R$, with mass squared splitting $\Delta m^2_{\tilde{t}} \approx 2\sqrt{6}m_t M_{SUSY}$. In our analysis below, we use $\tilde{A}_t > 0$. Negative values of $\tilde{A}_t$ introduce little changes to the numerical results. Since M_{3SQ} also controls the mass for $\tilde{b}_L$, there is a light $\tilde{b}_1 \sim \tilde{b}_L$ for the light M_{3SQ} case, assuming small sbottom left-right mixing and a decoupled $\tilde{b}_R$.

The mass spectra for stops and sbottom are shown in Fig. 1. In the minimal mixing case (left panel), $m_{\tilde{t}_L}$ ($m_{\tilde{t}_R}$), $m_{\tilde{b}_1} \sim M_{3SQ}(M_{3SU})$, especially for large M_{3SQ} (M_{3SU}). In the maximal mixing case (right panel), the mass difference between $\tilde{b}_1$ and $\tilde{t}_1$ is typically about 250 GeV while the mass difference between $\tilde{t}_2$ and $\tilde{t}_1$ is about 350 GeV or larger.

We used SUSY-HIT [23] to calculate the supersymmetric particle spectrum and decay branching fractions. In this section, unless otherwise specified, we have set the Bino-like LSP mass parameter $M_1 = 100$ GeV, the intermediate gaugino mass parameters $M_2, \mu = 300$ GeV in Cases IA and IB, respectively, and $\tan\beta = 10$.

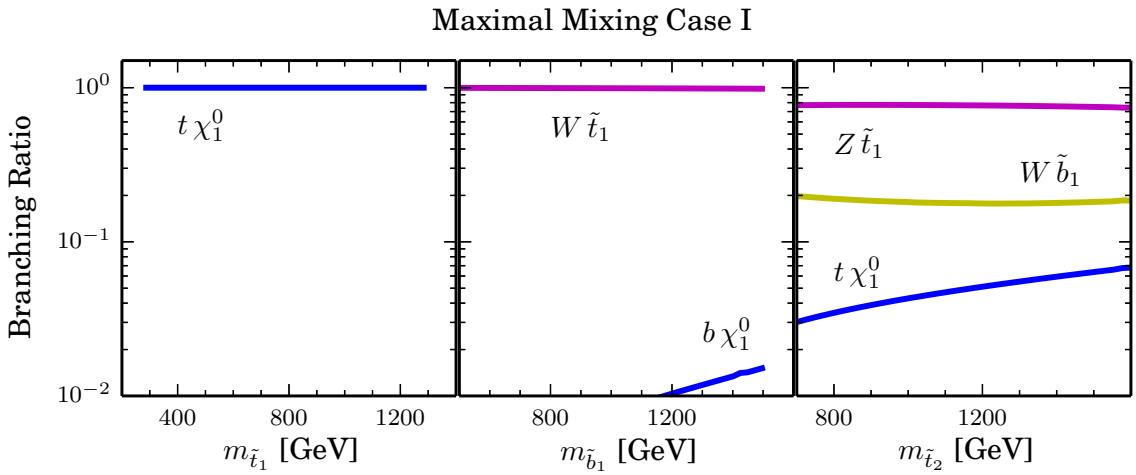

FIG. 2: Branching fractions for $\tilde{t}_1$ (left), $\tilde{b}_1$ (middle) and $\tilde{t}_2$ (right) in the maximal mixing scenario with a Bino-like LSP (Case I).

A. Case I: Bino-like LSP with decoupled Wino and Higgsino

The simplest case has a mass spectrum with stop(s), left-handed sbottom, and only the low-lying neutralino being the Bino-like LSP.

In the minimal mixing case with the light stop $\tilde{t}_1$ as a pure left- or right-handed state, $\tilde{t}_1$ either directly decays to $t\chi_1^0$ when it is kinematically accessible or through $bW^*\chi_1^0$ with 100% branching fraction. Similarly, in the case of small M_{3SQ}, $\tilde{b}_1$ decays directly through $b\chi_1^0$ with 100% branching fraction.

In the maximal mixing case, $\tilde{t}_1$, $\tilde{t}_2$, and $\tilde{b}_1$ appear in the spectrum, with a typical mass order $m_{\tilde{t}_1} < m_{\tilde{b}_1} < m_{\tilde{t}_2}$ with relatively large mass splittings of 150 GeV or larger. While the decay of $\tilde{t}_1$ is straightforward (100% into $bW^{(*)}\chi_1^0$), the decays of $\tilde{b}_1$ and $\tilde{t}_2$ could have multiple competing channels, as shown in Fig. 2. For $\tilde{b}_1$, it dominantly decays into $W\tilde{t}_1$ while the branching fraction of the conventional channel of $\tilde{b}_1 \to b\chi_1^0$ is only about a few percent or less. For $\tilde{t}_2$, it dominantly decays into a light stop/sbottom with a gauge boson: $Z\tilde{t}_1$ about 75% and $W\tilde{b}_1$ about 20%. The direct decay down to $t\chi_1^0$ is less than 10%.

The pair production of stops and sbottoms at the LHC, and their subsequent decays result in the appearance of various final states. In the left panel of Fig. 3, we show the $\sigma \times \mathrm{BR}$ of final states $tt/bbWW + \not{E}_T$ for $\tilde{t}_1$ in the minimal and maximal mixing scenarios, as well as $bb + \not{E}_T$ for $\tilde{b}_1$ in the minimal mixing scenario at the 14 TeV LHC. These are the

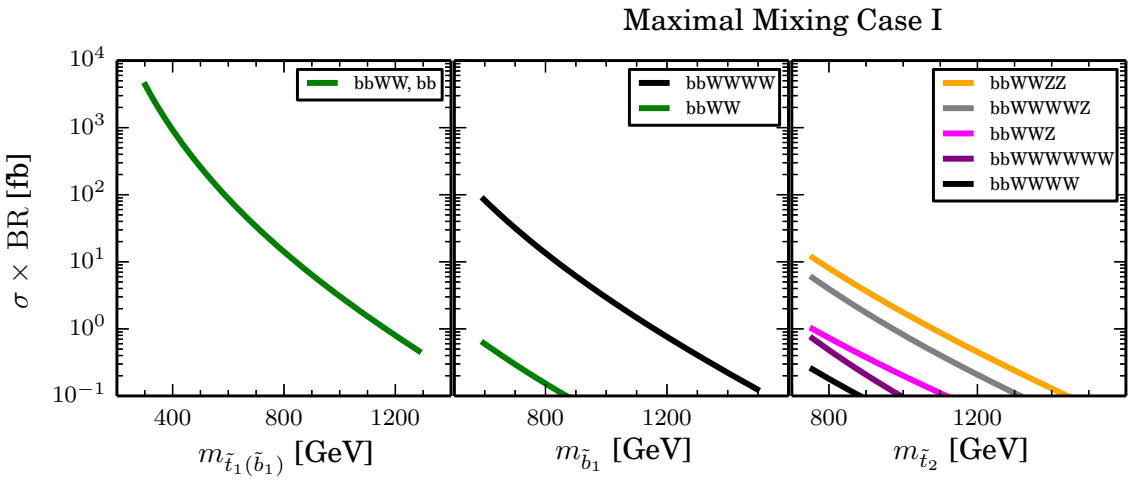

FIG. 3: Case I: left panel shows $\sigma \times$ BR of final states for $\tilde{t}_1$ pair production in both the minimal and maximal mixing scenarios, as well as $\tilde{b}_1$ pair production in the minimal mixing scenario. The middle and right panel show $\sigma \times$ BR for various final states of $\tilde{b}_1$ and $\tilde{t}_2$ pair production, respectively, in the maximal mixing scenario. All channels include $\not{E}_T$ in the final states.

conventional channels where $\tilde{t} \to t/bW\chi_1^0$ and $\tilde{b} \to b\chi_1^0$ dominate. $\sigma \times$BR is the same as the production cross sections for the stop pair and sbottom pair. The middle panel of Fig. 3 shows the $\sigma \times$BR for $\tilde{b}_1\tilde{b}_1$ pair production in the maximal mixing scenario. The conventional channel $bb+\not{E}_T$ is highly suppressed, while $bbWWWW+\not{E}_T$ becomes dominant. The right panel of Fig. 3 shows the $\sigma \times$ BR for $\tilde{t}_2\tilde{t}_2$ pair production in the maximal mixing scenario. The current experimentally searched channel $ttZ + \not{E}_T$ is subdominant, only 10% of the dominant channel of $ttZZ + \not{E}_T$. $ttWWZ$ is the second dominant channel. The cross section, however, is relatively small, less than about 10 fb for $m_{\tilde{t}_2} \gtrsim 750$ GeV, given the heaviness of the second stop. Note that the range of the stop and sbottom masses are controlled by the choice of parameter $M_{3SQ} = M_{3SU} = M_{SUSY} = 600 \ldots 1500$ GeV in the maximal mixing case(see Fig. 1). Also note that all the cross sections shown in the plots are leading order only. The next leading order K-factor for stop and sbottom pair production process is about 1.33 at the 14 TeV LHC [24, 25], which has been taken into account in our collider analysis below in Sec. V.

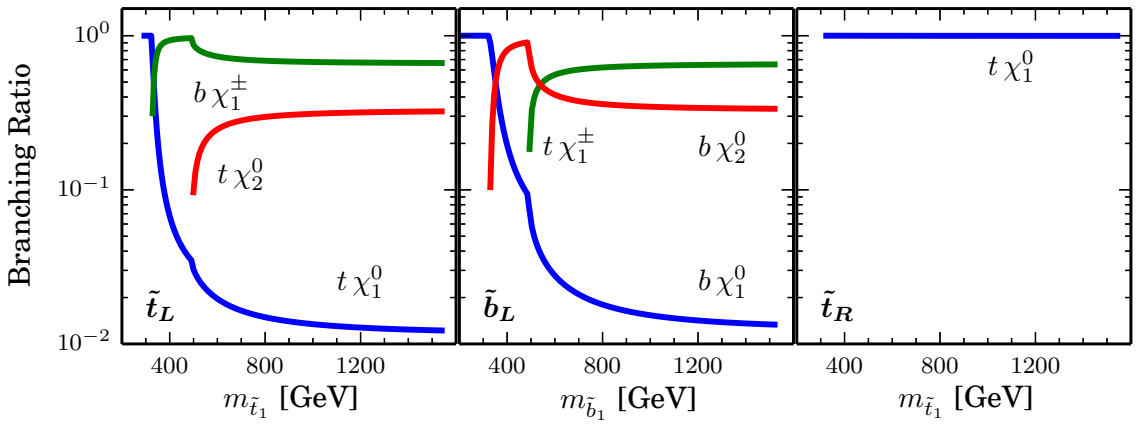

FIG. 4: Case IA: branching fractions for left-handed $\tilde{t}_1$ (left), $\tilde{b}_1$ (middle), right-handed $\tilde{t}_1$ (right) in the minimal mixing scenario.

B. Case IA: Bino LSP with Wino NLSP

The low lying neutralino/chargino spectrum in Case IA comprises of a Bino-like LSP, as well as a pair of Wino-like states: χ_2^0 and $\chi_1^\pm$ with nearly degenerate masses. In the minimal mixing scenario, the decay branching fractions are shown in Fig. 4 for left-handed $\tilde{t}_1$ (left), $\tilde{b}_1$ (middle), and right-handed $\tilde{t}_1$ (right). For the left-handed $\tilde{t}_1$, decays to $b\chi_1^\pm$ ($\sim$ 70% for large $m_{\tilde{t}_1}$) and $t\chi_2^0$ ($\sim$ 30% for large $m_{\tilde{t}_1}$) dominate over $t\chi_1^0$ once kinematically accessible, due to the stronger $\mathrm{SU}(2)_L$ coupling compared to the relatively weaker $\mathrm{U}(1)_Y$ coupling. Similarly, $\tilde{b}_1 \to t\chi_1^\pm$ ($\sim$ 65%) and $\tilde{b}_1 \to b\chi_2^0$ ($\sim$ 30%) dominate over the conventional channel of $b\chi_1^0$ for sbottom. Given the dominant decay channels of the Wino-like neutralino/chargino[1]: $\chi_1^\pm \to W\chi_1^0$, $\chi_2^0 \to Z/h\chi_1^0$, the dominant decay modes for $\tilde{t}_1$ and $\tilde{b}_1$ are: $\tilde{t}_1 \to bW\chi_1^0,\ tZ/h\chi_1^0$, $\tilde{b}_1 \to tW\chi_1^0,\ bZ/h\chi_1^0$. When $\tilde{t}_1$ is mostly right-handed, it decays to $t\chi_1^0$ almost 100%, since its couplings to the Wino-like neutralino/charginos are highly suppressed.

The left, middle and right panels of Fig. 5 show the $\sigma \times$BR for pure left-handed $\tilde{t}_1\tilde{t}_1$, $\tilde{b}_1\tilde{b}_1$ and pure right-handed $\tilde{t}_1\tilde{t}_1$ pair production, respectively, in the minimal mixing scenario

[1] For χ_2^0, whether it decays preferably to $Z\chi_1^0$ or $h\chi_1^0$ depends on the sign of μ, as explained in detail in Ref. [26].

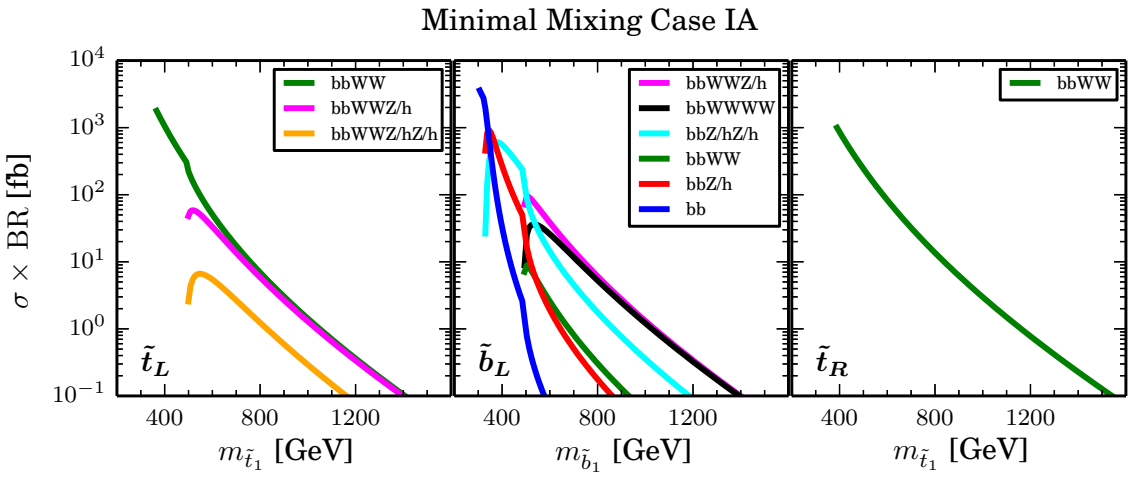

FIG. 5: Case IA: $\sigma \times$ BR of various final states for pair production of left-handed $\tilde{t}_1$ (left), $\tilde{b}_1$ (middle), and right-handed $\tilde{t}_1$ (right) in the minimal mixing scenario.

of Case IA. For pure left-handed $\tilde{t}_1$, $bbWWZ/h + \not{E}_T$ is as important as the conventional channel $bbWW + \not{E}_T$, which could be an important new search channel for the stop. For pure left-handed $\tilde{b}_1$, the conventional channel of $bb + \not{E}_T$ is highly suppressed. New final states of $bbWWZ/h$ and $bbWWWW$ are dominant and comparable in size, with $bbZ/hZ/h$ being subdominant, opening up new channels for sbottom searches. The final state for the pure right-handed $\tilde{t}_1$ is still the conventional channel of $bbWW + \not{E}_T$, despite the existence of light Wino NLSPs in the spectrum.

For the maximally mixed scenario, the decay of $\tilde{t}_1$, $\tilde{b}_1$ and $\tilde{t}_2$ are shown in the left, middle and right panels of Fig. 6, respectively. For $\tilde{t}_1$ with large mass, the decay to $b\chi_1^\pm$, $t\chi_2^0$ still dominates over $t\chi_1^0$, but the corresponding branching fractions are smaller compared to the pure left-handed case (Fig. 4) due to the decrease of the coupling to the Wino-like state caused by the right-handed stop component. For $\tilde{b}_1$, while $t\chi_1^\pm$ and $b\chi_2^0$ modes still dominate over $b\chi_1^0$ mode, the new decay channel of $W\tilde{t}_1$ opens up and even dominates over most of the mass range. Its branching fraction varies between 100% to about 40% for $m_{\tilde{b}_1}$ between 400 GeV to 1800 GeV. For $\tilde{t}_2$, in addition to $b\chi_1^\pm$ and $t\chi_{1,2}^0$ (about a few percent to 20%), decays to a light stop/sbottom plus a gauge boson become comparable or even dominant: about $50\% - 70\%$ for $Z\tilde{t}_1$ and about $20\% - 15\%$ for $W\tilde{b}_1$.

The left, middle and right panels of Fig. 7 show the $\sigma \times$ BR for $\tilde{t}_1\tilde{t}_1$, $\tilde{b}_1\tilde{b}_1$, and $\tilde{t}_2\tilde{t}_2$

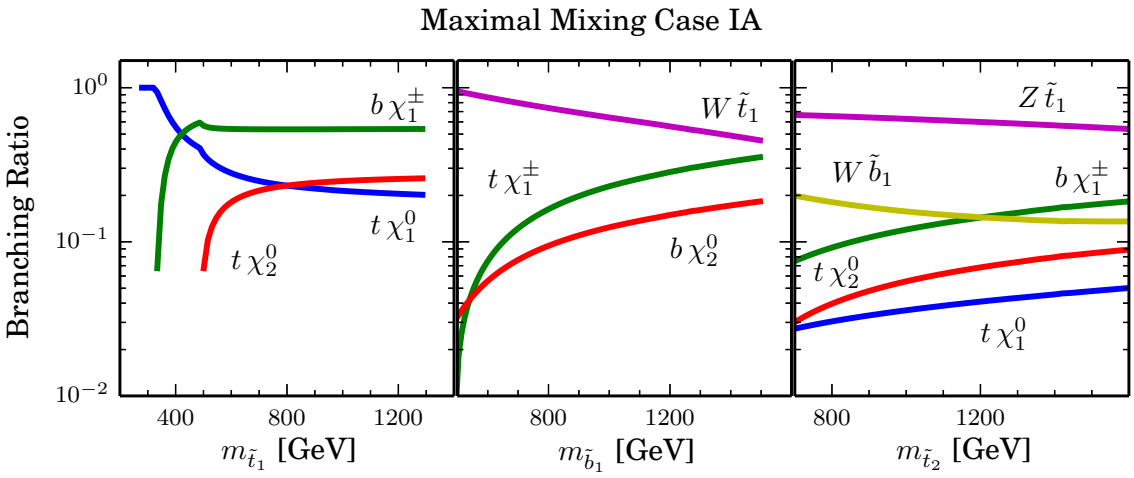

FIG. 6: Case IA: Branching fractions for $\tilde{t}_1$ (left), $\tilde{b}_1$ (middle) and $\tilde{t}_2$ (right) in the maximal mixing scenario.

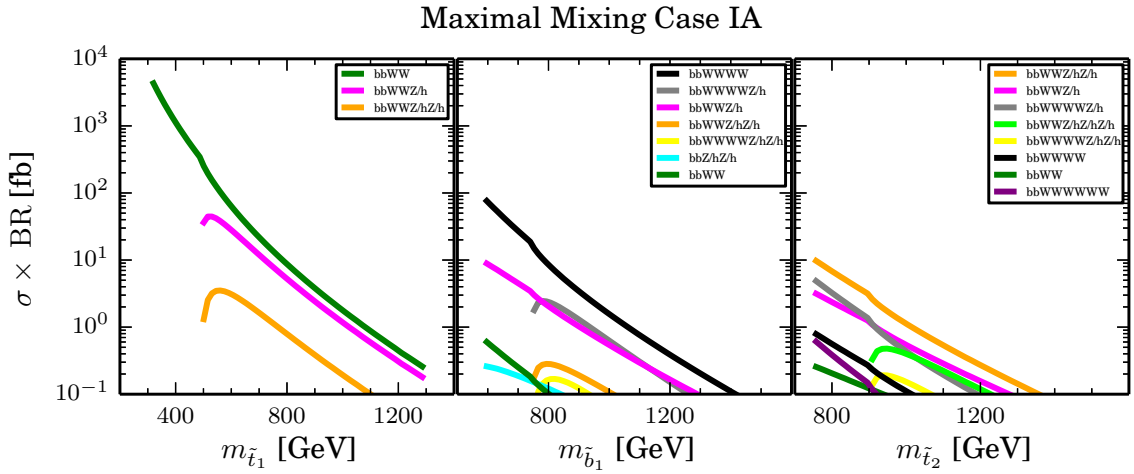

FIG. 7: Case IA: $\sigma \times$ BR of various final states for pair production of $\tilde{t}_1$ (left), $\tilde{b}_1$ (middle), and $\tilde{t}_1$ (right) in the maximal mixing scenario.

respectively for the maximal mixing scenario of Case IA at the 14 TeV LHC. For the light stop, while the dominant channel is the conventional $bbWW + \not{E}_T$, the subdominant channel $bbWWZ/h + \not{E}_T$ could still have a sizable cross section. For the light sbottom, $bbWWWW + \not{E}_T$ becomes dominant. For the heavy stop, multiple channels open, with $bbWWZ/hZ/h + \not{E}_T$ being dominant, followed by $bbWWZ/h + \not{E}_T$, $bbWWWWZ/h + \not{E}_T$, and $bbWWZ/hZ/hZ/h + \not{E}_T$.

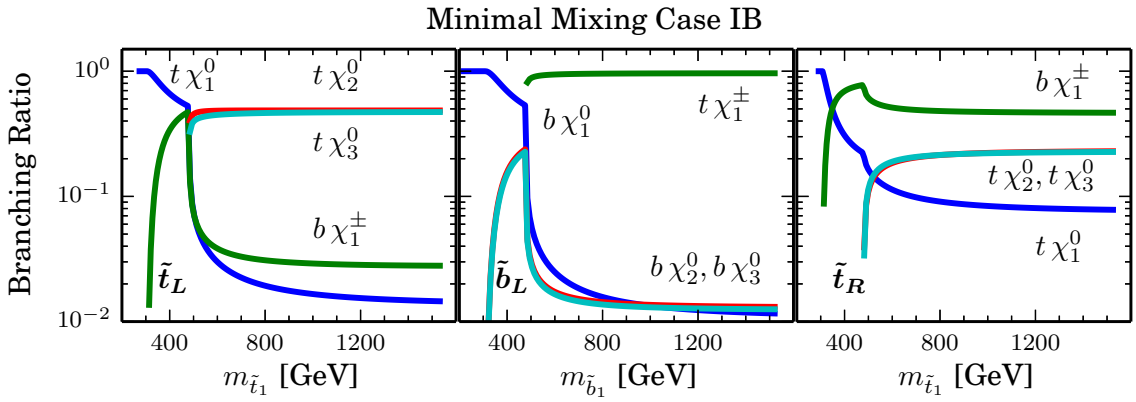

FIG. 8: Case IB: branching fractions for left-handed $\tilde{t}_1$ (left), $\tilde{b}_1$ (middle), right-handed $\tilde{t}_1$ (right) in the minimal mixing scenario.

C. Case IB: Bino-LSP with Higgsino-NLSP

The low lying neutralino/chargino spectrum in Case IB comprises of a Bino-like LSP, as well a pair of Higgsino-like neutralino states $\chi^0_{2,3}$ and chargino states $\chi^\pm_1$ with nearly degenerate masses. Fig. 8 shows the branching fractions of left-handed $\tilde{t}_1$ and $\tilde{b}_1$ and right-handed $\tilde{t}_1$ in the left, middle and right panels for the minimal mixing scenario. For $\tilde{t}_1$, decays to $t\chi^0_{2,3}$ dominate over $b\chi^\pm_1$ and $t\chi^0_1$ since the former ones are controlled by the large top Yukawa coupling, compared to the small bottom Yukawa coupling and $\mathrm{U}(1)_Y$ couplings for the latter two. However, for $\tilde{b}_1$, the decay of $t\chi^\pm_1$ becomes dominant since the $\tilde{b}_L\bar{t}_R\tilde{H}^+_u$ coupling is proportional to the top Yukawa while its couplings to $\chi^0_{2,3}$ and χ^0_1 are suppressed by the bottom Yukawa coupling and $\mathrm{U}(1)_Y$ couplings. For the right-handed $\tilde{t}_1$ case, it dominantly decays to $b\chi^\pm_1$, reaching almost 50%, while decays to $t\chi^0_2+t\chi^0_3$ are about 20%. All channels are controlled by the top Yukawa coupling while the latter ones have extra phase space suppression. Given the near degeneracy of the two Higgsino states $\chi^0_{2,3}$, contributions from final states involving $\chi^0_{2,3}$ are usually summed over in collider analyses.

Given the further decays of $\chi^\pm_1 \to W\chi^0_1$, $\chi^0_{2,3} \to Z\chi^0_1/h\chi^0_1$ as discussed in detail in [26], the pair production of stops and sbottoms lead to complicated final states at the collider. The left, middle and right panels of Fig. 9 show the $\sigma \times$ BR for pure left-handed $\tilde{t}_1\tilde{t}_1$, $\tilde{b}_1\tilde{b}_1$ and pure right-handed $\tilde{t}_1\tilde{t}_1$ pair production in the minimal mixing scenarios of Case IB. For pure left-handed $\tilde{t}_1$, $bbWWZ/hZ/h + \not{E}_T$ is the dominant final state with the

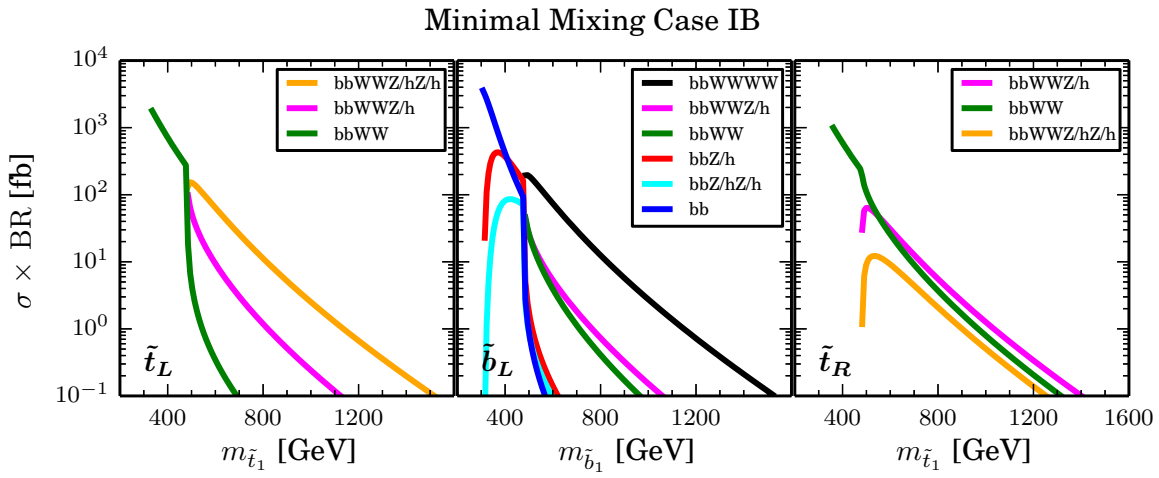

FIG. 9: Case IB: $\sigma \times$ BR of various final states for pair production of left-handed $\tilde{t}_1$ (left), $\tilde{b}_1$ (middle), and right-handed $\tilde{t}_1$ (right) in the minimal mixing scenario.

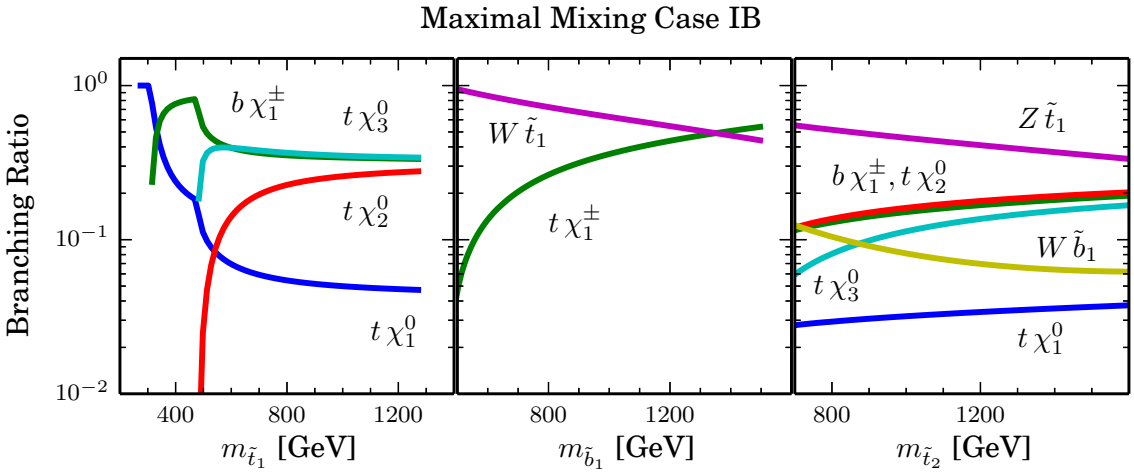

FIG. 10: Case IB: Branching fractions for $\tilde{t}_1$ (left), $\tilde{b}_1$ (middle) and $\tilde{t}_2$ (right) in the maximal mixing scenario.

conventional stop search channel $bbWW + \not{E}_T$ being highly suppressed. For pure left-handed $\tilde{b}_1$, $bbWWWW + \not{E}_T$ is the dominant channel. The dominant final states for pure right-handed $\tilde{t}_1$ are $bbWWZ/h + \not{E}_T$ as well as the conventional channel of $bbWW + \not{E}_T$.

For the maximal mixing scenario, the decay branching fractions for $\tilde{t}_1$, $\tilde{b}_1$, and $\tilde{t}_2$ are shown in the left, middle and right panels of Fig. 10, respectively. Since $\tilde{t}_1$ is an equal mixture of left- and right-handed components, the decays to $t\chi^0_{2,3}$ (dominant for $\tilde{t}_L$) and

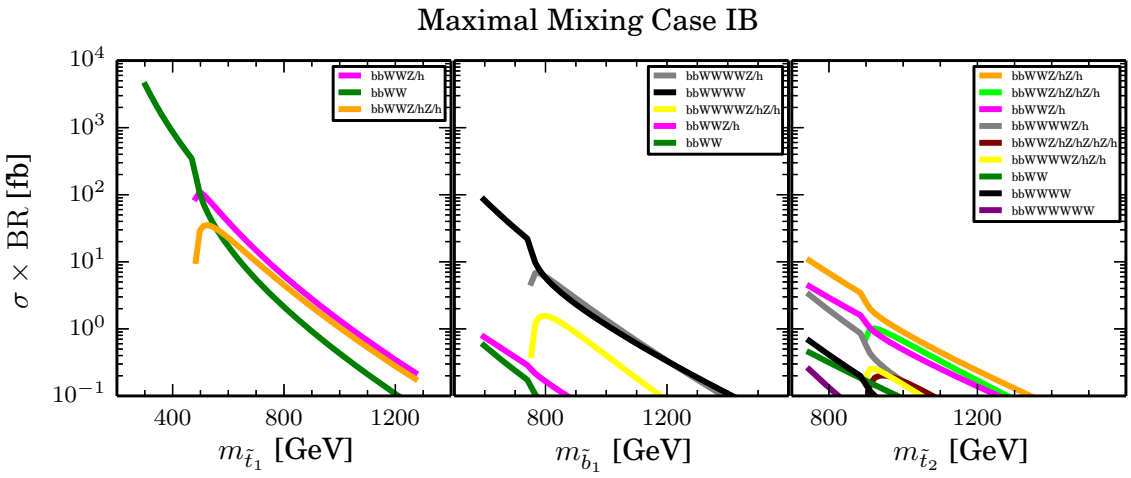

FIG. 11: Case IB: $\sigma \times$ BR of various final states for pair production of $\tilde{t}_1$ (left), $\tilde{b}_1$ (middle), and $\tilde{t}_2$ (right) in the maximal mixing scenario.

$b\chi_1^\pm$ (dominant for $\tilde{t}_R$) (see the left and right panel of Fig. 8) have roughly the same decay branching fraction, around 30% each. Decay to the conventional state of $t\chi_1^0$ is typically a few percent, unless other decay modes are kinematically unaccessible at small $m_{\tilde{t}_1}$.

For $\tilde{b}_1$, the relative strength of $t\chi_1^\pm$ and $b\chi_{2,3}^0$ is similar to that of the $\tilde{b}_1$ in the minimal mixing scenario, but the opening of the $W\tilde{t}_1$ mode dominates the decay for most of the mass range, leading to the suppression of the $t\chi_1^\pm$ and $b\chi_{2,3}^0$ modes. With increasing $m_{\tilde{b}_1}$, $t\chi_1^\pm$ becomes more and more important, which dominates over $W\tilde{t}_1$ when $m_{\tilde{b}_1} \gtrsim 1300$ GeV.

For $\tilde{t}_2$, decay to $Z\tilde{t}_1$ is dominant, about $60\% - 30\%$ for $m_{\tilde{t}_2}$ in the range of $700 - 1700$ GeV. Decays to $b\chi_1^\pm$, $t\chi_{2,3}^0$ are sub-dominant, around $10\% - 20\%$ for each channel. $\tilde{t}_2 \to W\tilde{b}_1$ is typically around 10% to about a few percent, while $\tilde{t}_2 \to t\chi_1^0$ is only at a few percent level.

The left, middle and right panel of Fig. 11 show the $\sigma \times$BR for $\tilde{t}_1\tilde{t}_1$, $\tilde{b}_1\tilde{b}_1$, and $\tilde{t}_2\tilde{t}_2$ for the maximal mixing scenario of Case IB at the 14 TeV LHC. For the light stop, the dominant channel is $bbWWZ/h + \not{E}_T$, followed by $bbWWZ/hZ/h + \not{E}_T$. The conventional channel $bbWW + \not{E}_T$ is suppressed by about a factor of 5. For the light sbottom, $bbWWWW + \not{E}_T$ and $bbWWWWZ/h + \not{E}_T$ are dominant. For the heavy stop, multiple channels open, with $bbWWZ/hZ/h + \not{E}_T$ being dominant, followed by $bbWWZ/hZ/hZ/h + \not{E}_T$ and $bbWWZ/h + \not{E}_T$.

IV. CURRENT COLLIDER SEARCH LIMITS ON STOP

113

Searches for direct stop pair production have been performed at both ATLAS and CMS, with about 20 fb^{-1} data at $\sqrt{s} = 8$ TeV, and about 5 fb^{-1} data at $\sqrt{s} = 7$ TeV [5–15]. The current searches mainly focus on two decay channels: $\tilde{t}_1 \to t^{(*)}\chi_1^0$ and $\tilde{t}_1 \to b\chi_1^\pm \to bW^{(*)}\chi_1^0$ [5–7, 9–11]. For small mass splitting $m_{\tilde{t}} - m_{\chi_1^0}$, channels of $\tilde{t} \to c\chi_1^0$, $bff'\chi_1^0$ have also been studied [12]. ATLAS results on fully hadronic final states exclude stops in the regions of $270 < m_{\tilde{t}_1} < 645$ GeV for $m_{\tilde{\chi}_1^0} < 30$ GeV, assuming both top squarks decay 100% via $\tilde{t}_1 \to t\chi_1^0$ [5]. Regions of $245 < m_{\tilde{t}_1} < 400$ GeV for $m_{\tilde{\chi}_1^0} < 60$ GeV, $m_{\chi_1^\pm} = 2m_{\chi_1^0}$ are excluded for the scenario where the top squark is assumed to decay 100% via $\tilde{t}_1 \to bW\chi_1^0$. For semileptonic channels, stop masses between 210 GeV and 640 GeV are excluded at 95% C.L. for a massless LSP [6] assuming BR($\tilde{t}_1 \to t\chi_1^0$) =100%. Stop masses up to 500 GeV are excluded when $\tilde{t}_1 \to b\chi_1^\pm$ dominates. Limits from the pure leptonic channels are much weaker [7]. Limits from CMS are similar [9–11]. Note that limits on the stop exclusion depend on the branching fractions of $\tilde{t}_1 \to t^{(*)}\chi_1^0$ and $\tilde{t}_1 \to b\chi_1^\pm$. For $\tilde{t}_1 \to b\chi_1^\pm$, the limits also depend on the mass of the intermediate chargino.

Searches for the second stop utilize the decay of $\tilde{t}_2 \to \tilde{t}_1 Z/h$, looking for signals including b-jets and large $\not{E}_T$ with either same flavor leptons reconstruction of the Z boson [8] and/or high p_T jet and b-jet multiplicities with additional leptons [13, 14]. The second stop mass is excluded up to about 600 GeV. Stop searches in scenarios with a Gravitino LSP are explored in Refs. [8, 15]. Stop searches in the R-parity violating MSSM can be found in Ref. [27].

There are other theoretical studies in the literature on the stop searches at the LHC, mostly focusing on the stop decaying to light generation quarks [28, 29] or a light stop with little missing energy, which mimics the WW signal at the LHC [30–34].

V. COLLIDER ANALYSIS

In this section, we study the detectability of the light stop in Case IA with a mass hierarchy of $M_1 < M_2 < M_{3SQ} \ll |\mu|, M_{3SU}$, resulting in a mass spectrum including a mostly left-handed stop and mostly left-handed sbottom, Wino-like NLSPs, and a Bino-like LSP. We choose a benchmark point with the specific set of parameters and the corresponding

mass spectrum shown in Table I. The value of $\tilde{A}_t$ is chosen such that the SM-like Higgs mass is around 125 GeV. Note that even though $\tilde{A}_t$ is set to a large value, the large mass splitting between M_{3SQ} and M_{3SU} results in a mostly left-handed $\tilde{t}_1$ and mostly right-handed $\tilde{t}_2$. Therefore, the decay patterns of $\tilde{t}_1$ and $\tilde{b}_1$ follow those of the Case IA: purely left-handed stop/sbottom in the minimal mixing scenario. 114

M_1	M_2	μ	$\tilde{A}_t$	M_{3SQ}	M_{3SU}	χ_1^0	χ_2^0	χ_1^+	$\tilde{t}_1$	h	$\tilde{b}_1$
150	300	2000	2750	550	2000	151	319	319	538	125	526

TABLE I: Mass parameters and mass spectrum of SUSY particles for the benchmark point. All masses are in units of GeV.

The decay channels for the light stop of the benchmark point are shown in Table II. While the dominant decay channel is $\tilde{t}_1 \to b\chi_1^+$ with 78% branching fraction, the subdominant channel $\tilde{t}_1 \to t\chi_2^0$ is about 20%, providing an interesting signal where χ_2^0 can either decay to a Higgs or a Z boson. For our choice of parameters with $\mu > 0$, χ_2^0 dominantly decays to $h\chi_1^0$, as shown in Table II. Flipping the sign of μ could lead to another interesting channel of $\chi_2^0 \to Z\chi_1^0$, which is left for future study.

Decay	Branching Fraction	Decay	Branching Fraction
$\tilde{t}_1 \to t\chi_1^0$	2%	$\chi_2^0 \to Z\chi_1^0$	3%
$\tilde{t}_1 \to t\chi_2^0$	20%	$\chi_2^0 \to h\chi_1^0$	97%
$\tilde{t}_1 \to b\chi_1^+$	78%	$\chi_1^+ \to W^+\chi_1^0$	100%

TABLE II: Decay branching fractions of $\tilde{t}_1$, χ_2^0 and χ_1^+ for the benchmark point.

For our benchmark point with the reduced branching fraction of $\mathrm{BR}(\tilde{t}_1 \to b\chi_1^\pm) = 78\%$, the current collider search limits on the stop are much more relaxed: less than about 400 $-$ 500 GeV for $m_{\tilde{t}_1}$. However, new search channels open up, which play a complementary role for stop searches at the LHC.

In our analysis, we study the stop pair production with one stop decaying via $\tilde{t}_1 \to t\chi_2^0 \to bWh\chi_1^0$ and the other stop decaying via $\tilde{t}_1 \to b\chi_1^+ \to bW\chi_1^0$. We consider semileptonic decays of the two Ws and the Higgs decay to two b-quarks. The signal contains four b-jets, two jets, one isolated lepton and large missing energy. The presence of a single lepton helps to reduce QCD backgrounds without significant branching fraction suppression.

The dominant SM backgrounds are $t\bar{t}$ and $t\bar{t}b\bar{b}$. While $t\bar{t}h$ is an irreducible background, the production cross section is typically small. Other backgrounds consist of $t\bar{t}W$, $t\bar{t}Z$ and $b\bar{b}WW$. 115

Event samples are generated using Madgraph MG5_aMC_V2_2_1 [35], processed through Pythia 6.420 [36] for fragmentation and hadronization and then through Delphes-3.1.2 [37] with the Snowmass combined LHC detector card [38] for detector simulation. Both the SM backgrounds and the stop pair production signal are normalized to theoretical cross sections, calculated including higher-order QCD corrections [24, 25, 39–43]. For the signal process, we scan the parameter range of $M_{3SQ} = 400 \ldots 1100$ GeV with step size of 25 GeV, and $M_1 = 3 \ldots 750$ GeV with step size of 25 GeV. We fix M_2 to be $M_2 = M_1 + 150$ GeV.

We apply the following event selection cuts:

- Events are required to have at least four isolated jets with

$$p_T^{j1,j2,j3} > 40 \text{ GeV}, \; p_T^{j4} > 25 \text{ GeV}, \; |\eta^j| < 2.5. \tag{7}$$

- Among the jets, at least two are b-tagged jets.

- One isolated lepton (e or μ) is required to have

$$p_T^{\ell} > 20 \text{ GeV with } |\eta^{\ell}| < 2.5. \tag{8}$$

Additional optimization cuts are applied to further enhance the signal and suppress the SM backgrounds:

- $\not{E}_T$, defined as the magnitude of the missing transpose momentum, $\mathbf{p}_T^{miss}$, ranging from 100 to 200 GeV, in increments of 20 GeV.

- H_T, defined as the scalar sum of the p_T of all surviving jets: $H_T = \sum p_T^{jet}$, ranging from 400 to 600 GeV, in increments of 50 GeV.

- Transverse mass m_T, defined as the invariant mass of the lepton and the missing transpose momentum:

$$m_T = \sqrt{2 p_T^{\ell} \not{E}_T (1 - \cos\phi(\mathbf{p}_T^{\ell}, \mathbf{p}_T^{miss}))}, \tag{9}$$

  ranging from 100 to 200 GeV, in increments of 20 GeV.

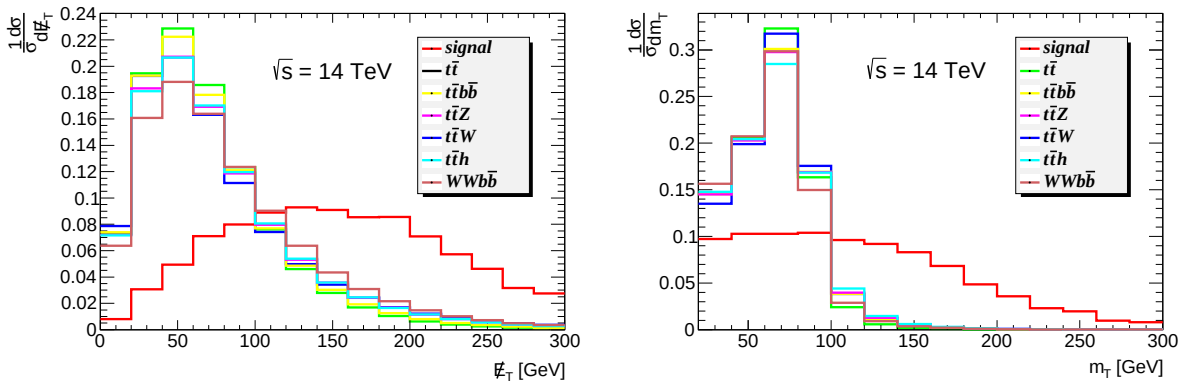

FIG. 12: The distribution of $\not{E}_T$ (left) and m_T (right) for the signal at the benchmark point and the SM backgrounds.

- N_j, the number of all surviving jets satisfying $p_T^j > 25$ GeV and $|\eta^j| < 2.5$, to be at least 4, 5, or 6.
- N_{bj}, the number of all tagged b-jets, to be at least 2, 3, or 4.

The distributions of $\not{E}_T$ and m_T for both the signal and the SM backgrounds are shown in Fig. 12. In the $\not{E}_T$ distribution, the $\not{E}_T$ for all the SM backgrounds comes only from the neutrino, which is typically smaller than that of the signal with additional $\not{E}_T$ contribution from the LSP. The transverse mass for the signal process extends beyond the SM threshold of the W boson mass. The H_T distribution of the signal is maximum at a higher value compared to the SM backgrounds.

In Table III, we present the cumulative cut efficiencies for the signal and dominant SM backgrounds with optimized cuts. By utilizing strong $\not{E}_T$, H_T and m_T cuts, we significantly reduce the SM backgrounds. The stop signal process typically generates multiple hard jets in our specified decay. The N_{bj} cut further plays an important role in cutting $t\bar{t}$, $t\bar{t}W$, $t\bar{t}Z$ and $b\bar{b}WW$ backgrounds. $t\bar{t}$ is the dominant background given its large cross section. $t\bar{t}b\bar{b}$ is the second dominant background given its relatively large cross section and similar final states to the signal process. $t\bar{t}h$, $t\bar{t}Z$, $t\bar{t}W$ and $b\bar{b}WW$ can be sufficiently suppressed due to low cross sections. We optimize the significance $S/\sqrt{B}$ for all the combinations of the advanced cuts. We impose a constraint on the number of signal events, $N_s \geq 3$ for 300 fb^{-1} in order to obtain sufficient statistics.

Description	$\tilde{t}_1\tilde{t}_1$	$t\bar{t}$	$t\bar{t}b\bar{b}$	$t\bar{t}h$	$t\bar{t}Z$	$t\bar{t}W$
CS (fb)	23	261230	2346	108	221	218
Basic cuts	38%	14%	24%	31%	30%	25%
$\not{E}_T > 200$ GeV	12%	0.23%	0.58%	1.2%	1.2%	1.2%
$H_T > 500$ GeV	7.6%	7.4×10^{-4}	0.29%	0.78%	0.77%	0.69%
$m_T > 160$ GeV	2.4%	1.8×10^{-6}	3.6×10^{-5}	6.6×10^{-5}	7.0×10^{-5}	6.0×10^{-5}
$N_j \geq 5$	2.0%	8.5×10^{-7}	2.1×10^{-5}	3.7×10^{-5}	3.8×10^{-5}	2.6×10^{-5}
$N_{bj} \geq 2$	1.2%	2.9×10^{-7}	1.1×10^{-5}	2.2×10^{-5}	1.1×10^{-5}	7.6×10^{-6}
CS (fb) after cuts	0.28	0.075	0.026	0.0023	0.0025	0.0017

TABLE III: The cumulative cut efficiencies for the signal at the benchmark point and all SM backgrounds. The cross sections shown in the second row are for the semileptonic final states.

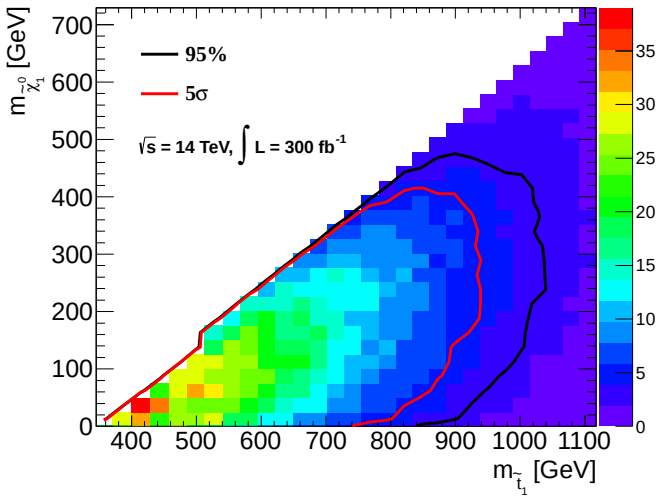

FIG. 13: The plot shows the 5σ discovery reach (red) and 95% exclusion limits (black) of the stop in the $m_{\tilde{t}_1} - m_{\chi_1^0}$ plane for 14 TeV LHC with 300 fb^{-1} of integrated luminosity. M_2 is fixed to be $M_1 + 150$ GeV and 10% systematic error is included.

In Fig. 13, we show the 95% C.L. exclusion limit and 5σ reach in the parameter space of $m_{\tilde{t}_1}$ versus $m_{\chi_1^0}$ for the 14 TeV LHC with 300 fb^{-1} luminosity. For the 5σ reach, stop masses up to 740 GeV can be reached for a massless LSP and about 940 GeV with $m_{\chi_1^0}$ = 250 GeV. The 95% C.L. exclusion limits are about 840 GeV for stops with a light χ_1^0, while the reach is 1040 GeV for $m_{\chi_1^0} = 250$ GeV.

VI. SUMMARY AND CONCLUSION

Most of the current stop and sbottom searches at the LHC have been performed considering the channels of $tt + \not{E}_T$, $bbWW + \not{E}_T$ for stop and $bb + \not{E}_T$ for sbottom, assuming the stop and sbottom decay 100% into these channels. However, in many regions of MSSM parameter space, these decay channels are subdominant, resulting in relaxed bounds from current LHC searches. In this work, we studied decays of the stop and sbottom in the cases of a Bino-like LSP with either Wino-like or Higgsino-like NLSPs in the low energy spectrum, for the left- and right-handed stops and left-handed sbottom in the minimal mixing scenario, and $\tilde{t}_{1,2}$, $\tilde{b}_1$ in the maximal mixing scenario. We found that new decay channels of $\tilde{t}_1 \to t\chi^0_{2,3}$, $\tilde{b}_1 \to b\chi^0_{2,3}, t\chi^\pm_1, W\tilde{t}_1$ open up, which could even dominate over conventional channels. For the heavier stop state, $\tilde{t}_2$, a new channel of $\tilde{t}_2 \to W\tilde{b}_1$ appears in addition to $\tilde{t}_2 \to Z\tilde{t}_1$ in the maximal mixing scenario. Given the further decays of $\chi^0_{2,3}$ and $\chi^\pm_1$, pair production of stops and sbottoms at the LHC typically leads to bb plus multiple gauge bosons plus $\not{E}_T$ final states. Conventional search channels of $bbWW + \not{E}_T$ and $bb + \not{E}_T$ could be highly suppressed.

We performed a detailed collider analysis for the reach of the stop at the 14 TeV LHC with 300 fb^{-1} integrated luminosity for one particularly interesting channel in the Bino-like LSP with Wino-like NLSP case. We considered left-handed stop pair production with one stop decaying via $\tilde{t}_1 \to t\chi^0_2 \to bWh\chi^0_1$ and the other stop decaying via $\tilde{t}_1 \to b\chi^\pm_1 \to bW\chi^0_1$, leading to $bbbbjj\ell + \not{E}_T$ final states. Our results show that for a LSP mass of 250 GeV, the 95% C.L. exclusion reach is about 1040 GeV for the stop and the 5σ reach is about 940 GeV. The reach decreases with smaller LSP mass.

Considering different low-lying neutralino/chargino spectra provides several promising channels for the stop and sbottom study. In this paper we focused on final states with a Higgs boson. Decays of χ^0_2 to $Z\chi^0_1$ could be dominant with a different choice of sign(μ). Furthermore, a different mass spectrum of neutralino/chargino with LSP being either Wino-like or Higgsino-like might give rise to more interesting final states. It is important to identify the leading decay channels in various regions of parameter space to fully explore the reach of the LHC for the third generation squarks, which has important implications for the stabilization of the electroweak scale in supersymmetric models. The strategy developed in our analysis can be applied to the study of top partners in other new physics

scenarios as well. 119

Acknowledgments

We would like to thank Felix Kling, Tao Han, Yongcheng Wu, Bing Zhang for helpful discussions. The work is supported by the Department of Energy under Grant DE-FG02-04ER-41298. This work was supported in part by National Science Foundation Grant No. PHYS-1066293 and the hospitality of the Aspen Center for Physics.

---

[1] G. Aad et al. (ATLAS Collaboration), Phys.Lett. **B716**, 1 (2012), 1207.7214.

[2] S. Chatrchyan et al. (CMS Collaboration), Phys.Lett. **B716**, 30 (2012), 1207.7235.

[3] S. Weinberg, Phys.Rev. **D13**, 974 (1976).

[4] M. Papucci, J. T. Ruderman, and A. Weiler, JHEP **1209**, 035 (2012), 1110.6926.

[5] G. Aad et al. (ATLAS Collaboration), JHEP **1409**, 015 (2014), 1406.1122.

[6] G. Aad et al. (ATLAS Collaboration), Tech. Rep. CERN-PH-EP-2014-143, CERN, Geneva (2014), 1407.0583.

[7] G. Aad et al. (ATLAS Collaboration), JHEP **1406**, 124 (2014), 1403.4853.

[8] G. Aad et al. (ATLAS Collaboration), Eur.Phys.J. **C74**, 2883 (2014), 1403.5222.

[9] C. Collaboration (CMS Collaboration), Tech. Rep. CMS-PAS-SUS-13-015, CERN, Geneva (2013).

[10] C. Collaboration (CMS Collaboration), Tech. Rep. CMS-PAS-SUS-14-011, CERN, Geneva (2014).

[11] S. Chatrchyan et al. (CMS Collaboration), Eur.Phys.J. **C73**, 2677 (2013), 1308.1586.

[12] C. Collaboration (CMS Collaboration), Tech. Rep. CMS-PAS-SUS-13-009, CERN, Geneva (2014).

[13] V. Khachatryan et al. (CMS Collaboration), Phys.Lett. **B736**, 371 (2014), 1405.3886.

[14] C. Collaboration (CMS Collaboration), Tech. Rep. CMS-PAS-SUS-13-021, CERN, Geneva (2013).

[15] S. Chatrchyan et al. (CMS Collaboration), Phys.Rev.Lett. **112**, 161802 (2014), 1312.3310.

[16] A. Chakraborty, D. K. Ghosh, D. Ghosh, and D. Sengupta, JHEP **1310**, 122 (2013), 1303.5776. 120

[17] C. Collaboration (CMS Collaboration), Tech. Rep. CMS-PAS-SUS-13-018, CERN, Geneva (2014).

[18] E. Alvarez and Y. Bai, JHEP **1208**, 003 (2012), 1204.5182.

[19] M. S. Carena, J. Espinosa, M. Quiros, and C. Wagner, Phys.Lett. **B355**, 209 (1995), hep-ph/9504316.

[20] N. D. Christensen, T. Han, and S. Su, Phys.Rev. **D85**, 115018 (2012), 1203.3207.

[21] M. Carena, S. Gori, N. R. Shah, and C. E. Wagner, JHEP **1203**, 014 (2012), 1112.3336.

[22] A. Belyaev, S. Khalil, S. Moretti, and M. C. Thomas, JHEP **1405**, 076 (2014), 1312.1935.

[23] A. Djouadi, M. Muhlleitner, and M. Spira, Acta Phys.Polon. **B38**, 635 (2007), hep-ph/0609292.

[24] W. Beenakker, S. Brensing, M. Kramer, A. Kulesza, E. Laenen, et al., JHEP **1008**, 098 (2010), 1006.4771.

[25] A. Broggio, A. Ferroglia, M. Neubert, L. Vernazza, and L. L. Yang, JHEP **1307**, 042 (2013), 1304.2411.

[26] T. Han, S. Padhi, and S. Su, Phys.Rev. **D88**, 115010 (2013), 1309.5966.

[27] C. Brust, A. Katz, and R. Sundrum, JHEP **1208**, 059 (2012), 1206.2353.

[28] R. Grober, M. Muhlleitner, E. Popenda, and A. Wlotzka (2014), 1408.4662.

[29] P. Agrawal and C. Frugiuele, JHEP **1401**, 115 (2014), 1304.3068.

[30] A. Delgado, G. F. Giudice, G. Isidori, M. Pierini, and A. Strumia, Eur.Phys.J. **C73**, 2370 (2013), 1212.6847.

[31] K. Rolbiecki and K. Sakurai, JHEP **1309**, 004 (2013), 1303.5696.

[32] D. Curtin, P. Meade, and P.-J. Tien (2014), 1406.0848.

[33] J. S. Kim, K. Rolbiecki, K. Sakurai, and J. Tattersall (2014), 1406.0858.

[34] M. Czakon, A. Mitov, M. Papucci, J. T. Ruderman, and A. Weiler (2014), 1407.1043.

[35] J. Alwall, R. Frederix, S. Frixione, V. Hirschi, F. Maltoni, et al., JHEP **1407**, 079 (2014), 1405.0301.

[36] T. Sjostrand, S. Mrenna, and P. Z. Skands, JHEP **0605**, 026 (2006), hep-ph/0603175.

[37] J. de Favereau et al. (DELPHES 3), JHEP **1402**, 057 (2014), 1307.6346.

[38] J. Anderson, A. Avetisyan, R. Brock, S. Chekanov, T. Cohen, et al. (2013), 1309.1057.

[39] M. Cacciari, S. Frixione, M. L. Mangano, P. Nason, and G. Ridolfi, JHEP **0809**, 127 (2008), 0804.2800. 121

[40] A. Bredenstein, A. Denner, S. Dittmaier, and S. Pozzorini, Phys.Rev.Lett. **103**, 012002 (2009), 0905.0110.

[41] W. Beenakker, S. Dittmaier, M. Kramer, B. Plumper, M. Spira, et al., Nucl.Phys. **B653**, 151 (2003), hep-ph/0211352.

[42] J. M. Campbell and R. K. Ellis, JHEP **1207**, 052 (2012), 1204.5678.

[43] A. Lazopoulos, T. McElmurry, K. Melnikov, and F. Petriello, Phys.Lett. **B666**, 62 (2008), 0804.2220.